Lappeenranta
University of Technology

Pasi Nuutinen

POWER ELECTRONIC CONVERTERS IN LOW-VOLTAGE DIRECT CURRENT DISTRIBUTION – ANALYSIS AND IMPLEMENTATION

Thesis for the degree of Doctor of Science (Technology) to be presented with due permission for public examination and criticism in the Auditorium 1383 at Lappeenranta University of Technology, Lappeenranta, Finland on the 18th of December, 2015, at noon.

Acta Universitatis
Lappeenrantaensis 677

Supervisors Professor Pertti Silventoinen
LUT Electrical Engineering
LUT School of Energy Systems
Lappeenranta University of Technology
Finland

Dr. Pasi Peltoniemi
LUT Electrical Engineering
LUT School of Energy Systems
Lappeenranta University of Technology
Finland

Reviewers Professor Kimmo Kauhaniemi
Department of Electrical Engineering
University of Vaasa
Finland

Professor Teuvo Suntio
Department of Electrical Engineering
Tampere University of Technology
Finland

Opponent Professor Kimmo Kauhaniemi
Department of Electrical Engineering
University of Vaasa
Finland

ISBN 978-952-265-890-6
ISBN 978-952-265-891-3 (PDF)
ISSN-L 1456-4491
ISSN 1456-4491
Lappeenrannan teknillinen yliopisto
Yliopistopaino 2015

Abstract

Pasi Nuutinen
Power Electronic Converters in Low-Voltage Direct Current Distribution – Analysis and Implementation
Lappeenranta 2015
102 pages
Acta Universitatis Lappeenrantaensis 677
Diss. Lappeenranta University of Technology
ISBN 978-952-265-890-6, ISBN 978-952-265-891-3 (PDF)
ISSN-L 1456-4491, ISSN 1456-4491

Over the recent years, smart grids have received great public attention. Many proposed functionalities rely on power electronics, which play a key role in the smart grid, together with the communication network. However, “smartness” is not the driver that alone motivates the research towards distribution networks based on power electronics; the network vulnerability to natural hazards has resulted in tightening requirements for the supply security, set both by electricity end-users and authorities. Because of the favorable price development and advancements in the field, direct current (DC) distribution has become an attractive alternative for distribution networks.

In this doctoral dissertation, power electronic converters for a low-voltage DC (LVDC) distribution system are investigated. These include the rectifier located at the beginning of the LVDC network and the customer-end inverter (CEI) on the customer premises. Rectifier topologies are introduced, and according to the LVDC system requirements, topologies are chosen for the analysis. Similarly, suitable CEI topologies are addressed and selected for study. Application of power electronics into electricity distribution poses some new challenges. Because the electricity end-user is supplied with the CEI, it is responsible for the end-user voltage quality, but it also has to be able to supply adequate current in all operating conditions, including a short-circuit, to ensure the electrical safety. Supplying short-circuit current with power electronics requires additional measures, and therefore, the short-circuit behavior is described and methods to overcome the high-current supply to the fault are proposed. Power electronic converters also produce common-mode (CM) and radio-frequency (RF) electromagnetic interferences (EMI), which are not present in AC distribution. Hence, their magnitudes are investigated.

To enable comprehensive research on the LVDC distribution field, a research site was built into a public low-voltage distribution network. The implementation was a joint task by the LVDC research team of Lappeenranta University of Technology and a power company Suur-Savon Sähkö Oy. Now, the measurements could be conducted in an actual environment. This is important especially for the EMI studies. The main results of the work concern the short-circuit operation of the CEI and the EMI issues. The applicability of the power electronic converters to electricity distribution is demonstrated, and suggestions for future research are proposed.

Keywords: Low-voltage direct current, LVDC distribution, smart grid, research site, converter, power electronics, CEI, common-mode, EMI, short circuit

Acknowledgments

The results of this doctoral dissertation are based on research projects carried out between 2007 and 2015 at the Department of Electrical Engineering, School of Energy Systems at Lappeenranta University of Technology. The research work was conducted as a part of research programs funded by the Finnish Funding Agency for Technology and Innovation (TEKES) and several companies involved.

I owe my deepest gratitude to the supervisor of this work, Professor Pertti Silventoinen for his valuable comments, guidance, and encouragement during the times when the focus became unclear, and to Professor Jarmo Partanen for giving me the opportunity to prepare my doctoral dissertation at LUT. Further, I want to thank both of you for the opportunity to do the research in a way that is perfectly suitable for me. I also want to thank the other supervisor, Dr. Pasi Peltoniemi, for his valuable comments that improved the result.

I thank the preliminary examiners, Professor Kimmo Kauhaniemi and Professor Teuvo Suntio, for their valuable feedback and suggestions on the manuscript. I am very grateful for your contribution.

I express my sincere gratitude to the LVDC research team that has been working like a well-oiled machine. Especially Mr. Tero Kaipia's assistance has been invaluable in many occasions, and it has been a privilege to work with you. Thank you Dr. Pasi Peltoniemi and Dr. Antti Pinomaa, for your help in the measurements and preparation of the publications. Dr. Andrey Lana, without your contribution to the research setup, getting the measurement results would have been very hard. Mr. Aleksi Mattsson, Mr. Janne Karppanen, and Mr. Pasi Salonen, thank you for your contribution in the implementation of the research setups and publications. I would also like to thank Dr. Markku Niemelä, and the staff at the laboratory and LUT Voima for your help while building the setups.

Juha Lohjala and Mika Matikainen from the companies Suur-Savon Sähkö Oy and Järvi-Suomen Energia Oy: thank you for supporting and enabling the practical research of the LVDC distribution.

Dr. Hanna Niemelä deserves special thanks for translating my writing into proper English. Your help has always been available, and I think the size of your bag of articles for me, which you many times mentioned, is not that big anymore.

The financial support of Walter Ahlström Foundation, Research Foundation of Lappeenranta University of Technology, Ulla Tuominen Foundation, and Emil Aaltonen Foundation is greatly appreciated.

Most importantly, I extend my deepest gratitude to my wife Sanna. Thank you for your tolerance over the years. And our children Silja and Luka – you are the world to me.

Kiitos äiskä ja iskä kaikesta siitä tuesta, jota olen elämäni aikana teiltä saanut. Kiitos iskä elämänohjeista ja kaikista niistä hetkistä autotallissa, jotka saivat hurahtamaan tekniikkaan. Vaikka et olekaan enää täällä, olet kuitenkin.

Lappeenranta, December 2015
Pasi Nuutinen

Contents

List of publications

Publication I
Nuutinen, P., Salonen, P., Peltoniemi, P., Silventoinen, P., and Partanen, J. (2009). "LVDC Customer-End Inverter Operation in Short Circuit." In *Proc. of EPE 2009*. 8–10 Sept. 2009, Barcelona, Spain.

Publication II
Nuutinen, P., Peltoniemi, P., and Silventoinen, P. (2013). "Short-Circuit Protection in a Converter-Fed Low-Voltage Distribution Network." *IEEE Trans. Power Electron.*, 28(4), pp. 1587–1597.

Publication III
Nuutinen, P., Pinomaa, A., Ström, J-P., Kaipia, T., and Silventoinen, P. (2014). "On Common-Mode and RF EMI in a Low-Voltage DC Distribution Network." *IEEE Trans. Smart Grid*, 5(5), pp. 2583–2593.

Publication IV
Nuutinen, P., Kaipia, T., Peltoniemi, P., Lana, A., Pinomaa, A., Mattsson, A., Silventoinen, P., Partanen, J., Lohjala, J., Matikainen, M. (2014). "Research Site for Low-Voltage Direct Current Distribution in an Utility Network - Structure, Functions, and Operation." *IEEE Trans. Smart Grid*, 5(5), pp. 2574–2583.

Publication V
Nuutinen, P., Mattsson, A., Kaipia, T., Peltoniemi, P., Pinomaa, A., Lana, A., Karppanen, J., and Silventoinen, P. (2014). "Power Electronic Losses of a Customer-End Inverter in Low-Voltage Direct Current Distribution." In *Proc. of EPE 2014*. 26–28 Aug. 2014, Lappeenranta, Finland.

The publications are in a chronological order. In this doctoral dissertation they are referred to as Publication I, Publication II, Publication III, Publication IV, and Publication V.

Nomenclature

Latin alphabet

C	Capacitance
E	Energy
f	Frequency
F	Factor
h	Order of harmonics
I,i	Current
$\hat{I}$, $\hat{i}$	Current peak value
k	Integer
L	Inductance
m, M	Modulation index
n	Integer
P	Active power
$\hat{P}$	Peak active power
R, r	Resistance
t	Time
U, u, V	Voltage
$\hat{U}$, $\hat{u}$	Voltage peak value
X	Reactance
Z	Impedance

Greek alphabet

φ	Phase angle
ω	Angular frequency

Superscripts

min	Minimum value

Subscripts

-	DC network minus pole
+	DC network plus pole
1	Transformer primary value
2	Transformer secondary value
1phase inv	Single-phase inverter
3phase inv	Three-phase inverter
a,b,c	Phases a, b, and c
add	Additional value
batt	Battery value

cap	Capacitor value
cc	Supply value
CE	Collector-emitter
CM	Common-mode
cond	Conduction
cust1,cust2,cust3	Customers 1, 2, and 3
D	Diode
DC	DC network value
ds(ON)	Drain-source on value
earth,EMI	EMI filter earth value
F	Forward value (diode)
filt	Filter value
I	IGBT
load	Load value
M	MOSFET
min	Minimum value
n, nom	Nominal value
off	Turn-off value
on	Turn-on value
out	Output value
peak	Peak value
rated	Rated value of a component
rec±	Rectifier-end plus and minus
rect	Rectifier value
ref	Reference value
ripple	Ripple value
rms	Root mean square
rr	Reverse recovery
sc	Short circuit
sw	Switching
T	Transistor
total	Combined value
transf.	Transformer

Abbreviations

1PFB	Single-phase full-bridge
1PHB	Single-phase half-bridge
2L	Two-level
3L	Three-level
3P4L	Three-phase four-leg
3PHB	Three-phase half-bridge
3PM	Three-phase modular
AC	Alternating current

ADSL	Asymmetric digital subscriber line
BESS	Battery energy storage system
CCB	Controlled circuit breaker
CEI	Customer-end inverter
CM	Common-mode
DC	Direct current
DG	Distributed generation
DOD	Depth of discharge
DSO	Distribution system operator
DSP	Digital signal processor
EMI	Electromagnetic interference
GaN	Gallium nitride
HERIC	Highly efficient and reliable inverter concept
HF	High-frequency
HSAR	High-speed auto-reclosing
HVDC	High-voltage direct current
IGBT	Insulated gate bipolar transistor
IT	Terrain-isolated functionally unearthed network
LV	Low-voltage
MOSFET	Metal-oxide-semiconductor field-effect transistor
MV	Medium-voltage
N	Neutral
NB	Narrowband
PE	Protective earth
PLC	Power line communication
PV	Photovoltaics
PWM	Pulse-width modulation
RCD	Residual current device
RF	Radio frequency
SiC	Silicon carbide
SOA	Safe operating area
SOC	State of charge
THD	Total harmonic distortion
TN-C	Earthed network with combined neutral and protective earth
TN-S	Earthed network with separated neutral and protective earth
UPS	Uninterruptible power supply

1 Introduction

Power electronic converters have been used in power transmission and power supply applications for decades. High-voltage DC (HVDC) systems are currently used around the world, and with high voltage levels, they are an efficient solution to long-distance and high-power transmission, and for interconnecting AC networks. In industrial environments, small-scale DC distribution has been used to feed common DC buses to which motor inverters are connected. Similarly, DC distribution has been proposed to replace AC networks in various applications, such as in data center supply (Salato et al., 2012) and marine vessel power systems (Zahedi and Norum, 2013). DC has also been proposed for residential microgrids (Kakigano et al., 2010) and nanogrids (Cvetkovic et al., 2012), and studies concerning direct DC supply in household appliances and protection of home DC grids have been published (Lucía et al., 2013), (Rodríguez-Otero and O'Neill-Carrillo, 2008), (Makarabbi et al., 2014a), (Makarabbi et al., 2014b). Still, AC has been the only choice for public low-voltage (LV) electricity distribution. A typical LV electricity distribution network in Finland is a three-phase 400 V 50 Hz AC network supplied by a 20 kV medium-voltage (MV) network. Over the past decade, a few major storms have generated high interruption costs, and every winter, snow causes supply interruptions in the MV network. Interruptions caused by trees are common in overhead line rural MV networks, because MV branch line paths often go through forests, and therefore, achieving tightening supply security requirements set by the Finnish legislation is more challenging with an overhead line MV network. Secondly, the network is aging and requires renovation. To overcome these challenges and to enhance supply security, one option is to increase underground cabling (Haakana, 2013); however, especially rural power companies have numerous low-power MV branch lines, to which MV cabling is an expensive solution. In these areas, some power companies have adopted 1000 V AC distribution (Lohjala, 2005), (Lohjala et al., 2005) to avoid MV cabling, but 1000 V AC distribution is still a fairly seldom used solution. To this end, power-electronics-based solutions that exploit DC in power distributions have also been studied.

1.1 Low-voltage DC distribution

The development in power electronics and the rising public attention to smart grids have resulted in intense research globally, and smart grids have increased their attractiveness. For instance in (Li, 2010), each smart transmission grid is regarded as an integrated system that functionally consists of three interactive, smart components, in other words, smart control centers, smart transmission networks, and smart substations. Consequently, the structure of the distribution networks is changing and the power transmission is no longer unidirectional, that is, from the power plants to the customer. The number of small-scale power generation units, energy storages, and electric vehicles is increasing, and almost all of them share one essential feature: DC voltage. The low-voltage DC (LVDC) distribution network enables easy connection of distributed generation to the grid, and in most cases, power conversion is required to match the voltage level to the grid voltage but no synchronization is required.

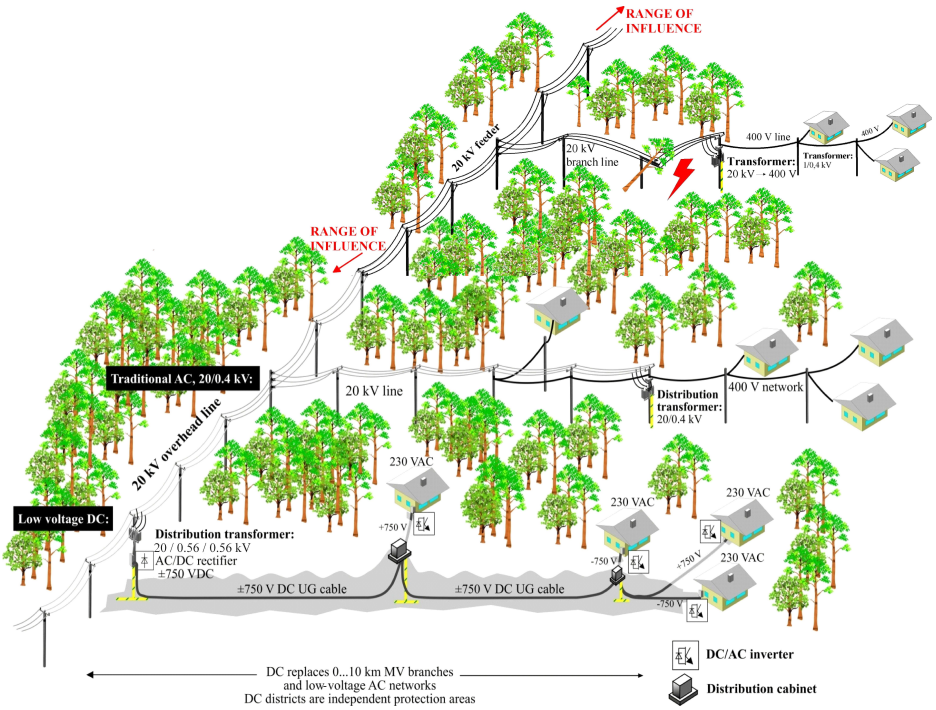

Figure 1.1: LVDC distribution system replacing a medium-voltage branch line and a low-voltage AC network (LUT, 2010).

In rural-area distribution, LVDC is a development step from the 1000 V AC distribution. In the public network LVDC distribution system concept, DC is applied in a larger scale than in the applications mentioned above. The LVDC distribution uses DC together with power electronics to replace 20 kV MVAC overhead branch lines and a 400 V AC network by an undergrounded DC network that can be built with LV cables. In Figure 1.1, the concept of the LVDC distribution is presented, and the LVDC is used in a rural environment. Advantages are, for instance, lower grid investment costs, enhanced end-user voltage quality, and various smart grid functionalities enabled by the use of smart power electronic converters (Kaipia et al., 2006), (Lassila et al., 2008), (Lassila et al., 2009). In the interconnection point to the MVAC network, an AC/DC conversion is required, and further, at every electricity end-user connected to the LVDC network, electricity supply is provided by a customer-end inverter (CEI) or a DC/DC converter, if the end-user can exploit DC supply. Power electronics enables the customer-end voltage quality control (Peltoniemi et al., 2013), and the integrated communications (Pinomaa, 2013) allows smart grid functions, such as the customer-end load control and the intelligent network management. The feasibility of the LVDC distribution relies on the use of the highest allowed DC voltage level of 1500 V defined by the low-voltage directive LVD 2006/95/EC (LVD, 2006). With a bipolar LVDC system applying the maximum voltage level (-750 VDC, 0 VDC, +750 VDC), the power transmission capacity can be 15 times that of the

400 V AC distribution with the same cable cross section (Figure 1.2), because higher voltage drop can be allowed with DC. Because the LVDC distribution enables the use of low-voltage cables and the transmission capacity is higher, the LVDC network provides a cost-effective way to develop distribution networks.

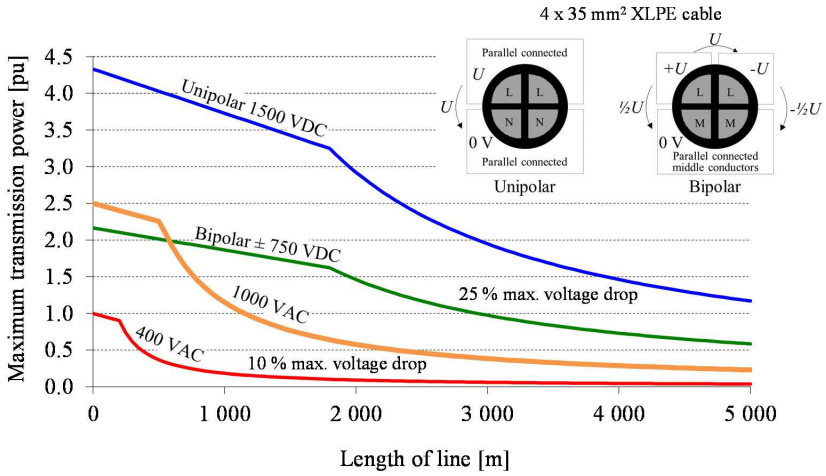

Figure 1.2: Comparison of maximum transmission powers (Kaipia, 2014).

1.2 Motivation of the work

DC microgrids and nanogrids are usually proposed for different purposes, for instance residential applications and data center power supply, as was discussed above. Despite the manifold activities in the smart grids field, similar applications of the LVDC distribution have not been presented in the literature so far. The LVDC distribution system that is in the focus of this doctoral dissertation is used for public electricity distribution, and it is designed to be an alternative to a traditional AC distribution system based on MV branch lines and a 400 V AC distribution network. The DC network and the smart power electronic converters open up opportunities to more efficient and diversified distribution network control. Many functionalities are required from the converters, but their relevance can be questioned. For instance, the requirements for the rectifier are different in a simple unidirectional network than in a network having energy storages and local generation. From the CEI point of view, both three-phase and single-phase solutions have to be studied, although the typical customer-end supply in Finland is provided as a three-phase one; the LVDC distribution may introduce new openings for the single-phase supply.

The customers already supplied with the AC distribution require solutions that are compatible with the system today. Consequently, the CEI has to be able to meet the requirements set by the voltage quality and electrical safety. The short-circuit operation of the

CEI is important from the electrical safety point of view, because if the CEI has to be compatible with present protection devices, that is, fuses and circuit breakers, it has to be able to supply sufficient short-circuit current. The question is whether there are any other alternatives available. Finally, when power electronics are applied to the electricity distribution, high-frequency disturbances arise, and it has to be studied if these disturbances have an effect on the operation of the system or even deteriorate the electrical safety of the customer.

1.3 Objective of the work and research methods

The first hypothesis is that the public network LVDC distribution system, based on power electronic converters, can be implemented. In this doctoral dissertation, the design and operating requirements for the power electronic converters are addressed. In this application, certain features are required from the rectifier and the CEIs. For example, the rectifier plays the key role in the power flow control between the MV network and the DC network. On the customer premises, the CEI alone is supplying the electricity, and it is responsible for the voltage quality. At the same time, the CEI has to enable smart grid functionalities, and meet the requirements set for the fault protection and electrical safety. Finally, to be economically feasible, the energy efficiency of the converters have to be optimized for this application; the efficiency of the electricity supply from the power plant to the distribution network is good and therefore, the losses produced in the 'last mile' are highly significant. Furthermore, the reliability of the converters has to be high, because the service life of a distribution network is decades, and thus, the need to replace the converters frequently degrades the overall feasibility.

The second hypothesis is that the power electronic converters can be feasibly implemented to meet the set requirements. The main objectives of the work are to introduce applicable converter topologies and analyze them against the functionalities and requirements set by this application. The main research issues for the rectifier involve the requirements and functionalities for the rectifier and consideration of the applicable topologies. At the customer end of the DC network, one research question concerns the CEI structures. Secondly, the LVDC network being a potential replacement for AC networks today, fault protection and clearance in a customer-end network have to be taken into account, especially when the protection is implemented with traditional, short-circuit current dependent devices. In this case, the CEI has to (1) supply sufficient current for the protection devices and (2) keep the current in the safe operating area (SOA) of the CEI. The question is: What does the short-circuit current supply requirement mean from the CEI point of view, and is it possible to manage the situation by applying other, low-current protection methods? Finally, as the power electronics is the key element in the power conversion and supply, an analysis of the conducted and radiated interferences is required. The research site, introduced below, plays a key role in the electromagnetic interference (EMI) study; the measurements can be conducted in an actual distribution network.

Even though the economic point of view is important for the LVDC concept, the research questions of this doctoral dissertation mainly involve technical issues, and economic considerations represent only a limited part of the work. The reason is that in the course of the research, the objective has been to develop and verify structures and methodologies that enable the proof of concept. However, it is pointed out that the optimization of the converters is not in the scope of the study. To sum up, the work focuses on analyzing the converters for the LVDC system, and considers the functionalities required for the reliable power supply.

A literature study is made to survey and elaborate on potential topologies and their properties. The main research methods applied are calculations, simulations, and experimental measurements, of which the empirical research covers the most of the study. Simulations are performed in Simplorer and Matlab Simulink environments. The analysis is mainly based on measurements carried out on a public distribution network research site (Publication IV), (Nuutinen et al., 2013), (Nuutinen et al., 2015), built by LUT in cooperation with a Finnish power company Suur-Savon Sähkö Oy. The research site was established to allow practical studies, concerning different areas of the LVDC distribution; the LVDC distribution is a novel approach to public electricity distribution, and the objective was to combine a fully functional LVDC system with a flexible research platform. The research site is addressed in Chapter 6. Furthermore, a laboratory setup at Lappeenranta University of Technology (LUT) (Nuutinen et al., 2011b) was used.

1.4 Outline of the work

The doctoral dissertation consists of a summary section and the appended original publications. The contents of the summary are divided into seven chapters as follows.

Chapter 1 introduces the LVDC distribution system concept, and discusses in brief the use of power electronics in the LVDC distribution and the requirements for the converters in this application. The chapter describes the background and motivation of the dissertation, presents the research objective and methods, and provides the scientific contributions.

Chapter 2 elaborates on the requirements for the rectifier. Topologies for the rectifier are presented and they are compared against the requirements set for the rectifier in LVDC distribution. The main analysis is made for a diode bridge rectifier, a half-controlled thyristor bridge rectifier, and a PWM grid-tie rectifying converter. First, the start-up of the LVDC distribution network using a diode bridge rectifier and a half-controlled thyristor bridge rectifier is analyzed by a case study. Next, the opportunities enabled by the more advanced control over the DC network voltage such as the option to connect a battery energy storage system (BESS) directly to the DC network, are addressed. Finally, other rectifier topologies are introduced.

Chapter 3 focuses on the customer-end inverter. Five two-level (2L) topologies are introduced and after an analysis, three applicable topologies are selected for a more detailed comparison, where their characteristics and losses are analyzed (Publication V). The losses for three topologies (single-phase full-bridge, three-phase full-bridge, and modular three-phase) are calculated using nine commercially available switches (IGBT, MOSFET, and SiC MOSFET).

Chapter 4 is devoted to the overcurrent supply capability and short-circuit operation of the CEI. Because the CEI is supplying an actual customer with protection devices and equipment that require current higher than the nominal current, the current supply requirements for the CEI are discussed. First, the short-circuit behavior of the galvanically nonisolating CEI structure is described (Publication I). Next, a similar analysis is performed for a galvanically isolating three-phase CEI structure used on the research site (Publication II). Consequently, the challenges in protection both from the electrical safety and equipment points of view are considered, and different methods for short-circuit protection are proposed to overcome the challenges with the short-circuit current supply.

Chapter 5 analyzes the electromagnetic interference (EMI) on the LVDC distribution research site (Publication III). First, common-mode EMI in the customer-end network is studied, and the effect on the operation of the system and the electrical safety of the electricity end-user are considered by using measurement data collected from the research site. Next, the common-mode EMI in the DC network and its effect on the use of PLC communication is studied. Finally, radio frequency EMI generated by the power electronic converters is analyzed. In addition to the results of the system with a half-controlled thyristor rectifier (Publication III), some new measurement results with the PWM grid-tie rectifying converter are presented and analyzed against previous results.

Chapter 6 introduces the LVDC public network research site (Publication IV). The background of the of the site is outlined and the structure of the setup is described.

Chapter 7 is the final chapter before the appended publications. Conclusions are made and suggestions are provided for future work.

1.5 Summary of publications

This doctoral dissertation consists of five publications, three of which are refereed journal articles and two are refereed conference publications. The first publication was published in 2009, and the last publication included in the dissertations was published in 2015. The author of this dissertation is the primary author of all the publications.

Publication I addresses the operation, current supply capability, and current limitation of the CEI in a short-circuit. The CEI studied in the publication is a single-phase galvanically nonisolating inverter implemented in the laboratory. The publication presents three methods for short-circuit protection in different inverter structures and makes a compar-

ison between them. In this publication, the author of the doctoral dissertation has developed and implemented the protection methods.

Publication II studies the short-circuit operation of the three-phase CEI, implemented for the LVDC distribution system research network. It introduces the control scheme for the short-circuit current control and analyzes alternative short-circuit protection solutions to overcome the problem of high fault current injection. In this publication, the present author analyzed the CEI operation in a short-circuit and developed alternative protection methods. The control scheme of the CEI was developed by Dr. Peltoniemi.

Publication III investigates common-mode (CM) and radio frequency (RF) electromagnetic interferences (EMI) on the LVDC distribution system research site. CM currents in the DC network and the customer-end networks are studied by on-site measurements with the objective to determine whether there are disturbances that exceed the requirements of the standards or whether the CM current could cause safety issues in the converter-fed user-end network. Moreover, RF disturbances are measured and discussed. In this publication, the present author is responsible for the analysis of the RF EMI and customer-end network CM current issues. The effect of the CM current on the feasibility of power line communication (PLC) in the DC network was analyzed by Dr. Pinomaa.

Publication IV introduces an LVDC distribution system research site, which was established in the course of the doctoral work to enable practical studies on different areas of LVDC distribution. The publication focuses on investigating the design, structure, functionalities, and operation of the site using the experiences of use and the measurement results gathered during continuous operation. The major functionalities and other important system properties are demonstrated. The research site has been implemented in cooperation by the LVDC research team of Lappeenranta University of Technology (LUT), and the present author has played the key role in the development and implementation of the research site, converters, converter functionalities, and protection systems. The publication was also written by the author.

Publication V considers the power electronic losses of the feasible single- and three-phase CEI topologies. The losses are calculated using nine different power switches: three commercially available IGBT, MOSFET, and SiC MOSFET power switches are selected for comparison. Further, the effect of the supply voltage level on the losses of the CEI is calculated for the nine power transistors in single- and three-phase topologies. The publication was written by the present author.

The author of the doctoral dissertation has also been the primary author or a coauthor in the following publications on closely related topics. These publications are excluded from the doctoral dissertation.

Nuutinen, P., Lana, A., Salonen, P., and Silventoinen, P. (2011a). “Start-up of the LVDC Distribution Network.” In *Proc. of CIRED 2011*. 6–9 Jun. 2011, Frankfurt, Germany.

Nuutinen, P., et al. (2011b). “Implementing a Laboratory Research Platform for an LVDC Distribution System.” In *Proc. of IEEE SmartGridComm 2011*. 17–20 Oct. 2011, Brussels, Belgium.

Nuutinen, P., et al. (2012). “Commissioning Inspection of an LVDC Distribution Network.” In *Proc. of NORDAC 2012*. 10–11 Sept. 2012, Espoo, Finland.

Nuutinen, P., et al. (2013). “Experiences from Use of an LVDC System in Public Electricity Distribution.” In *Proc. of CIRED 2013*. 10–13 Jun. 2013, Stockholm, Sweden.

Nuutinen, P., et al. (2015). “Implementing a Battery Energy Storage System with a Converterless Direct Connection to an LVDC Distribution Network.” In *Proc. of CIRED 2015*. 15–18 Jun. 2015, Lyon, France.

Nuutinen, P., Pinomaa, A., and Silventoinen, P. (2016). “Grid-Tie Rectifying Converter Impact on Common-Mode and RF EMI in a Low-Voltage DC Distribution Network.” *IEEE Trans. Smart Grid*. In review.

Peltoniemi, P. and Nuutinen, P. (2013). “Fault Detection Method for Phase-to-Ground Faults in Three-Phase Inverter Applications.” In *Proc. of IECON13*. 10–13 Nov. 2013, Vienna, Austria.

Peltoniemi, P., Nuutinen, P., and Pyrhonen, J. (2013). “Observer-based Output Voltage Control for DC Power Distribution Purposes.” *IEEE Trans. Power Electron.*, 28(4), pp. 1914–1926.

Mattsson, A., et al. (2014a). “Galvanic Isolation and Output LC Filter Design for the Low-Voltage DC Customer-End Inverter.” *IEEE Trans. Smart Grid*, 5(5), pp. 2593–2601.

Mattsson, A., et al. (2014c). “Implementation of a Modular Customer-end Inverter for a Low Voltage DC Distribution Network.” In *Proc. of EPE 2014*. 26–28 Aug. 2014, Lappeenranta, Finland.

Mattsson, A., et al. (2015b). “Life-Cycle Cost Analysis for the Customer-end Inverter Used in Low Voltage DC Distribution.” In *Proc. of ICDCM 2015*. 31 Mar.–1 Apr. 2015, Charleston, SC, USA.

Mattsson, A., et al. (2015a). “Evaluation of Isolated Converter Topologies for Low Voltage DC Distribution.” In *Proc. of IECON 2015*. 9–12 Nov. Yokohama, Japan.

Lana, A., et al. (2014b). “On Low-Voltage Dc Network Customer-End Inverter Energy Efficiency.” *IEEE Trans. Smart Grid*, 5(6), pp. 2709–2717.

Lana, A., et al. (2015a). “Control and Monitoring Solution for the LVDC Power Distribution Network Research Site.” In *Proc. of ICDCM 2015*. 31 Mar.–1 Apr. 2015, Charleston, SC, USA.

Lana, A., et al. (2015b). “Control of directly connected energy storage in LVDC distribution network.” In *Proc. of ACDC 2015*. 10–12 February 2015, Edgbaston Stadium, Birmingham, UK.

Kaipia, T., et al. (2012). “Field Test Environment for LVDC Distribution – Implementation Experiences.” In *Proc. of CIRED Workshop 2012*. 29–30 May 2012, Lisbon, Portugal.

Kaipia, T., et al. (2013). “A System Engineering Approach to Low-Voltage DC Distribution.” In *Proc. of CIRED 2013*. 10–13 Jun. 2013, Stockholm, Sweden.

Karppanen, J., et al. (2015). “Effect of Voltage Level Selection on Earthing and Protection of LVDC Distribution Systems.” In *Proc. of ACDC2015*. 10–12 February 2015, Edgbaston Stadium, Birmingham, UK.

1.6 Scientific contributions

The scientific contributions of this doctoral dissertation are:

- Analysis and definition of the requirements, applicable topologies, and functionalities for the rectifier in LVDC distribution.
- Analysis and definition of the requirements, applicable topologies, and functionalities for the CEI in LVDC distribution.
- Analysis of the CEI overcurrent supply and operation in a short-circuit.
- Methods for the customer-end network short-circuit protection.
- Loss analysis of the CEI structures.
- Analysis of common-mode and RF EMI originating from the power electronics and their effect on the system and customer-end network operation and electrical safety.
- Implementation and verification of the developed methodologies and technologies.
- Design, implementation, and analysis of a fully functional LVDC system with an energy storage, built into a public rural-area distribution network.

2 Rectifier

This chapter presents rectifier topologies applicable to LVDC distribution and compares them against the requirements set for the rectifier in this particular application. Depending on the DC network structure and desired functionalities, at least the following technical requirements are set for the rectifier:

- Unidirectional/bidirectional power flow
- DC voltage and power control
- High energy efficiency
- Low grid current distortion
- Low EMI
- Remote control and monitoring
- High-resolution measurements
- Complies with distribution network standards

Not all of the requirements have to be met in every LVDC application. For instance, accurate DC network voltage control is not needed in the simplest structure. In addition, an unidirectional rectifier may also be suitable in applications where power does not have to be supplied from the DC network to the supplying grid. These issues are addressed later in this chapter.

As it was mentioned in Chapter 1, the feasibility of the LVDC distribution requires the highest allowed DC voltage level of 1500 V. Hence, the LVDC network can be constructed at least as a unipolar or bipolar structure with 1500 VDC or $\pm$750 VDC voltage levels, respectively. The unipolar solution is not feasible with the 1500 V voltage level as it requires switches with a high rated voltage in the CEI, if two-level CEI topologies are used. Besides, these components are designed for industrial, traction, or other high-current applications, and therefore, they are overdimensioned for this purpose. In addition, the losses become high because of the high-voltage switch technology. However, 3.3 kV SiC MOSFETs are being developed, but they are not yet feasible. In Figure 2.1, cost trends of 1200 V and 3.3 kV SiC MOSFETs are shown, and it is evident that the price/amps for 3.3 kV components is notably higher and will remain such in the near future. With the $\pm$750 V bipolar structure, the use of 1200 V switches is enabled, which significantly increases the availability of the components. In addition to the IGBT technology, the development has been rapid, and novel, low-switching-loss silicon carbide (SiC) and gallium nitride (GaN) power switches have become, or are becoming, commercially available (Figure 2.2). Consequently, the DC network in this doctoral dissertation is considered a bipolar structure.

If the bipolar DC network is constructed by connecting two rectifiers in series, a single rectifier supplies either the top or bottom (plus or minus) half of the network, that is, voltage levels between +750 V and 0 V or 0 V and -750 V, respectively. If a two-tier transformer feeds a rectifier with 1500 V output DC voltage, split output capacitors are used to constitute the middle point of the DC network. In Figure 2.3, these two options of the rectifier supply are presented using a half-controlled thyristor bridge rectifier as an

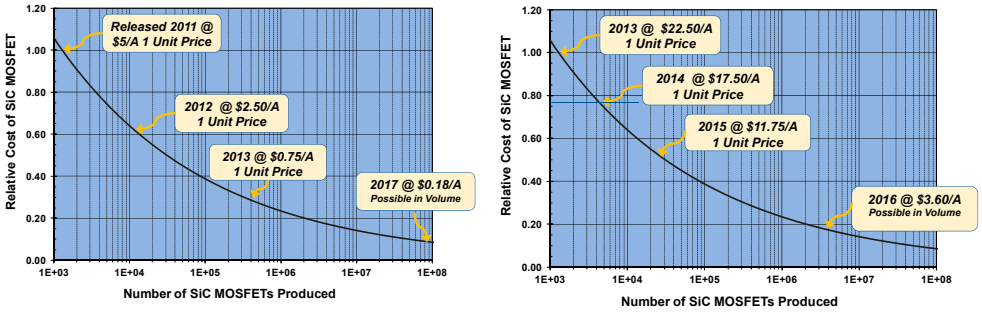

(a) (b)

Figure 2.1: Projected cost trends of a) 1200 V and b) 3.3 kV SiC MOSFETs (Cree Inc., 2014).

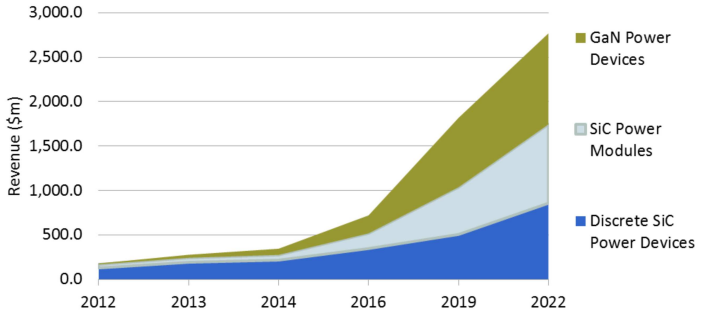

Figure 2.2: Overall SiC and GaN power semiconductor market 2012–2022 (Eden, 2013).

example. In Figure 2.3b, a high capacitance is required to keep the voltage equal at both voltage levels (poles), and the control of the DC voltage of an individual pole is not attainable. It is, however, possible to use an additional balancing leg to balance the voltages of the capacitors, but it adds more complexity to the circuit and degrades the efficiency of the rectifier (Alahuhtala and Tuusa, 2008). The split capacitor structure is also challenging in special situations such as a high current unbalance between the poles. The unbalance also produces a DC component to the transformer. The worst case is a single-pole DC short-circuit, shown in Figure 2.3b. If the voltage of the bottom pole $U_{\mathrm{DC}-}$ becomes 0 V during the short-circuit, the voltage of the top pole $U_{\mathrm{DC}+}$ doubles from 750 V to the rectifier output voltage 1500 V. This may result in a failure in the converters connected to the healthy pole. Finally, if the DC network protection is implemented using devices based on fault current injection and the energy of the faulty pole capacitor is not adequate to trip the protection, the short-circuit and overvoltage conditions will remain until other protection measures are performed.

In this application, the topology of the rectifier is determined by the network structure and the requirements of the LVDC network, and therefore, a single topology is not suit-

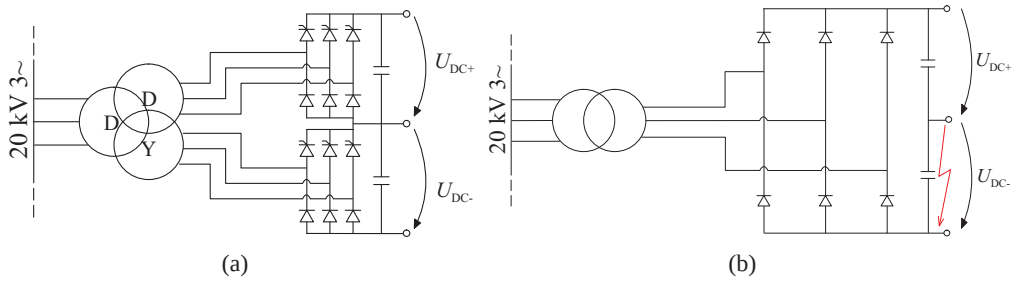

(a) (b)

Figure 2.3: A) Double-tier transformer and two series-connected half-controlled thyristor bridge rectifiers. B) Two-tier transformer supplying a half-controlled thyristor bridge rectifier with a split output capacitance. The lightning symbol indicates a short-circuit.

able for every situation. The requirements for the rectifier are different in a DC network structure where the power is transferred only from the supplying network to the customer than in a situation where DC voltage control and/or bidirectional power flow are required. Consequently, also the most feasible rectifier structure is different in both situations. A three-phase rectifier can be categorized, for example, as a controlled/uncontrolled, unidirectional/bidirectional, and two-level/three-level one. In this section, three rectifier topologies are analyzed: a diode bridge, a half-controlled thyristor bridge, and a grid-tie rectifying converter. Other topologies are also discussed in brief.

In the literature, different terms such as 'two-level line converter' and 'PWM full-bridge rectifier' have been used for the grid-tie rectifying converter topology. In this dissertation, the term 'grid-tie rectifying converter' is used to emphasize its differences to previous topologies: the diode bridge rectifier and the thyristor bridge rectifier are only used to rectify AC to DC whereas the grid-tie rectifying converter enables more versatile functionalities. Secondly, also the term 'rectifier' is used for an LVDC network front-end supply device, and it covers all topologies. This is for clarification purposes only, and no modifications are made to the topologies themselves.

2.1 Diode bridge

A diode bridge rectifier (Figure 2.4) is a low-cost choice with very low losses. The lack of control and measurement electronics results in a simple rectifier structure. Because the diode bridge is a passive topology, neither the current nor the voltage can be controlled. In this case, the minimum DC voltage $U_{\mathrm{DC,min}}$ required for the nominal AC voltage output $U_{\mathrm{AC,nom}}$ at the customer-end inverter is

$$U_{\mathrm{DC,min}} = \sqrt{2} u_{\mathrm{AC,nom}}. \tag{2.1}$$

With $u_{\mathrm{AC,nom}} = 400V$, 2.1 gives $U_{\mathrm{DC,min}} = 566V$. Because the nominal DC voltage level is 750 V and the minimum required voltage level is 566 V with the three-phase CEI, the

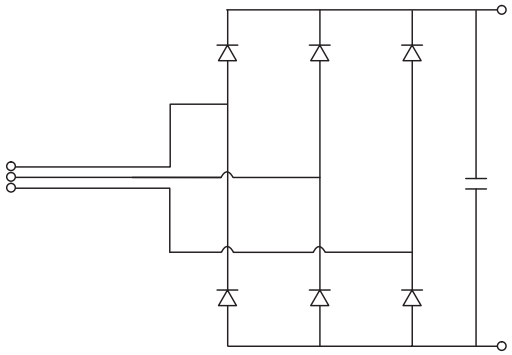

Figure 2.4: Diode bridge rectifier.

voltage can vary in a wide range, and from the CEI point of view, no DC voltage control or regulation is required. Actually, an advantage of the LVDC system is that the customer-end voltage can be kept at the nominal level even if the voltage in the DC network varies, which may result from the disturbances and voltage sags in the MV network.

Measurement results from the LVDC public network research site (Publication IV) are shown in Figure 2.5. A high-speed auto-reclosing (HSAR), caused by a climatic over-voltage, has occurred in the feeding MV network. The duration of the HSAR is approx. 0.4 s, and the DC network capacitances, discussed later in this chapter, are feeding the DC network. It can be seen that the phase a voltage of the CEI (a) is kept constant until the voltage in the DC network (b) decreases below 610 V. In this case, a higher voltage limit was selected to ensure that the DC voltage is high enough for the CEI voltage control and above the limit, customer-end voltage is not influenced by the decreasing DC voltage. To increase the CEI operating time of the DC network capacitor supply, the output voltage is decreased by 15% at voltages below 610 V. This has an effect on the customer-end power consumption if the load is linear. Therefore, if there are no other devices connected to the DC network that require DC voltage requlation, a diode bridge can be used. However, there are other issues addressed below that decrease the feasibility of the diode bridge.

2.1.1 DC voltage ripple and grid current harmonics

The diode bridge rectifier produces voltage ripple of the sixth harmonic of the fundamental frequency to the DC voltage (Mohan et al., 2003). Therefore, a capacitance is required in the DC network similarly as in the intermediate circuit of a motor inverter. A difference is that in the LVDC distribution the length of the intermediate circuit can be kilometers. In (Peltoniemi, 2010) and (Lana, 2014), the allowable voltage ripple is limited to 5% (10% peak-to-peak). The DC network capacitance sizes affect both the technical performance and economy of the LVDC distribution network; for instance, the power losses of the LVDC network depend on the dimensioning of the capacitors (Lana et al., 2011). As a result, the size of the minimum capacitance required in the DC network is

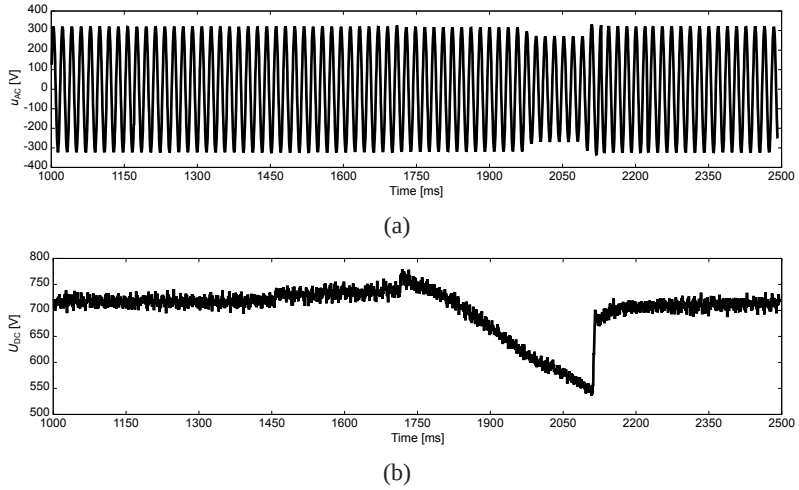

Figure 2.5: Phase a voltage of the CEI (a) and DC voltage (b) during an HSAR (Publication IV).

$$C_{\mathrm{rec}\pm} = 30\ \tfrac{\mu F}{kW},$$
$$C^{min}_{1\mathrm{phase\ inv}} = 44\ \tfrac{\mu F}{kW},$$
$$C^{min}_{3\mathrm{phase\ inv}} = 15\ \tfrac{\mu F}{kW},$$

where $C_{\mathrm{rec}\pm}$ is the rectifier-end, $C^{min}_{1\mathrm{phase\ inv}}$ the single-phase CEI end, and $C^{min}_{3\mathrm{phase\ inv}}$ the three-phase CEI end capacitance (Lana et al., 2011). If the maximum DC network voltage drop of 20% is taken into account (Lana, 2014), the CEI end capacitances become

$$C^{min}_{1\mathrm{phase\ inv}} = 71\ \tfrac{\mu F}{kW},$$
$$C^{min}_{3\mathrm{phase\ inv}} = 24\ \tfrac{\mu F}{kW}.$$

It is widely known that the line current of the diode bridge rectifier is not sinusoidal. To improve the harmonic content of the grid current, the rectifier is supplied with a double-tier transformer shown in Figure 2.3a. With a phase shift of 30 degrees between the secondaries, low-order harmonics are canceled and the rectifier line current has harmonics h of the order

$$h = 12k \pm 1, \tag{2.2}$$

where k is an integer (Mohan et al., 2003). In this case, two 6-pulse rectifiers constitute a 12-pulse rectifier, and the current in the middle conductor is 0 A. This is, however, an ideal situation because the loads in the top and bottom poles of the DC network vary continuously. Hence, the harmonic spectrum of the grid current depends on the load

conditions of the DC network. If one pole is under a light and one under a heavy load, the 12-pulse rectifier becomes a single 6-pulse rectifier, which has the following harmonics of the line current (Mohan et al., 2003)

$$h = 6k \pm 1. \tag{2.3}$$

This is the worst case, and no benefits are gained with the double-tier transformer in this situation. It also has an effect on the losses of the supply transformer, which should be designed for the rectifier supply to prevent saturation. The nominal power of a DC network, supplied with a single rectifier, is usually considerably lower than the nominal power of an MV network, and the line current harmonics have a minor effect on the MV network voltage quality. Nevertheless, the situation becomes different when more rectifiers (and DC networks) are connected to the same MV network. In this case, additional filtering may be required. Consequently, every network has to be individually studied to ensure proper operation and keep the voltage and current harmonics at the standardized level.

2.1.2 Capacitor charging

The lack of controllability results in problems in the DC network start-up situation. The total capacitance of the DC network is always significantly higher if compared with the traditional AC network. When the LVDC network is started up, the capacitances take charging current. If the current is not properly controlled, the outcome can be (1) a rectifier failure or (2) a protection device trip, and if the rectifier and the protection devices can withstand the high charging current, (3) overvoltages in the DC network. In (Nuutinen et al., 2011a), the start-up of an LVDC network is investigated. The result is that depending on the network structure and length, the overvoltage in the DC network varies from tens to hundreds of volts. The main reason is the rectifier-end capacitance connected directly to the output pole of the rectifier. This causes a high charging current, which together with the transformer inductance results in an overvoltage. This can be seen in Figure 2.6, where charging of the capacitances is simulated. The charging current exceeds 2 kA, and the overvoltage of the capacitor Cx is 250 V during the charging. When charging is completed, the steady-state voltage becomes 900 V. It is obvious that even if the overvoltage is at an acceptable level, the charging current has to be limited.

To overcome the charging current issue, an external charging device is required. The charging device can be a resistor in series with the rectifier, and during the normal operation, the resistor is bypassed using a mechanical contactor. The resistor has to be properly dimensioned; the control electronics power supplies of the CEIs start up above a certain voltage level, and if the resistance is too high, the voltage loss in the resistor becomes too high and the charging fails. Secondly, the resistor also has to withstand a short-circuited DC network charging attempt, which could be a challenge with a low resistance. As a result, a simple control circuit is required to monitor the voltages and detect abnormal charging behavior. It is also possible to use a power electronic switch for current limi-

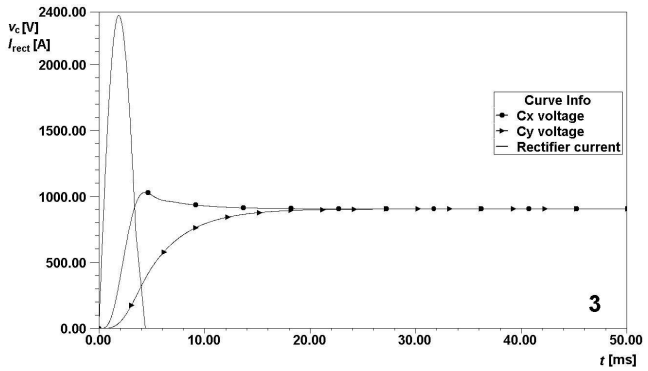

Figure 2.6: Rectifier current and capacitor voltages when the capacitors are charged with a diode bridge rectifier (Nuutinen et al., 2011a).

tation. With a fast switch and a PWM control circuit, the charging current and time can be controlled. When charging is completed, the switch can be turned on and a bypass contactor is not required. However, there is conduction loss in the switch, which could be higher than the losses in the diode bridge, which degrades the efficiency of the rectifier.

2.2 Half-controlled thristor bridge

When three diodes are replaced with thyristors (Figure 2.7), the rectifier becomes controlled. However, the controllability of the DC voltage is limited, and it can be used only in certain situations. The accuracy of the control is adequate for the current limitation during the network start-up process, and with the half-controlled thyristor bridge rectifier, charging challenges mentioned above can be avoided. This is evident in Figure 2.8, where a situation similar to Figure 2.6 is managed using a half-controlled thyristor bridge rectifier. Even though the maximum charging current still exceeds 500 A, no overvoltages arise. By increasing the charging time, the charging current can be decreased. As a result, a 12-pulse half-controlled thyristor bridge rectifier was in use on the research site.

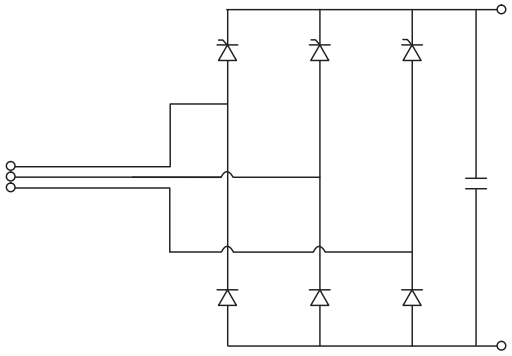

Figure 2.7: Half-controlled thyristor bridge rectifier.

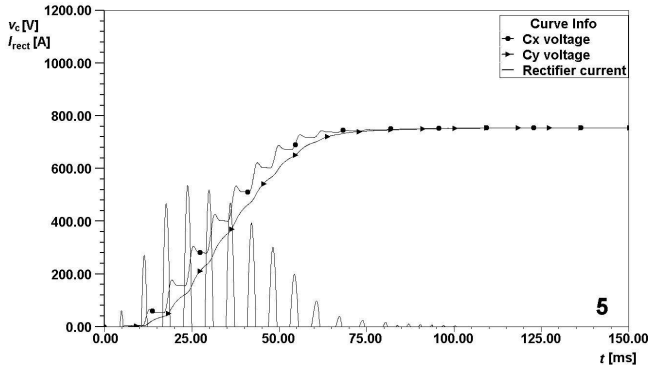

Figure 2.8: Rectifier current and capacitor voltages when the capacitors are charged with a half-controlled thyristor bridge rectifier (Nuutinen et al., 2011a).

When charging is completed, a thyristor control phase angle of 0 degree is used, and the operation corresponds with the diode bridge rectifier. Therefore, replacing the diodes with thyristors gives no benefits in the normal operation. Similarly, issues concerning the DC voltage ripple, the DC network capacitor dimensioning, and the grid current harmonics are equal to the diode bridge. Also in the HSAR situation shown in Figure 2.5, the rectifier is a half-controlled thyristor bridge, but it is operating as a diode bridge. During the HSAR, the DC voltage is not low enough, and the charging current is not controlled because the current remains at an acceptable level and no overvoltages occur. The measurement data were automatically collected from the research site, and the measurements in Figure 2.5 are from the CEI 1. Fast data recording at the rectifier-end was introduced later with the grid-tie rectifying converter, and with the thyristor rectifier, the rectifier currents during charging could not be collected, unfortunately.

2.3 Grid-tie rectifying converter

If bidirectional power flow is required, previous topologies have to be abandoned. It is required if there are energy storages or local generation connected to the DC network, or if the power from the customer-end network is required to be supplied back to the MV network. A two-level grid-tie rectifying converter is shown in Figure 2.9. It can be seen that this topology is a typical full-bridge three-phase six-pack inverter installed backwards. Therefore, without control it is a diode bridge rectifier, and the minimum voltage of the grid-tie rectifying converter is defined by the diode bridge. Therefore, the DC voltage can only be stepped up, for which inductance is required between the grid (transformer) and the rectifier. The bidirectional power flow also enables reactive power control. The 12-pulse half-controlled thyristor bridge rectifier of the research site was replaced with two series-connected grid-tie rectifying converters (Chapter 6).

Sinusoidal current is drawn from the supplying grid, and it is enabled by the grid-side LCL filter and boosting of the DC voltage. The boosting produces losses in the switches and the LCL filter, which results in a poor efficiency especially with low power levels. The

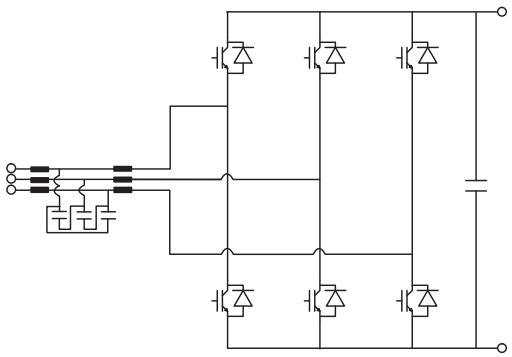

Figure 2.9: Two-level PWM grid-tie rectifying converter.

losses also depend on the DC voltage level; higher voltages require more boosting, which increases losses in the LCL filter. Therefore, the design of the filter and the selection of the inductor core materials are crucial to the feasibility of this topology. Similarly to other PWM switching topologies, the power electronics losses will decrease when new switch components become commercially available. This topology also shares the same drawback with the diode and thyristor bridge rectifiers: the charging current of the DC network capacitors cannot be controlled, and an external charging device is required. For instance, in the public network research site rectifier (Publication IV), which is a commercial grid-tie rectifying converter, charging is managed with a resistor and a bypass contactor. However, a DC network with this topology usually includes energy storages and/or local generation capable of feeding the network during a reconnection, and thus, slow charging after reconnection is not an issue.

2.3.1 Battery energy storage and system power flow control

A direct-connected battery energy storage (BESS), connected to the LVDC research site DC network, is introduced in (Nuutinen et al., 2015). Because the grid-tie rectifying converter enables the DC voltage control and a bidirectional power flow, the BESS is implemented without an interface converter between the DC network and the BESS. Therefore, the voltage of the BESS equals the voltage of the DC network. In this case, the DC network voltage can be varied between 710 V and 790 V, which represents empty and full BESS voltages, respectively. By using the voltage and current measurements shown in Figure 2.10, the DC network voltage control, the BESS current control, and the rectifier current control are enabled. These three control modes allow a comprehensive use of the BESS. Because the BESS is directly connected to the DC network, the power flow is controlled by varying the DC voltage of the rectifier. The reference variable in the rectifier can be current or voltage, but in this setup, the commercial rectifier accepts only a DC voltage reference as the control input, with a resolution of 1 V. Therefore, an external digital signal processor (DSP) based control and measurement card is used for the power flow control (Nuutinen et al., 2015). The card measures the required currents and voltages and uses them in the control input signals. The control output signal is the DC voltage.

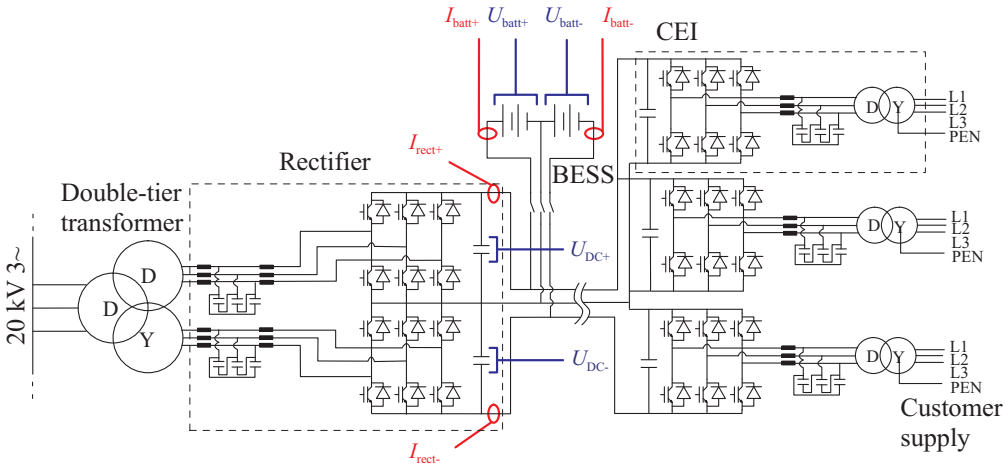

Figure 2.10: Current and voltage measurement points required for the BESS and the DC network power flow control.

DC network voltage control When the BESS is reconnected to the DC network, the voltage control has to be used to match the DC network voltage with the BESS voltage before the interconnection. The prime use of the voltage control is the constant voltage charging stage of the BESS. When the BESS is charged with a constant current and the voltage reaches a preset value, the voltage is kept constant. The signals for this control are $U_{\mathrm{batt}-}$ and $U_{\mathrm{DC}-}$, and $U_{\mathrm{batt}+}$ and $U_{\mathrm{DC}+}$ for the minus- and plus-pole-connected halves of the storage, respectively. In Figure 2.11a and b, the voltage control is presented. The BESS current control mode is changed over to the DC voltage control mode at 2 s and the voltage reference U_{ref} = 788 V is given. It can be seen that the actual battery voltage U_{batt} follows the reference. Still, the control resolution of 1 V is noticeable because there is an error between the actual and reference voltages.

BESS current control In this mode, the current of the BESS is kept constant and $I_{\mathrm{batt}-}$ and $I_{\mathrm{batt}+}$ are the control signals. The BESS current control is mainly for the charging current control of the BESS, but the discharge current of the BESS can be controlled, and therefore, the power taken from the BESS can also be controlled. If required for single BESS battery cell protection, the battery management system (BMS) can override the current reference or even disconnect the BESS from the network. This, however, is enabled in every operating mode. In Figure 2.11c and d, a current reference step I_{ref} is made from -15 A (discharge) to +15 A (charge). It can be seen that the step response of the actual current I_{batt} is quite slow. Faster response times are possible, but the implemented control is fast enough for this purpose, and it is assumed that stability is reached in every situation. The 1 V rectifier reference voltage resolution is evident also in this mode.

Rectifier current control This control mode is similar to the BESS current control mode, but the input signals are minus and plus pole rectifier currents $I_{\mathrm{DC}-}$ and $I_{\mathrm{DC}+}$,

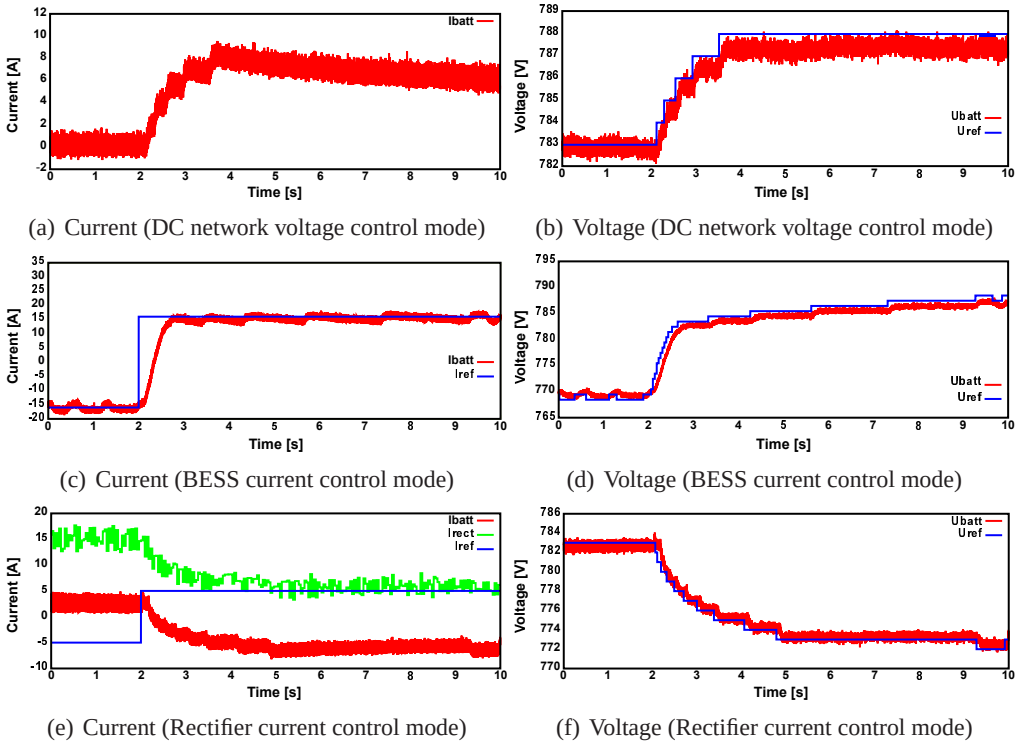

(a) Current (DC network voltage control mode)
(b) Voltage (DC network voltage control mode)
(c) Current (BESS current control mode)
(d) Voltage (BESS current control mode)
(e) Current (Rectifier current control mode)
(f) Voltage (Rectifier current control mode)

Figure 2.11: BESS control modes (Nuutinen et al., 2015).

respectively. Hence, the power taken from the MV grid and the power supplied back to the grid can be controlled. Therefore, it is also possible to limit the grid power to a certain level and take the remaining power from the BESS. When the DC network power decreases below the grid power limit, the excess power is used for the charging of the BESS. In Figure 2.11e and f, the 783 V DC network voltage reference is changed to a 5 A rectifier current reference I_{ref}. Because of the manner of illustration, U_{ref} is not shown in Figure 2.11e, and -5 A is an old value of I_{ref}, which is not in use. It can be seen that before the change in the control, the actual current of the rectifier I_{rect} is 15 A, and the BESS is charged with a 2 A current (I_{batt}), which results in a 13 A DC network current. After the change in the control mode, $|I_{\mathrm{batt}}|$ = 8 A and I_{rect} = 5 A, to which it is controlled. Again, the DC network current is 13 A.

Although the voltage reference resolution is 1 V, the accuracy in the control is adequate for this purpose. The poor resolution is, however, only a feature of the commercial converter, and it can be enhanced. The results show that the power flow of the BESS and the DC network can be controlled only by controlling the rectifier voltage. This is an advantage in the LVDC network and reduces the number of converters required for the system.

2.4 Other topologies

The previous three topologies are the most commonly used topologies in commercial rectifiers. There are also other topologies available; three topologies that could also be applicable in certain situations are introduced in brief below.

2.4.1 VIENNA rectifier

The VIENNA rectifier, presented in Figure 2.12, is a combination of a three-phase diode bridge and a DC/DC boost converter. It enables a sinusoidal mains current, controlled output voltage, and a low blocking voltage stress on the power transistors (Kolar and Zach, 1997). Compared with the diode and thyristor bridge rectifiers, the losses of the VIENNA rectifier are notably higher, resulting from the losses of the controlled switches and the LCL filter (Rekola et al., 2012). However, when compared with the controlled topologies (two-level and three-level grid-tie rectifying converters), the VIENNA rectifier is found between them, having lower losses than the two-level topology and higher ones than the three-level one (Rekola et al., 2012). In (Viitanen and Tuusa, 2002), a loss comparison between a 50 kW VIENNA and a two-level grid-tie rectifier is made with similar results; a higher efficiency and smaller filter components are achieved with this topology.

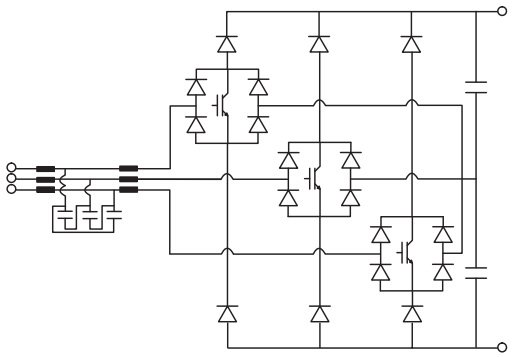

Figure 2.12: VIENNA rectifier.

If the start-up of the DC network is considered, the VIENNA rectifier has similar challenges to the diode bridge rectifier and the two- and three-level grid-tie rectifiers; the charging current of the network capacitances cannot be controlled without an external device. The major drawback of this topology is the unipolar power flow, which also disables the reactive power control. Consequently, the unipolar power flow limits the use of this topology with the DC networks having local generation and energy storages. Without a bidirectional power flow, the controllability of the DC voltage is not a beneficial feature in this application, because the CEIs can operate with a wide input voltage range, and the DC voltage regulation brings no significant advantages to the system. Therefore, the only benefit of the VIENNA rectifier is the sinusoidal grid current and the lower total harmonic distortion (THD) compared with the diode and thyristor bridge rectifiers.

Therefore, the key issues guiding the rectifier selection have to be studied in every case individually. It was discussed above that the nonsinusoidal current of the diode and thyristor bridge rectifiers increases the losses in the supplying transformer and has an influence on the medium-voltage network voltage quality. These can be avoided with the VIENNA rectifier, but at the cost of higher losses and investment costs. However, with novel low-switching-loss components becoming soon commercially available, the feasibility of the VIENNA rectifier may be different.

2.4.2 Three-level grid-tie rectifying converter

The grid-tie rectifying converter can be implemented as a three-level topology, shown in Figure 2.13. The three-level structure enables the use of switches with a lower voltage rating, which usually results in lower switching losses. For instance in (Rekola et al., 2012), the three-level full-bridge converter has lower power electronics losses than the two-level full-bridge converter because of the lower switching losses. Secondly, the three-level converter has higher conduction losses. Therefore, the situation may be different with modern switch components. The three-level structure also requires lower inductance on the converter side of the LCL filter (Rekola et al., 2012), which results in lower losses. Again, with other inductor core materials than laminated iron, the difference between the losses may decrease.

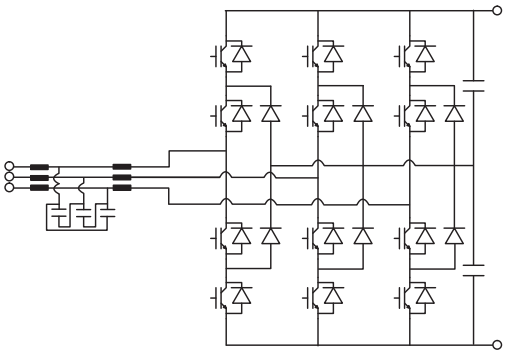

Figure 2.13: Three-level PWM grid-tie rectifying converter.

2.4.3 Multilevel grid-tie rectifying converter

It is possible to use multilevel converters with a high-frequency isolation transformer to construct a rectifier without a 50 Hz isolation transformer. For instance in (Islam et al., 2014), an analysis is made for a high-frequency link multilevel cascaded medium-voltage converter having 11 kV grid-side voltage (Figure 2.14), and in (Rashed et al., 2010), a 650 V DC bus is interfaced to a 11 kV MV grid with a multilevel converter. However, the multilevel converter faces challenges: it has a complicated converter structure, and it requires a fast processing speed and a high number of PWM control channels. Circulating current mitigation has also been addressed in (Chen et al., 2015) and (He et al., 2015). The MV

voltage being 20 kV, a 50 kV withstand voltage between the primary and the secondary is required according to the insulation coordination standard IEC 60071-1 (IEC, 2006), which could result in long creepage distances, high costs, and a large physical size. However, high-voltage and low-loss switch components will enhance the applicability of this topology, and fewer levels are required in the converter. In Figure 2.15, the projected cost trend of 10 kV SiC MOSFETs are depicted. It can be seen that the components are becoming commercially available and the cost trend is downward. Hence, the applicability of the multilevel converter should be studied in the future.

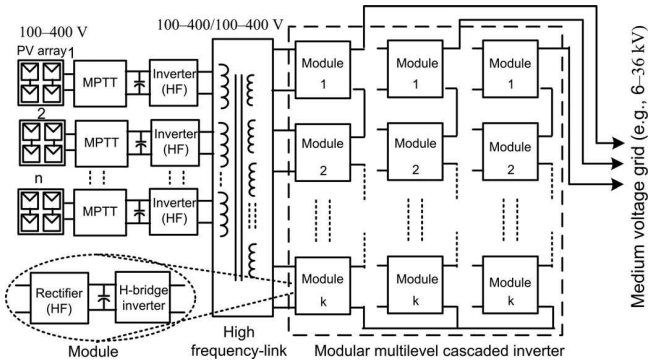

Figure 2.14: Multilevel converter system with high-frequency-link galvanic isolation for direct MV grid interconnection (Islam et al., 2014).

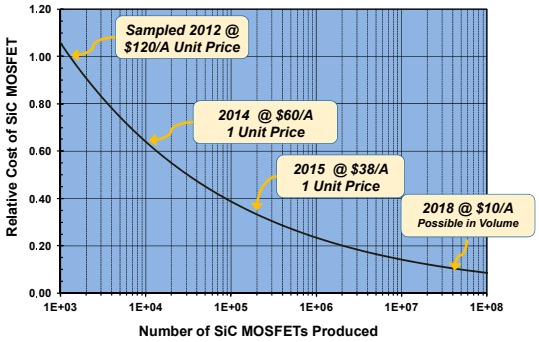

Figure 2.15: Projected cost trend of 10 kV SiC MOSFETs (Cree Inc., 2014).

2.5 Conclusions

The requirements for the rectifier and applicable rectifier topologies were addressed. The half-controlled thyristor bridge rectifier is, from the perspective of its properties, suitable for an LVDC distribution network where unidirectional power flow is adequate. Typically,

no control over DC voltage is required in this kind of a network structure. However, grid current harmonics might require additional filtering in some cases. The grid-tie rectifying converter should be selected when bidirectional power flow and DC voltage control are required. Energy storages and/or DG in the DC network are situations where a more advanced control is justified. With the grid-tie rectifying converter, implementing a BESS with a direct connection to the DC network is possible, as it was demonstrated. Other topologies were also introduced, but an in-depth analysis is out of the scope of this work. Nevertheless, they should be kept in mind for future purposes.

3 Customer-end inverter

In this chapter, solutions for the CEI are considered. In Publication V, both single-phase and three-phase topologies are introduced, and the losses are analyzed for the most applicable topologies. In this doctoral dissertation, two-level (2L) topologies are studied, but three-level (3L) converters are excluded from the study. 3L converters for this application are, however, discussed for instance in (Rekola and Tuusa, 2011) and (Rekola et al., 2012). It was mentioned above that the feasibility of the LVDC distribution, especially in rural areas, involves the use of the 1500 V DC voltage level. With the two-level CEI topologies, the bipolar $\pm$750 V structure is the only choice, because with the 1500 V unipolar network, 3.3 kV switch components have to be used, and their price/amps value (Figure 2.1b) is typically higher than that of 1200 V rated components (Figure 2.1a). Therefore, the CEI is connected either to the plus or minus pole of the bipolar network.

3.1 CEI requirements

The CEI is solely responsible for the customer-end power supply. Therefore, it has to meet the voltage quality and electrical safety requirements. Similar requirements are also found in uninterruptible power supplies (UPS) used to provide reliable electricity supply for sensitive loads. At least the following technical requirements are set for the CEI:

- High energy efficiency
- Low EMI
- Measurements applicable for customer billing
- Short-circuit current supply
- Bidirectional power flow (for local generation)
- Remote control and monitoring
- Complies with voltage quality standards
- Complies with electrical safety and EMI standards

Similarly to the rectifier, not all of the requirements have to be met in every LVDC application. However, some features such as electrical safety, high energy efficiency, and voltage quality are mandatory. The voltage quality requirements set by the standard EN 50610 (EN 50160, 1994) are introduced in Table 3.1. Because the CEI can constantly maintain good-quality supply, tighter requirements for the voltage quality are introduced and they are also shown in Table 3.1. These are the values that are used as the technical design criteria for the research site.

From the electrical safety point of view, the CEI and the other LVDC system installations have to meet the requirements set by the national low-voltage standard series SFS 6000 (SFS 6000, 2012), based on HD 60364, IEC 60364, and IEC60664, where applicable. The electrical safety and the protection are considered in Publication IV and (Nuutinen et al., 2012), and the short-circuit operation of the CEI in Chapter 4. In addition to the voltage quality requirements, there are also other standards that include specifications for the CEI such as the IEC 61000 series (relevant equipment standards) and IEC 60664-1

(insulation coordination for equipment within low-voltage systems), but these are not discussed further in this dissertation. The application of power electronics to the electricity distribution enables numerous new functionalities that can be used for protection, control, and measurement purposes. For example, a customer-end energy measurement is already embedded in the CEI because it uses the voltage and current measurements required for the CEI control. Still, the measurement accuracy have to meet the requirements set for billing, which have to be ensured in the design process. Similarly, the fast processing speed allows various protection functions. Finally, the communication network enables remote control and monitoring of the entire LVDC system, which can be used for smart grid functionalities, including power flow control, optimized control of active resources, and demand response. Although these are not requirements for the CEI, many of these functionalities use the CEI, and therefore, the control system has to be able to provide them or adapt itself to the new functionalities to be introduced.

Table 3.1: Voltage quality requirements.

Property	Standard/recommended value	Target value
Nominal voltage	230/400 V_{rms}	230/400 V_{rms}
Frequency	50 Hz $\pm$1% (99.5%[1]) 50 Hz +4%, -6% (100%[2])	50 Hz $\pm$0.1% (100%[1])
Variation	$\pm$10% (95%[3]) -15%, +10% (100%[4])	$\pm$1% (100%[3])
Distortion (THD)	$<$8%	$<$5%

1) Of 10 s mean values of a year

2) Of 10 s mean values of a year

3) Of 10 min mean RMS values during each one-week period

4) Of 10 min mean RMS values of supply voltage

3.1.1 Galvanic isolation

Studies have shown that implementing the DC network as a TN system results in dangerous contact voltages especially when the resistance of the earth is high, for instance, in Finland. Thus, the DC network should be constructed as a terrain-isolated functionally unearthed (IT) system to meet the electrical safety requirements (Karppanen et al., 2015), (Salonen et al., 2008). Customer-end networks in Finland are typically built as functionally earthed (TN), and therefore, a galvanic isolation is required between the unearthed DC and the earthed customer-end networks, if no modifications are made on the customer premises. Consequently, if the customer-end inverter is implemented without a galvanic isolation, also the customer-end network needs to be an IT system. However, setting up the customer-end network as unearthed calls for the following actions:

1. Required modifications to the existing network, in the case of TN-C/TN-S systems.
2. Insulation/isolation monitoring device in the customer-end network.
3. Mitigation of common-mode (CM) disturbances originating from the CEI and other power electronic converters connected to the DC network.

In some cases, the first item requires entire customer-end network renovation, which is not feasible. The second one requires a commercial device or a monitoring functionality implemented in the CEI. A customer-end monitoring device is required if the signal of the DC network monitoring device is blocked by the CEI power stage, and therefore, the device is not able to detect an earth fault in the customer-end network. Further, when the system is operated with a DC network earth fault, which is allowed in some cases, the customer-end network earth fault has to result in an immediate CEI shutdown, because it could lead to a short-circuit and a risk of an electric shock. The item number three is challenging; the switching frequency of the CEI and its harmonics and other CM sources in the DC network have only a minor effect on the DC network, but cause troubles in the customer-end network. If there is an electromagnetic interference (EMI) filter in the equipment in the customer-end network, the high-frequency CM current can induce a filter failure, a risk of fire, or a risk of an electric shock. These issues are addressed in more detail in Chapter 5, where the CM and radio-frequency (RF) EMI in the LVDC research site are discussed.

If galvanic isolation is used between the DC network and the customer-end network, the challenges discussed above can be avoided. The galvanic isolation can be implemented either by using a 50 Hz transformer at the output of the CEI (1) or an isolating DC/DC converter at the input of the CEI (2). The first option is simple: a commercial transformer is installed after the output filter of the inverter (Figure A.2). With the three-phase CEI, the use of a delta-wye transformer constitutes a neutral point for the TN network. The drawbacks of the 50 Hz transformer are the price, the physical size, and the losses. For instance, the 16 kVA transformer of the CEI used on the LVDC research site weighs over 90 kg. The energy loss distribution of the CEI on the LVDC research site is presented in Figure 3.1a. It can be seen that the transformer losses are almost half of the overall losses of the CEI. This degrades the feasibility of the LVDC distribution. The second choice is to use an isolating DC/DC converter at the input of the CEI. This option has been covered in (Mattsson et al., 2014a) and (Mattsson et al., 2014b), and the isolating DC/DC converter for DC power supply in (Hayashi et al., 2014) and (Simanjorang et al., 2010). As a result, the input voltage of the CEI can be optimized so that the overall losses of the CEI and the DC/DC converter can be minimized without having an effect on the DC network voltage level. In Figure 3.1b, the measurement results are compared with the calculated results with the DC/DC converter. It can be seen that an efficiency of over 95% could be achieved with modern switching components. However, experimental results are required to verify the results.

3.2 Customer-end inverter topologies

The CEI can be implemented as a single-phase or three-phase one. The customer-end supply in Finland today is provided as three-phase, and hence, the CEI on the LVDC research site is also constructed as a three-phase one. The three-phase supply is mainly needed for electric motors, and there are numerous applications where a single-phase supply would be adequate. Therefore, also single-phase CEI structures are analyzed.

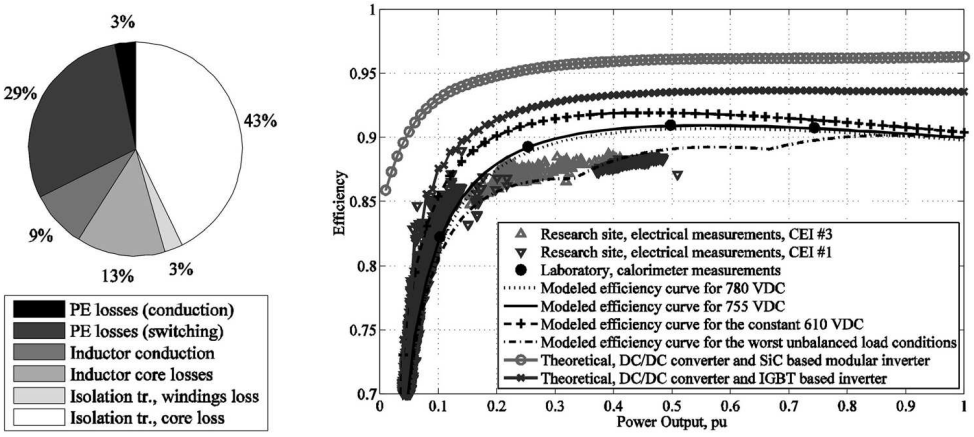

(a) (b)

Figure 3.1: Energy loss distribution on the LVDC research site during a four-week period (a), and loss comparison of measurement data and proposed new technology (b) (Lana et al., 2014b).

3.2.1 Single-phase half-bridge

The simplest single-phase topology is the half-bridge (1PHB) one, which consists of one switching leg and two series-connected capacitors. The load is connected between the capacitors, and the energy to the load is taken from the capacitors, as can be seen in Figure 3.2a.

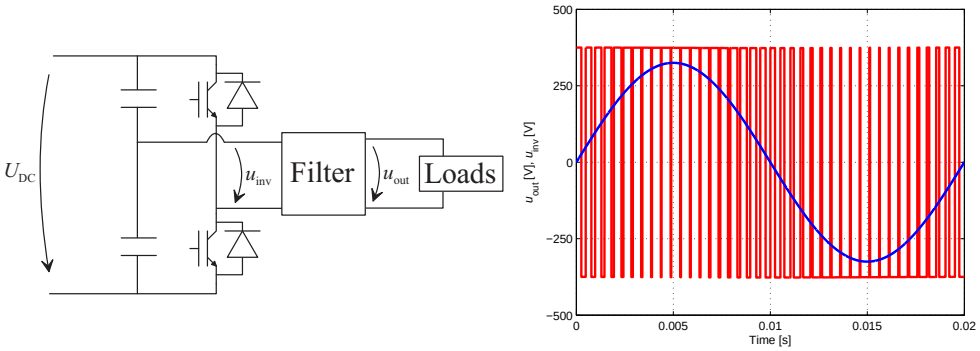

(a) (b)

Figure 3.2: Half-bridge inverter topology (a) and the output voltage waveform (b).

The maximum output voltage $\hat{u}_{\mathrm{out}}$ of the 1PHB topology, produced from the DC voltage U_{DC}, is

$$\hat{u}_{\mathrm{out}} = \frac{U_{\mathrm{DC}}}{2}. \tag{3.1}$$

Therefore, if U_{DC}=750 V, the maximum output voltage peak value of the CEI is 375 V (Figure 3.2b), which corresponds to 265 $\mathrm{U_{rms}}$. With 230 $\mathrm{V_{rms}}$, the minimum required output voltage is 325 V, and thus, DC voltage levels lower than 650 V cannot be used. However, the voltage level being 750 V in the bipolar network, this is not a limitation in normal operation. The sizes of the capacitors depend on the output power P_{out}. Because a single capacitor supplies the load during one half-cycle, the line frequency f_{out} defines the required power supply time of the capacitor. With the 50 Hz line frequency, the duration of the half-cycle is 10 ms. To derive an equation for the capacitance, the capacitor energy E_{cap} has to be calculated as

$$E_{\mathrm{cap}} = \frac{1}{2}CU^2, \tag{3.2}$$

where C is the capacitance and U the capacitor voltage. Because the energy is taken from the capacitors, their voltage fluctuate, and therefore, the minimum and maximum voltages of the capacitors are used in the calculations as

$$E_{\mathrm{cap}} = \frac{1}{2}CU_{\mathrm{max}}^2 - \frac{1}{2}CU_{\mathrm{min}}^2, \tag{3.3}$$

where

$$U_{\mathrm{min}} = \frac{U_{\mathrm{DC}}}{2} - \frac{U_{\mathrm{ripple}}}{2}, \text{and} \tag{3.4}$$

$$U_{\mathrm{max}} = \frac{U_{\mathrm{DC}}}{2} + \frac{U_{\mathrm{ripple}}}{2}. \tag{3.5}$$

U_{ripple} is the desired capacitor ripple voltage. With a sinusoidal output voltage, we get

$$E_{\mathrm{cap}} = \hat{P_{\mathrm{out}}}\int_0^{0.01} \sin(\omega t), \tag{3.6}$$

where P_{out} is the output power of the CEI. Based on Equations (3.3)–(3.6), the capacitance as a function of P_{out} and U_{ripple} can be written as

$$C = \frac{4P_{\mathrm{out}}\int_0^{0.01}\sin(\omega t)}{(\frac{U_{\mathrm{DC}}}{2}+\frac{U_{\mathrm{ripple}}}{2})^2 - (\frac{U_{\mathrm{DC}}}{2}-\frac{U_{\mathrm{ripple}}}{2})^2}. \tag{3.7}$$

Equation 3.7 applies only when the modulation index m is 1. It can be derived from the CEI output voltage u_{out} and the DC voltage U_{DC} as

$$m = \frac{u_{\text{out}}}{U_{\text{DC}}/2}. \tag{3.8}$$

Because the modulation index affects the capacitor current and the capacitor voltage ripple, it has to be taken into account when calculating the capacitance value. Hence, the final equation for the capacitance is

$$C = \frac{4P_{\text{out}} \int_0^{0.01} \sin(\omega t)}{(\frac{U_{\text{DC}}}{2} + \frac{U_{\text{ripple}} m}{2})^2 - (\frac{U_{\text{DC}}}{2} - \frac{U_{\text{ripple}} m}{2})^2}. \tag{3.9}$$

When the nominal output power of the CEI equals 10 kW, the ripple voltage is selected to be 250 V, and the modulation index is 0.87, the capacitance value derived from 3.9 is 1561 µF. If the ripple voltage is decreased to 50 V, the capacitance becomes 7805 µF. The 1PHB topology was simulated with Matlab Simulink, by using both 250 V and 50 V ripple voltages (1561 µF and 7805 µF, respectively). The simulation model is shown in Figure 3.3, and the simulation parameters in Table 3.2. The output filter parameters are for a full-bridge topology with bipolar modulation (Peltoniemi et al., 2008).

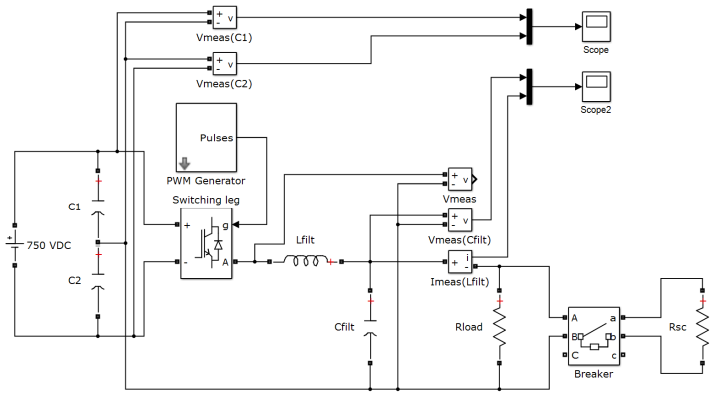

Figure 3.3: Simulation model of the half-bridge topology.

The results are shown in Figure 3.4. In the simulations, 10 kW resistive load is used. It can be seen from Figure 3.4a that the capacitor voltages (yellow and green) are very close to the output voltage (red) of the CEI. Therefore, if the capacitor voltage ripple is increased, that is, the capacitances are decreased, 230 V_{rms} cannot be produced. When the capacitance is increased (Figure 3.4b), the gap between the capacitor voltage and the output voltage gets wider. The sizes of the capacitors also affect the maximum output current of the CEI. In Figures 3.4c and d, a short-circuit, with a duration of 55 ms, is made using a breaker. It can be seen that the short-circuit current is higher with the

Table 3.2: Simulation parameters.

Parameter	Simulation 1	Simulation 2
U_{DC}	750 V	
u_{out}	230 V	
R_{load}	5.29 Ω	
R_{sc}	0.5 Ω	
U_{ripple}	250 V	50 V
C	1561 µF	7805 µF
m	0.87	
f_{sw}	10 kHz	
L_{filt}	535 μH	
C_{filt}	8 μF	

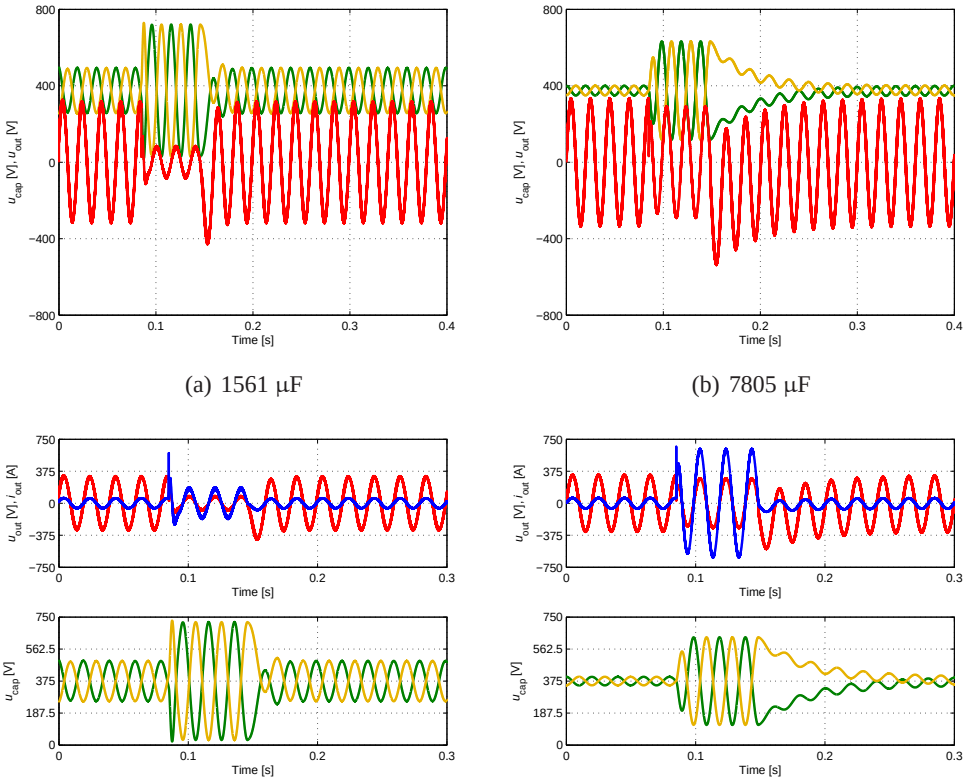

(a) 1561 µF

(b) 7805 µF

(c) 1561 µF

(d) 7805 µF

Figure 3.4: Simulated voltages and currents of the 1PHB.

larger capacitors because of the higher output voltage. Therefore, the output voltage may fluctuate during high-current load steps, if the capacitance is minimized. Finally, to achieve a capacitance of millifarads, electrolytic capacitors had to be used. Moreover, the physical size of the capacitors and the CEI become large because of the rather high voltage rating of the capacitors. Therefore, large and expensive capacitors with a limited service life prevent the use of this topology.

3.2.2 Single-phase full-bridge

In a single-phase full-bridge topology (1PFB), the large capacitors are replaced with a switching leg (Figure 3.5a). With the second leg, the voltage amplitude shown in Figure 3.5b is double the amplitude with the 1PHB topology (Figure 3.2b). The use of the 1PFB topology also enables the use of unipolar modulation, which results in three voltage levels (+DC, 0, -DC) at the output instead of two in the 1PHB (-DC/2 and DC/2). The unipolar modulation also effectively doubles the switching frequency (Mohan et al., 2003), and therefore, the switching frequency on the output is 2* f_{SW}. This reduces the size of the filter components, because the output voltage ripple is lower (Peltoniemi et al., 2008).

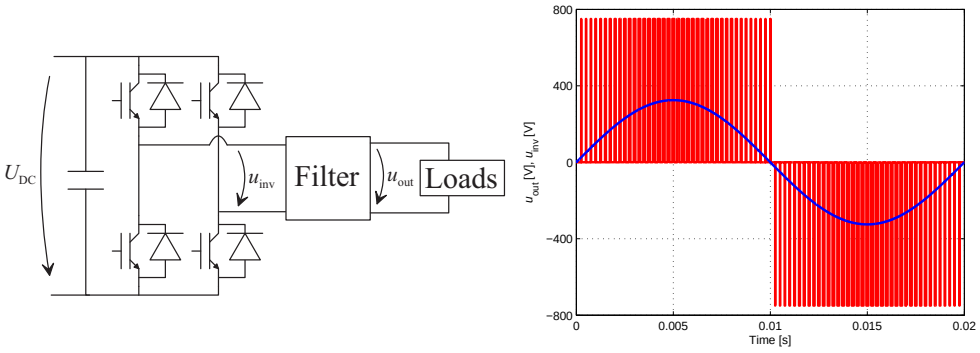

(a) (b)

Figure 3.5: Full-bridge inverter topology and the output voltage waveform.

However, it is discussed in (Kerekes, 2009) that high-frequency voltage components are present in the measurements between the -DC terminal and the ground connection, leading to a very high leakage ground current, which prevents the use of unipolar PWM in transformerless PV systems. Although this application has galvanic isolation, similar common-mode voltages are present, but the leakage current is reduced. According to Kerekes, this drawback can be avoided with bipolar modulation. Kerekes also introduces other single-phase topologies: a highly efficient and reliable inverter concept (HERIC) from Sunways, an H5 from SMA, and a single-phase topology with DC decoupling from Ingeteam, which are developed from the full-bridge topology. These are, however, not discussed in this doctoral dissertation. The drawbacks of the 1PHB are avoided with the 1PFB topology. However, the additional switches increase the switching losses, and the

topology may suffer from CM interference. Still, the 1PFB is the only feasible single-phase topology.

3.2.3 Three-phase half-bridge

The CEI on the LVDC distribution research site comprises a six-pack power stage and galvanic isolation based on a 50 Hz transformer at the output of the CEI, as shown in Figure 3.6a. Despite the aforementioned drawbacks, this structure was selected mainly because it provides simple implementation, and therefore, the research site could be completed at short notice. The output neutral (N) connection of the CEI was also achieved with the delta-wye transformer. If a galvanically isolating converter is used instead of the 50 Hz transformer, a similar six-pack topology cannot be used, because it does not provide neutral for the unbalanced loads. By adding a capacitor leg similarly to the 1PHB topology (Figure 3.2a, the neutral can be provided between the capacitors. The resulting three-phase half-bridge (3PHB) topology is shown in Figure 3.6b.

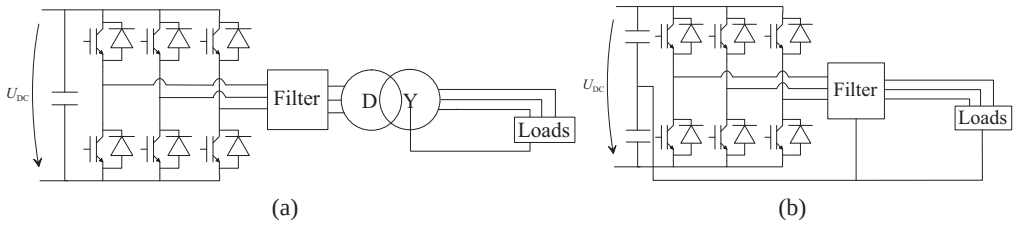

Figure 3.6: A) Three-phase topology and the 50 Hz isolation transformer with a Dyn vector group. B) Three-phase half-bridge topology.

This topology shares the same drawback as the single-phase one: large capacitors are required. If the output power of the three-phase CEI is selected to be 16 kVA, the nominal power of a single phase becomes 5.33 kVA. The worst-case situation is a pure single-phase load, and by using 3.9, the capacitance becomes 833 μF with U_{ripple}=250 V. The unbalance situation is simulated with a 5.33 kW load in phase 3, and phases 1 and 2 without load. It can be seen in Figure 3.7a that the capacitor voltage ripple distorts the voltage of the second phase (blue). Still, the calculated capacitance is adequate for the third phase (grey), and no distortion is evident. It can be seen that the nominal 230 V rms voltage cannot be achieved in every three phase. Because of the nature of the three-phase system, the situation becomes different when the 5.33 kW load is connected to phase 2, leaving only phase 1 without load. It is shown in Figure 3.7b that phase 3 is now distorted and its rms voltage is lower. It is obvious that the capacitance is not sufficient and the voltage ripple has to be decreased. By using U_{ripple}=50 V, the capacitance becomes 4163 μF. The results from similar load conditions to those in Figures 3.7a and b are shown in Figures 3.7c and d. It can be seen that all of the voltage waveforms are of good quality, and there are no differences in the rms values between the three phases. Thus, the half-bridge topology is not suitable for the three-phase supply either because of the large capacitors.

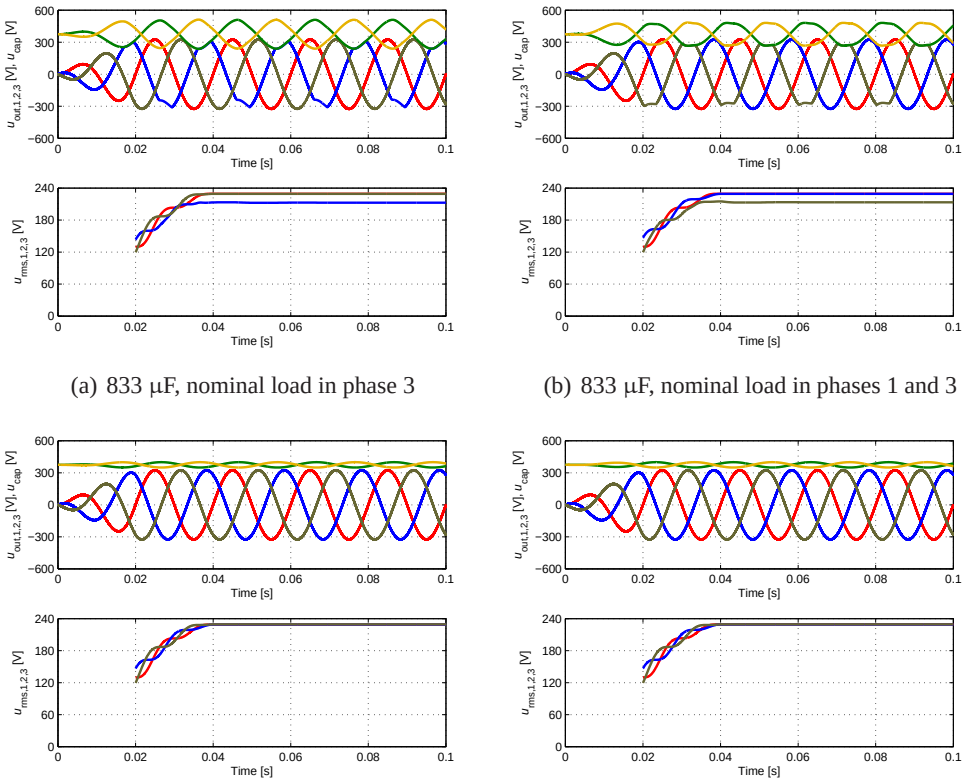

(a) 833 µF, nominal load in phase 3

(b) 833 µF, nominal load in phases 1 and 3

(c) 4163 µF, nominal load in phase 3

(d) 4163 µF, nominal load in phases 1 and 3

Figure 3.7: Simulated output voltage waveforms, capacitor voltage waveforms, and output voltage rms values.

3.2.4 Three-phase four-leg topology

In three-phase four-leg topology (3P4L), the capacitors are replaced by a fourth switch leg, as can be seen in Figure 3.8a. The voltage of the neutral point is controlled by modulating the fourth leg with PWM or space vector modulation. As a result, the large capacitances are avoided, but the switching losses are increased because of the additional two switches. In Zhang (1998), a comprehensive analysis of the four-leg topology and its control is made, and three-dimensional space vector modulation schemes for the four-legged power converters are proposed. In Figure 3.8b, Zhang's simulation results of a 150 kW four-leg inverter with the proposed modulation scheme and unbalanced loads of I_A=180 A, I_B=90 A, and I_C=90 A are presented. It can be seen that the output voltage is kept nominal despite the power unbalance. Thus, the three-phase four-leg topology could be used in the LVDC application.

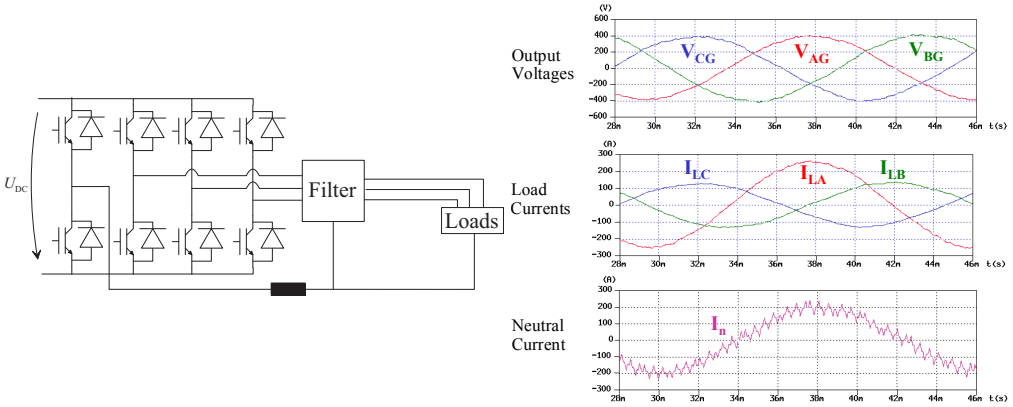

Figure 3.8: a) Three-phase four-leg topology. b) Simulation results from an unbalanced 150 kW three-phase four-leg inverter (Zhang, 1998).

3.2.5 Modular three-phase topology

In the modular three-phase topology (3PM) shown in Figure 3.9, the three-phase output is implemented by using 1PFB modules. The modules are supplied with three individual DC/DC converters, because a galvanic isolation is required between the module inputs. This topology enables accurate control over the phase voltages and also allows the use of parallel, low-power modules. In Figure 3.10, a modular CEI structure is presented (Mattsson et al., 2013). In the solution proposed by Mattsson et al., the inverter has separate single-phase modules, and multiple modules are also in parallel per phase. In this kind of a structure, a single module can be operated close to its peak efficiency, and parallel modules are switched on and off depending on the required CEI output power. Parallel modules also increase the redundancy of the power supply, because a failure in a single module results only in maximum power reduction, because the remaining modules continue the power supply. Therefore, this topology is also suitable for this application.

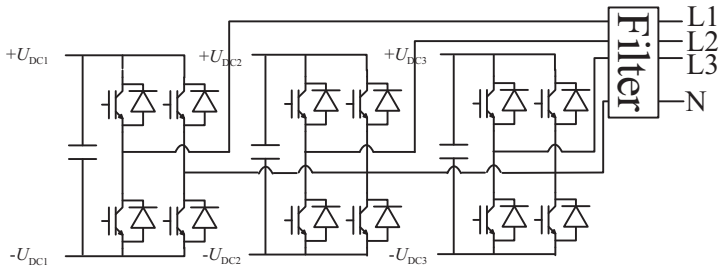

Figure 3.9: Modular three-phase topology (Publication V).

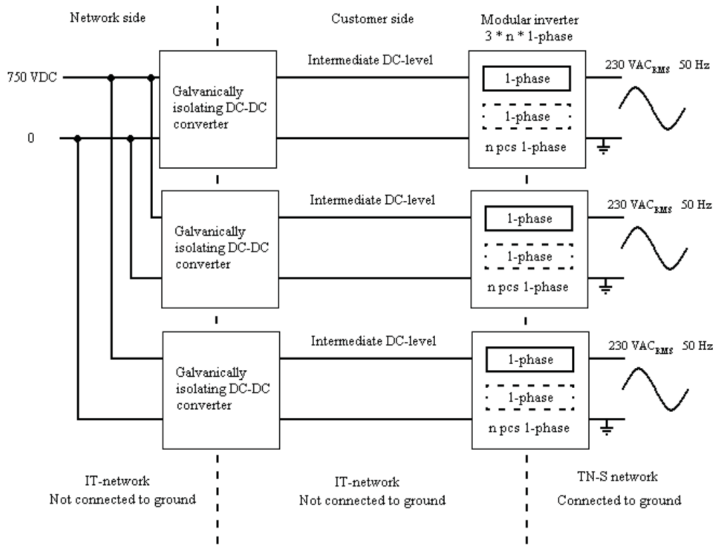

Figure 3.10: Block diagram of the modular inverter (Mattsson et al., 2013).

3.3 Losses

In Publication V, losses are calculated for three applicable topologies: 1PFB, 3P4L, and 3PM. The losses are calculated using nine different, commercially available power electronic switches; three of each type of IGBT, MOSFET, and SiC MOSFET. Their properties are presented in Table 3.3. 800/900 V rated MOSFETs are for lower-current applications and require considerable paralleling. Further, preliminary loss calculations of 1700 V IGBTs indicated essentially higher losses. Hence, they were left out of the comparison. The short-circuit current behavior, addressed in Chapter 4, was not taken into account either when selecting the components, because the purpose is to compare losses in the previous three topologies. Hence, the switches are not dimensioned for short-circuit current supply, and other protection methods will be used.

Table 3.3: Properties of the transistors under study (Publication V).

Switch	U_{nom} [V]	$I_{\mathrm{max}(25^\circ\mathrm{C})}$	V_{ce0} [V]	r_{CE} [mΩ]	$R_{\mathrm{ds(ON)}}$ [mΩ]
IGBT 1	600	100	1.1	15	
IGBT 2	1200	114	1.04	21	
IGBT 3	1200	85	2.2	20	
MOSFET 1	650	68			96
MOSFET 2	600	100			18
MOSFET 3	650	48			41
SiC MOSFET 1	1200	90			63
SiC MOSFET 2	650	29[1)]			156
SiC MOSFET 3	1200	40[2)]			125

1) Three switches in parallel.

2) Two switches in parallel.

The losses consist of conduction and switching losses of the transistor and the diode, $P_{\mathrm{cond,T}}$, $P_{\mathrm{cond,D}}$, $P_{\mathrm{sw,T}}$, and $P_{\mathrm{sw,T}}$, respectively. The total losses of the CEI P_{total}, with control and cooling losses P_{add}=20 W can be calculated for an n number of switches as

$$P_{\mathrm{total}} = (P_{\mathrm{cond,T}} + P_{\mathrm{cond,D}} + P_{\mathrm{sw,T}} + P_{\mathrm{sw,D}}) * n + P_{\mathrm{add}}. \tag{3.10}$$

The conduction losses of the IGBT $P_{\mathrm{cond,I}}$, the MOSFET $P_{\mathrm{cond,M}}$, and the diode $P_{\mathrm{cond,D}}$ can be calculated using Equations (3.11), (3.12), and (3.13), respectively. In all of the calculations, the power factor $cos(\varphi) = 0.9$. Temperature coefficients are not taken into account, but worst-case values are used. The switching losses of the IGBT $P_{\mathrm{sw,I}}$, the MOSFET $P_{\mathrm{sw,M}}$, and the diode $P_{\mathrm{sw,D}}$ can be calculated using (3.14), (3.15), (3.16), and (3.17), respectively. There are two equations for the switching losses of the diode, and they are used depending on the datasheet values available. Derivation of these equations is found in Publication V.

$$P_{\mathrm{cond,I}} = V_{\mathrm{ce0}}\hat{i}_{\mathrm{out}}\left(\frac{1}{2\pi} + \frac{M\cos(\varphi)}{8}\right) + r_{\mathrm{CE}}\hat{i}^2_{\mathrm{out}}\left(\frac{1}{8} + \frac{M\cos(\varphi)}{3\pi}\right) \tag{3.11}$$

$$P_{\mathrm{cond,M}} = R_{\mathrm{ds(ON)}}\hat{i}^2_{\mathrm{out}}\left(\frac{1}{8} + \frac{M\cos(\varphi)}{3\pi}\right) \tag{3.12}$$

$$P_{\mathrm{cond,D}} = V_{\mathrm{F}}\hat{i}_{\mathrm{out}}\left(\frac{1}{2\pi} - \frac{M\cos(\varphi)}{8}\right) + r_{\mathrm{F}}\hat{i}^2_{\mathrm{out}}\left(\frac{1}{8} - \frac{M\cos(\varphi)}{3\pi}\right) \tag{3.13}$$

$$P_{\mathrm{sw,I}} = \frac{1}{\pi} f_{\mathrm{sw}} E_{\mathrm{sw}} \left(\frac{\hat{i}_{\mathrm{out}}}{I_{\mathrm{rated}}}\right)^{K_{\mathrm{i}}} \left(\frac{V_{\mathrm{cc}}}{V_{\mathrm{rated}}}\right)^{K_{\mathrm{v}}} \tag{3.14}$$

$$P_{\mathrm{sw,M}} = \frac{1}{\pi} f_{\mathrm{sw}} (E_{\mathrm{on,M}} + E_{\mathrm{off,M}}) \tag{3.15}$$

$$P_{\mathrm{sw,D}} = \frac{1}{\pi} f_{\mathrm{sw}} E_{\mathrm{rr}} \left(\frac{\hat{i}_{\mathrm{out}}}{I_{\mathrm{rated}}}\right)^{K_{\mathrm{i}}} \left(\frac{V_{\mathrm{cc}}}{V_{\mathrm{rated}}}\right)^{K_{\mathrm{v}}} \tag{3.16}$$

$$P_{\mathrm{sw,D}} = \frac{1}{\pi} f_{\mathrm{sw}} E_{\mathrm{on,D}} \tag{3.17}$$

The losses are calculated using different output powers and input voltages for each com-

ponent and topology, and the parameters are shown in Table 3.4. The minimum input voltage level of the 1PFB and the 3PM is 326 V, which results from the 230 $\mathrm{U_{rms}}$ output voltage. In the 3P4L topology, at least 566 V is required for the 400 $\mathrm{U_{rms}}$ three-phase output voltage, and hence, only 1200 V switches can be used. 15 V higher voltages (340 V and 580 V) are used in the calculations, and the maximum DC voltages are 400 V and 800 V for 600/650 V and 1200 V rated switches, respectively. Note that only power electronic losses are calculated, and for example, filter losses are neglected. It is also stated in Publication V that the input voltage of the CEI, that is, the output voltage of the isolating DC/DC converter, also affects the losses of the DC/DC converter, and the results of the DC/DC converter and the CEI losses have to be combined to achieve the optimal overall result. This is left for future studies.

Table 3.4: Loss calculation parameters.

Topology	output power range [kVA]	DC voltage range [V]	f_{sw} [kHz]
Single-phase full-bridge	1–10	340–800[1)]	10
Three-phase four-leg[2)]	1–16	580–800	10
Three-phase modular	1–16	340–800[1)]	10

1) 340–400 V and 340–800 V for 600/650 V and 1200 V components, respectively.

2) Only 1200 V components.

3.3.1 Analysis

The results of the loss calculations can be found in Publication V together with the analysis of the loss charts. Therefore, they are not reproduced here, but the conclusions of the results are considered.

Because the power is supplied only to a single phase in the 1PFB topology, the output current is higher than in the other two topologies. Hence, transistors with low conduction losses are required to achieve a high efficiency, especially at high power levels. However, it is discussed in (Mattsson et al., 2014c) that the annual average power consumption of the customer is less than 3 kVA. Therefore, higher losses at higher power levels might be be acceptable. It is also obvious that the lowest number of switches (1PFB) also results in the best efficiency when the CEI is run at low power levels. The 1PFB topology also enables the use of IGBTs with the 600 V rating. As a result, a similar or higher efficiency can be achieved with the 600 V IGBT if compared with the 600/650 V MOSFETs. This arises from the lower conduction losses of the IGBT, which is beneficial at higher power levels. The 600 V IGBT is even better than the SiC MOSFETs at higher power levels, and the SiCs have a better efficiency only at very low powers.

With the IGBTs, the 3P4L has a better efficiency than the 1PFB at low powers, even though the number of the switching components is higher. Because the current per transistor is lower, the losses of the SiCs are lower, and the efficiency becomes almost 99 % at the nominal power. The efficiency of the 3P4L with the SiC MOSFETs is almost constant between 3 kW and 16 kW. The 3P4L topology is calculated with symmetrical

loads, because the analysis of the results becomes complicated if also the loads are varied between the phases. During the unbalanced supply, the losses are higher in the fourth leg, but they are also lower in the phase legs. The losses also depend on the selected switching strategy as presented in Demirkutlu and Hava (2009) and Kim et al. (2004). Hence, the loss calculations for the 3P4L topology may be somewhat optimistic, and a more in-depth analysis requires verification with experimental results.

The number of switches is highest in the 3PM topology, but the three-phase structure decreases the current of a single transistor. As a result, a better efficiency than with the 1PFB can be achieved, except at low power levels. It can be concluded that only the components with low switching losses are suitable for the 3PM because of the high number of switches. Further, the SiCs in the 3PM topology have a better efficiency above 2 kW power, but the losses are slightly higher at lower powers. This results from lower conduction losses, which compensate for the higher switching losses at power levels above 2 kW. A similar behavior with the MOSFETs is visible when the 3PM and 1PFB topologies are compared, but the difference in the low-power efficiencies is significant. With the 1200 V IGBTs, there are only slight differences between the 1PFB and 3PM topologies. If the 3P4L and the 3PM are compared, the 3P4L topology stands out with a higher efficiency with every switch. It can be concluded that the modular three-phase topology combines the benefits of the previous two topologies: the use of 600/650 V switches is possible, the efficiency is better at higher power levels (if compared with the 1PFB), especially with MOSFETs having a high $R_{\mathrm{ds(ON)}}$, and three-phase supply is enabled. Still, the 3PM with a high number of swiches requires low switching losses to be feasible.

With every topology, the effect of the DC input voltage is similar: the higher the voltage is, the higher the losses are. With the 600/650 V switches, the possible DC voltage levels are 340–400 V, and therefore, the effect is negligible. With the 1200 V components, the effect is visible; more with IGBTs than SiC MOSFETs. Hence, if only the losses of the CEI are taken into account, the use of higher DC voltages is not profitable. As it was discussed above, the results of the loss calculations of the isolating DC/DC converter and the CEI have to be combined before selecting the output voltage level of the DC/DC converter.

3.4 Conclusions

The requirements of the customer-end inverter, galvanic isolation, topologies, and losses were addressed. Five topologies were introduced, and the single-phase full-bridge (1PFB), the three-phase four-leg (3P4L), and the modular three-phase (3PM) were found to be applicable. Other two topologies, the single-phase and the three-phase half-bridge (1PHB and 3PHB) were rejected because of the requirement for huge capacitances. The losses were calculated for the selected CEI topologies using nine commercially available IGBT, MOSFET, and SiC MOSFET switches. According to the results, the variation in the CEI efficiency is very high between the transistors and also between the CEI topologies. Thus, the 1PFB topology should be used with the single-phase CEI. With the three-phase sup-

ply, both 3P4L and 3PM are applicable, and the fourth leg in the 3P4L topology enables nominal output voltages also with unbalanced loads. However, other issues such as the manufacturing costs, size, filtering losses, and the losses of the DC/DC converter have also to be taken into account before decisions on the optimal CEI structure can be made.

4 Customer-end short-circuit protection

Short-circuit protection in AC distribution networks is implemented by using fuses and circuit breakers. These well-standardized protection devices provide adequate protection for both the network components and the customer-end equipment. Although these devices require a high short-circuit current to operate, the current required for the protection devices is available in most of the AC networks. The short-circuit current level available in the customer-end network is defined by the distribution transformer and the 400 V low-voltage network between the transformer and the customer. Reaching the required protection level seldom poses any problems, and the required protection device trip times can be easily achieved. However, in weak grids, the short-circuit current level at the customer decreases, which may require additional measures in the customer-end network such as installation cables with a larger cross-section and protection devices with a lower current rating or a different trip characteristic curve. Nevertheless, achieving satisfactory results is not challenging, because there are no such network components in the shorting circuit that are sensitive to current notably higher than the rated current of the components.

This chapter elaborates on the short-circuit protection of the customer-end network when the customer is supplied with a power electronic converter. The focus of this chapter is to consider the challenges that the CEI-based supply poses and investigate solutions that do not compromise the electrical safety of the customer. In Publication I, short-circuit operation of a galvanically nonisolated single-phase CEI is studied, and in Publication II, a three-phase galvanically isolated CEI is covered. In both cases, the short-circuit operation of the CEI is simulated and verified by laboratory measurements. Finally, alternative methods to fault current injection are proposed and demonstrated by measurements.

4.1 Fault current injection

If the LVDC distribution system has to be compatible with existing customer-end installations, electrical safety can only be ensured by supplying short-circuit current. Because the CEI supplies an actual network, it has to meet the requirements set by the electrical safety standards. In the Finnish national standard SFS 6000 (SFS 6000, 2012), which is based on the European standards HD 60364, IEC 60364, and IEC60664, the recommendation for the minimum single-phase short-circuit current is 250 $\mathrm{A_{rms}}$. Further, the required protection trip time is less than 0.4 s in the protection of branch circuits in the customer-end networks. However, a 5 s trip time is accepted in the customer main feeder cable protection. The current recommendation aims at ensuring protection and voltage quality in AC installations, and therefore, the 250 $\mathrm{A_{rms}}$ current is not a strict limit that applies to every installation. Still, 0.4 s and 5 s trip times have to be reached in every situation.

Feeding current that meets the recommendations causes challenges especially in a CEI that has a low nominal current and a high short-circuit current. A short-circuit current to nominal current ratio ($i_{\mathrm{sc}}/i_{\mathrm{n}}$) can be used to illustrate the situation. A typical end-user in Finland has a three-phase AC supply with 3x25 A fuses or circuit breakers. Thus, if the

250 A_{rms} current supply capability of the CEI is required, the current ratio becomes 10. For instance, the maximum overcurrent capability of the IGBTs is usually 2–3 times the nominal collector current, and the maximum allowable duration of the overload is from tens of microseconds to milliseconds. Therefore, the short-circuit current has to be taken into account when selecting the switching components. The situation is different if the current ratio is lower. In (Niiranen et al., 2010), a point-to-point LVDC system with a high-power inverter is discussed. In this application, a single inverter is used to supply a group of customers. Hence, the nominal power of the inverter is high, and actually, the short-circuit current equals the nominal current (Figure 4.1). This facilitates the converter design, and overrating of the components is not required.

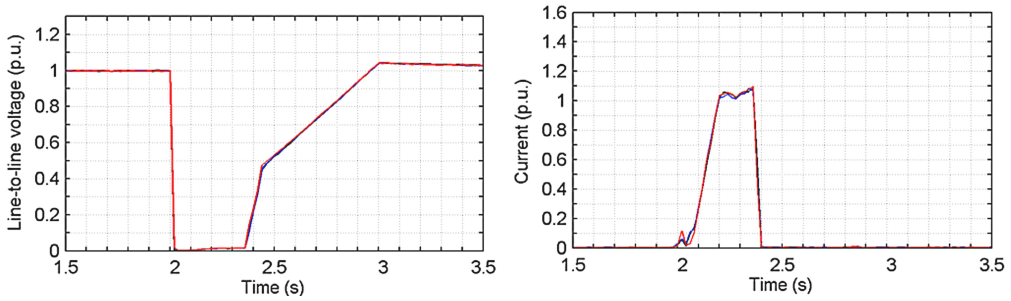

(a) (b)

Figure 4.1: Voltage (a) and current (b) during a three-phase fault situation; 32 A gG fuse (Niiranen et al., 2010).

4.1.1 Nonisolated single-phase CEI

In the course of the research, a single-phase CEI was implemented first to verify and demonstrate LVDC distribution in laboratory conditions (Nuutinen et al., 2011b). The CEI uses a nonisolated structure and a 1PFB topology, and therefore, the customer-end network in the laboratory is an unearthed (IT) network. The setup is illustrated in Figure A.1a. In Publication I, the short-circuit operation of this CEI has been studied. Although the nonisolated customer-end network is not practical, the short-circuit operation of the CEI corresponds to a structure where the galvanic isolation is provided by using an isolating DC/DC converter before the CEI, as was discussed in Chapter 3. In the laboratory setup, the CEI is supplied directly from the DC network, having 200 m of cable between the rectifier and the CEI. The DC network is able to feed short-circuit current, and the situation is similar if there is an isolating DC/DC converter capable of high-current supply. Direct connection to the DC can be considered the worst-case situation.

Because the CEI comprises IGBT modules with a nominal collector current of 80 A, the short-circuit current peak value is also limited to 80 A. The output current can be kept sinusoidal, which is addressed later in this chapter, or limitation can be very straightforward and the current is simply limited to the preset level. The latter solution results in

a square-wave current waveform, as can be seen in Figure 4.2. Still, the voltage during a short-circuit is very low, and the other devices supplied by the CEI see the situation almost as a blackout. Thus, the square-wave voltage waveform can be accepted.

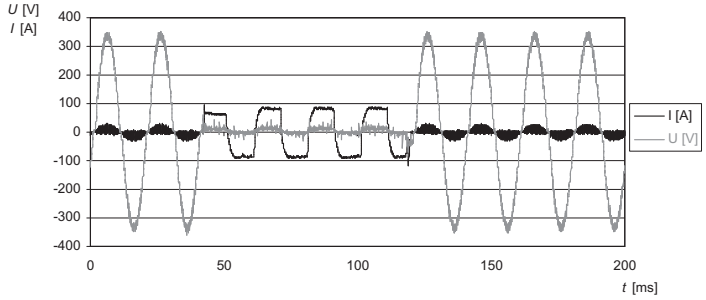

Figure 4.2: Measured capacitor voltage and choke current during a short-circuit. A 16 A B-type circuit breaker is used (Publication I).

The nonisolated system also poses challenges to the CEI short-circuit protection, because the CEI directly supplies the loads at the customer. Hence, the only inductance affecting the rate of current rise is the output filter choke, and if the nominal current of the CEI is close to the maximum current of the switches, their maximum current may be exceeded. When modern transistors enable high switching frequencies, the inductance of the filter choke decreases, and the rate of current current rise may increase such that the current control is unable to detect the fault in time. Therefore, the time step of the current control cannot be longer than the actual short-circuit current rise, which directly affects the computational burden of the system and requires very fast current measurement sensors.

4.1.2 Isolated three-phase CEI

The three-phase CEI, developed for the LVDC research site, uses a six-pack IGBT bridge together with a 50 Hz delta-wye isolation transformer at the output of the CEI. With the transformer, the galvanic isolation is enabled and the customer-end neutral connection is achieved. In the laboratory, the CEI is connected to the DC network similarly to the single-phase CEI. The structure of the CEI is shown in Figure A.1b and Figure A.2. The short-circuit operation of the three-phase CEI is analyzed in Publication II. The higher inductance caused by the transformer dramatically decreases the rate of current rise, which enables the current-control-based detection of the short-circuit in time without any additional actions. The short-circuit operation can be divided into three tasks: (1) short circuit recognition by applying the fault detection method presented in (Peltoniemi and Nuutinen, 2013), (2) switching from the voltage control to the current control for the current limitation, and (3) switching from the current control to the voltage control after the fault is recognized to be cleared. This sequence can be seen in Figure 4.3. Because the aforementioned 250 $\mathrm{A_{rms}}$ short-circuit current is a recommendation, lower current values can be used if the required 0.4 s trip time can be achieved. In load group protection, a type

C16 circuit breaker is considered to have the highest trip current. According to the standard IEC 60947-2 (IEC, 2013), electromagnetic release of the type C circuit breaker has trip times of $\geq$0.1 s and $<$0.1 s with rated currents (I_n) of 5 x I_n and 10 x I_n, respectively. Therefore, 160 $\mathrm{A_{rms}}$ is the current that guarantees the trip.

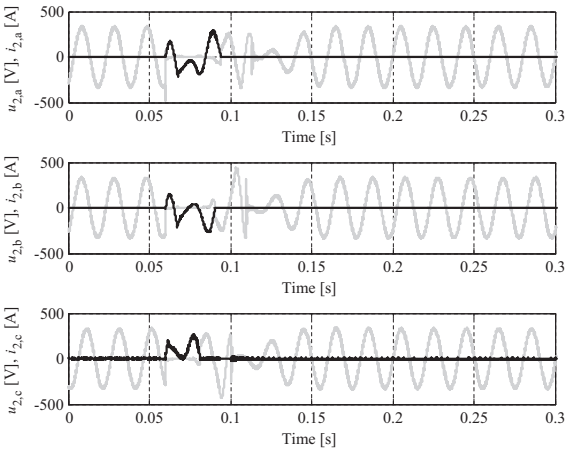

Figure 4.3: Voltages and currents of phases a–c, when a single-phase short-circuit is made at every phase at the CEI of the research site. The three results are from separate occasions. A type C20 circuit breaker is used (Publication IV).

Because the three-phase IGBT module has a rated current of 330 A, a 200 $\mathrm{A_{rms}}$ controlled short-circuit current was the target. A single-phase short circuit was made at the output of the isolation transformer, which is the supply point of the customer, and a gG25 fuse was used for short-circuit protection. 285 $\mathrm{A_{peak}}$ was set as a reference for the current controller. The situation is illustrated in Figure 4.4. The secondary current of the transformer (middle) is sinusoidal, and the reference value is reached. The trip time is also clearly shorter than the required 5 s, because the gG25 fuse is not used in the load group protection. It is obvious that the required trip times are easily achieved with the type C16 circuit breaker. However, the primary current of the transformer i_1 (top) and the current drawn from the DC network i_dc (bottom) are highly distorted. The current exceeds the allowed maximum current of the IGBT module, which is 600 A, permitted only for a duration of one millisecond. As a result, both the reliability of the CEI is degraded and the customer-end electrical safety are decreased. The distortion is caused by the saturation of the filter core, in which case the inductance of the choke collapses and the current at the switching frequency increases. Because the secondary fault current is almost purely sinusoidal, it indicates that the saturation of the transformer is not significant.

To avoid saturation, the components can be designed according to the short-circuit operation, or the short-circuit current has to be decreased until satisfactory performance is

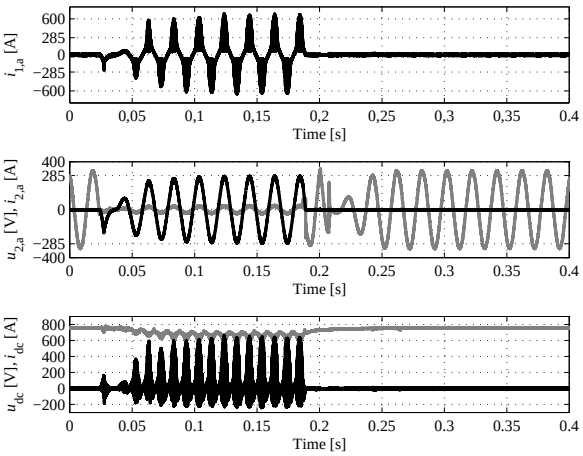

Figure 4.4: Measured short-circuit situation with a 285 $\mathrm{A_{peak}}$ reference. A gG25 fuse is used (Publication II).

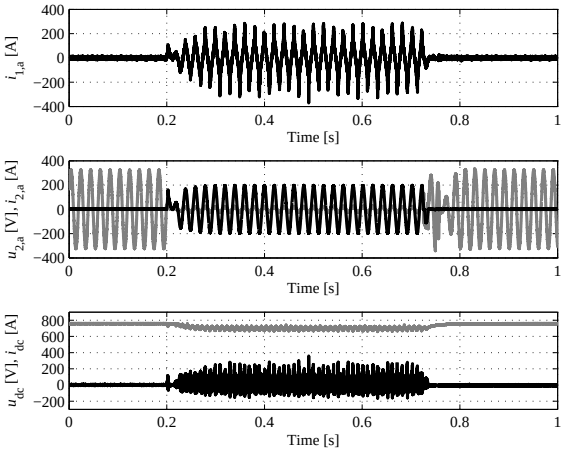

Figure 4.5: Measured short-circuit situation with a 200 $\mathrm{A_{peak}}$ reference. A gG25 fuse is used (Publication II).

achieved. Dimensioning the components for a short-circuit results in bulky and expensive inductive components, and therefore, lower current is a more feasible solution. In Figure 4.5, the results with 200 $\mathrm{A_{peak}}$ (141 $\mathrm{A_{rms}}$) are shown. It can be seen that only minor saturation occurs during the short-circuit, if compared with Figure 4.4. The duration of the short-circuit is over 0.5 s, which meets the 5 s requirement. Moreover, it is assumed that the type C16 circuit breaker trips in less than 0.4 s. This was also ensured before the commissioning of the LVDC research network, where actual customers are involved, by

testing the short-circuit operation with a type C20 circuit breaker. The results in Figure 4.3 indicate that the 0.4 s trip time is achieved with a clear margin.

4.2 Other protection methods

Today, only the use of standardized protection devices is allowed. However, smart grid research activities will result in the development of smarter and quicker protection devices such as solid state circuit breakers, which should be taken into account in the standardization work related to the LVDC. Present protection devices operate well with AC systems, because short-circuit current is easily available. To avoid overdimensioning of the CEI, alternative solutions for the short-circuit protection are studied and developed. The objective is to manage the short-circuit situation without using excessive current, but still maintain the required electical safety level. Still, overcurrent supply is also required for high short-term currents in normal operation. Customers may have equipment and electric motors that may cause high inrush currents, and therefore, the CEIs have to be capable of feeding current. In addition, false protection trips cannot be accepted. Consequently, the supply has to be rigid enough to prevent voltage fluctuation in these situations.

4.2.1 Overcurrent trip

When the customer-end supply is provided by power electronics, the control of the current can be carried out quickly and accurately. Typical converter protection relies on short-circuit detection and converter overcurrent shutdown, because it is the most feasible type of protection for instance in motor drives. In these applications, short-circuit current injection would further aggravate the fault situation. Figure 4.6a presents a single-phase customer-end network with several loads, supplied with a single CEI. In this structure, shutdown of the CEI is not an option as it results in customer-end blackout. The situation is different if every load group is supplied with an individual CEI, as depicted in Figure 4.6b. As was discussed above, the short-term overcurrent supply requirement poses challenges for the overcurrent-trip-based protection. If the trip is based on exceeding a certain strict current limit, it may cause false tripping. This can be avoided by setting the limit high enough, but it may be a challenge without the use of switches with a higher current rating. It is possible to use a high trip setting with low-current switches, if the fault detection time is short enough. But if the current in a normal overcurrent situation is close to the trip setting, protection is not tripped even though the current exceeds the safe current of the switches. Hence, the switches have to be overdimensioned to ensure proper operation. Moreover, current limitation can be used together with the overcurrent trip. In this case, the current is limited to a level that is acceptable in terms of power electronics, but it is sufficient to supply current in normal high-current situations. As a result, when a short-circuit occurs, the current is limited until the protection trips. In Figure 4.7, operation of a single-phase CEI with the current limitation and the overcurrent trip are demonstrated. The current is limited to 80 $\mathrm{A_{peak}}$, and after 8 ms, the inverter is turned off.

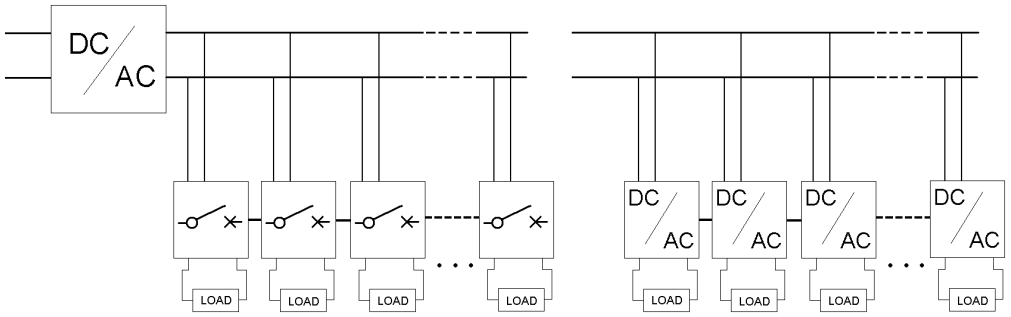

(a) (b)

Figure 4.6: Customer-end network supply using a) single CEI feeding load groups and b) individual CEIs for every load group.

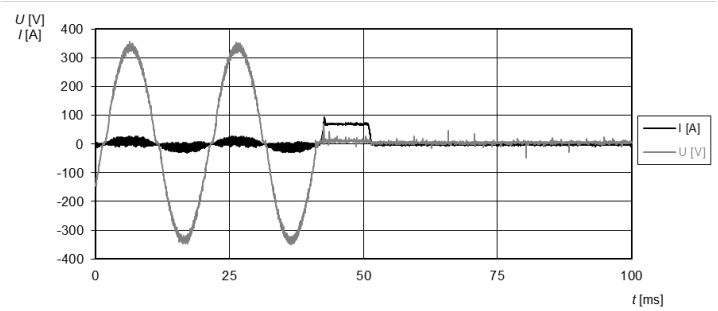

Figure 4.7: Measured capacitor voltage and choke current during a short-circuit. Overcurrent trip with current limitation is used (Publication I).

4.2.2 Controlled circuit breakers

If the short-circuit current is decreased, the trip times with conventional protection devices become unacceptable. However, if the circuit breaker could be externally tripped during the short-circuit, the time and the current amplitude needed for the operation of the protection device would decrease. In Publication I, controlled circuit breakers (CCB) are introduced and analyzed using the single-phase laboratory setup, and in Publication II, operation of the CCB is also verified with a three-phase setup. The CCB is a device that can be externally tripped, and therefore, short-circuit current injection is not required. The trip circuit detects overcurrent and controls the device. This protection method can be employed with a network structure using a single CEI, presented in Figure 4.6a.

With the CCB, the trip can similarly be based on (1) current trip or (2) current limitation. The first option is demonstrated in Figure 4.8 and the second in Figure 4.9. The trip limit is set to 70 $\mathrm{A_{peak}}$, which is the absolute value above which the CEI initiates shutdown and the CCB trips. The purpose of the shutdown is to extinguish the arc between the contact gap of the CCB immediately without waiting the 50 Hz sine wave to reach the

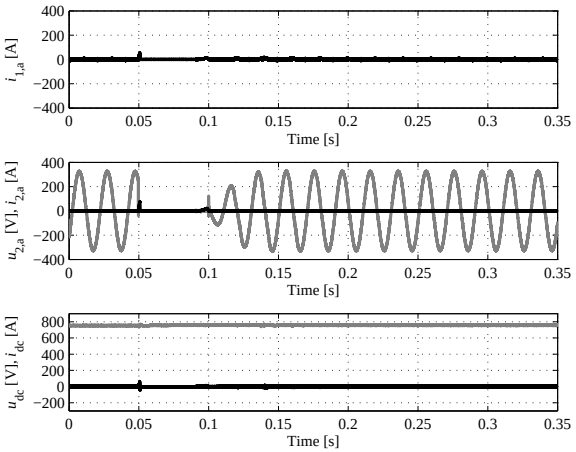

Figure 4.8: Measured short-circuit protection using the CCB with current trip (Publication II).

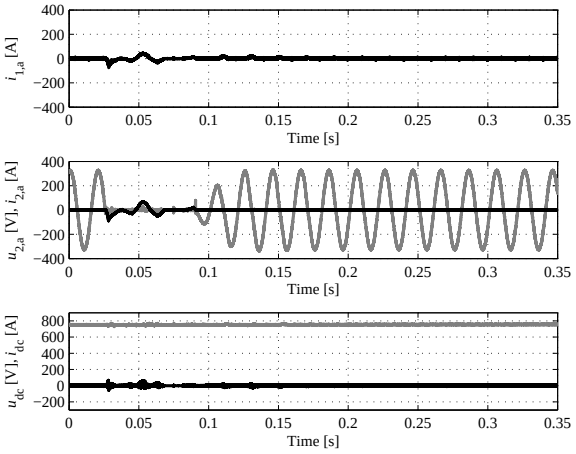

Figure 4.9: Measured short-circuit protection using the CCB with current limitation (Publication II).

zero crossing. The CEI then waits for 50 ms to ensure that the CCB is operated and then restarts. If compared with Figures 4.4 and 4.5, the trip time is notably shorter, and, most importantly, the current is very low and the aforementioned inductor saturation does not take place. It is also evident that although the trip limit is relatively low, i_2 does not exceed the trip value, which results from the higher inductance of the isolated system. If the CCB is based on a semiconductor switch, there is no need for the dead time, because the switch opens immediately. The short-circuit behavior of the CCB with current limitation is presented in Figure 4.9. The secondary current of the transformer is limited to 70 $\mathrm{A_{peak}}$

(middle), and no saturation is present in the transformer primary current i_1 (top) or the DC current i_{dc} (bottom). The CEI feeds the limited current for 40 ms after which it initiates shutdown and trips the CCB. The CEI is similarly restarted after a 50 ms dead time.

4.3 Conclusions

Three short-circuit control methods were introduced and demonstrated. All of them have their pros and cons, and none of them is a solution for every purpose. Even though the need for fault current injection makes the design of the CEI more challenging, it is still the only option for areas where the LVDC network is used to replace existing networks. Usually, changes cannot be made on the customer premises, and therefore, the new system has to be compatible with the protection devices already installed. The CCB could be a compatible solution, but the lack of commercially available products prevents its use. The control and trip circuits, discussed briefly in Publication I, also require standardization. The overcurrent trip method can be used in applications where the CEI supplies a single load group or a small number of load groups, such as in apartments. It provides low-current protection and requires no component overdimensioning; however, the current standardization does not allow only a semiconductor for protection. Therefore, it can be concluded that without changes in the standardization and before novel commercially available protection devices, the fault current injection is the only applicable protection method.

5 Electromagnetic interference

When a customer-end network is completely supplied with power electronics instead of a public low-voltage AC distribution network, the magnitudes of common-mode (CM) and radio frequency (RF) electromagnetic interferences (EMI) have to be studied. In Publication III, EMI issues of the LVDC research setup are analyzed. At the time of writing the publication, the rectifier was a thyristor bridge rectifier, depicted in Figure A.2a. When the rectifier was upgraded to a grid-tie rectifying converter shown in Figure A.2b, new measurements were conducted, and they will be analyzed in a future publication. However, some of the measurement results are introduced in this doctoral dissertation, and they are compared with the previous results.

5.1 Standardization

It was discussed in Publication III that the standardization is not satisfactory from the LVDC perspective, because in short, the standards mainly concern electricity consuming appliances. In particular, the problem lies in the most important frequency range from the 40th fundamental frequency harmonic (2 kHz) to 150 kHz. EN 50065-1 (EN 50 065-1, 1991), which is a standard for signaling at low-voltage electrical installations in the frequency range from 3 kHz to 148.5 kHz, concerns disturbances produced by the communication devices, not the allowed disturbances originating from the LV network itself. From the RF EMI point of view, CISPR 18-2 CISPR 18-2 (2010) does not provide limits for frequencies below 150 kHz, and no limits are defined for radiating disturbances for frequencies between 9 kHz and 30 MHz in EN 50065-1. The standard only covers conducted disturbances measured with an artificial network. According to (Dong et al., 2012), the AC-side measurements have been applied also to the DC side in different cases. In (Burkart and Kolar, 2012), the solution was to extrapolate German BDEW (Bundesverband der Energie- und Wasserwirtschaft) EMI limits between 2 and 9 kHz for the MV side to range it up to 150 kHz. It is clearly seen that there has been a need for standardization that would also cover disturbances below 150 kHz. Even the most present document, while writing this dissertation, *IEC TS 62578:2015-04: Power electronics systems and equipment - Operation conditions and characteristics of active infeed converter (AIC) applications including design recommendations for their emission values below 150 kHz* (IEC, 2015) states:

> In the frequency range from 2 to 150 kHz, up to now, no conducted emission limit has been defined in the CISPR 11 or in the IEC product standards dealing with power electronic systems and equipment. Manufacturers have no obligation to check them and these emissions are most of the time not known.

Therefore, the interference analysis is based on in situ measurements conducted on site. On-site measurements were the only way to gain knowledge about the CM and RF EMI in an LVDC distribution system in a public distribution network. Publication III addresses

three types of measured interferences: 1) CM currents in the customer-end networks, 2) CM current in the DC network, and 3) RF interferences close to the LVDC research site.

5.2 CM current in a DC network

It is shown in Figure 5.1a that the rectifier and the CEIs connected to the unearthed DC are the common-mode sources in the LVDC distribution. Of course, if there are other converters such as PV converters connected to the DC network, they also act as disturbance sources. In a DC network, there are no devices, except for the CEIs and other possible converters, that are directly connected to the DC network. Therefore, the CM current in the DC network has no effect on the electrical or equipment safety. However, the CM current in the DC network produces RF disturbances, discussed later in this chapter. Therefore, the converters have to be designed properly to keep especially radiating interferences as low as possible. Although the disturbances originating from a single LVDC distribution network can be at an acceptable level, several networks in a nearby area aggravate the situation.

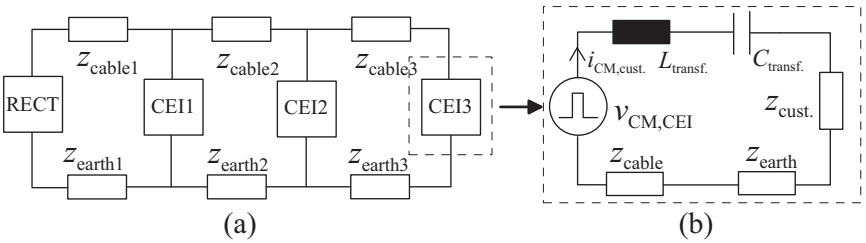

Figure 5.1: Equivalent circuits of the system (a) and a single CEI (b).

The CM current and impulsive noise generated by the power converters have also an impact on the feasibility of the power line communication (PLC) in the DC cable. Because the grid is branched, and comprises changing impedances and the ends of the DC grid are terminated to switched-mode power electronics, that is, the rectifier and the CEIs, the channel is very challenging for the high-frequency (HF) band PLC. For instance, it has been shown that HF band PLC is a feasible data transmission method, but because of the signal attenuation, the communication distances in the LVDC grid are limited (Pinomaa, 2013). In (Pinomaa et al., 2014), applicability of narrowband (NB) PLC in the LVDC research site is studied. As a conclusion, a reliable communication link without repeaters can be provided with the novel NB PLC technique, namely the G3-PLC, which operates in the 150–500 kHz frequency band. However, the data rates provided by the G3-PLC are insufficient for the current grid monitoring application implemented on the active power electronic devices used in the LVDC system (Lana, 2014), (Lana et al., 2015a).

In Publication III, the DC network CM current $i_{\text{CM,DC}}$ was measured at the rectifying substation, at the beginning of the DC cable with a current transducer. In Figure 5.2a, the structure of the system and the current measurement points are shown, and in Figure 5.2b, the measurement of the CM current in the DC cable is in progress. A Rohde & Schwarz

ESHS 30 EMI test receiver was applied in all measurements, together with a Rohde & Schwartz EZ-17 current transducer. Two frequency ranges of 10–150 kHz and 150 kHz – 1 MHz were used, and the settings of the test receiver for both ranges are shown in Table 5.1. The measurements were conducted using peak and quasi-peak detectors, and the quasi-peak values are indicated by 'x' in the figures.

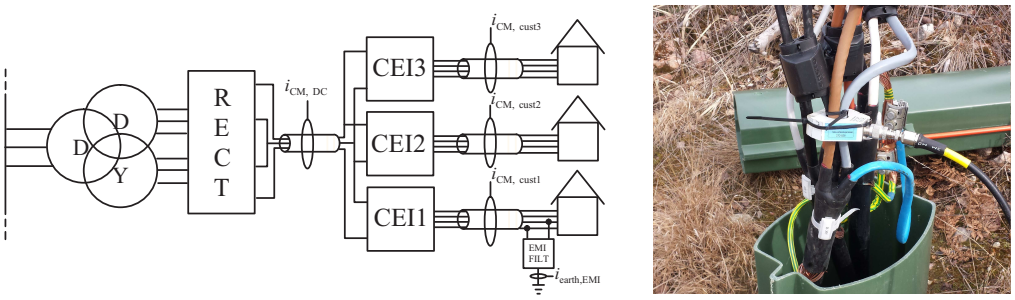

(a) (b)

Figure 5.2: Structure of the system and the CM current measurement points (a). CM current measurement using the current transducer (b).

Table 5.1: EMI test receiver settings (Publication III).

Value	Frequency range 1	Frequency range 2
Start frequency [Hz]	10k	150k
Stop frequency [Hz]	150k	1M
Frequency step [Hz]	100	5k
IF bandwidth [Hz]	200	10k
Meas. time (peak) [ms]	100	20
Meas. time (quasi-peak) [s]	1	1

The measurement results are shown in Figure 5.3. It was expected that with the thyristor bridge rectifier (Figure A.2a), the CM current is low, because in normal operation, the thyristor bridge rectifier corresponds with the diode bridge rectifier. The current is less than 70 dBµA (3.2 mA) throughout the frequency range, and only at 300 kHz, 80 dBµA (10 mA), the current peak value is higher. However, the quasi-peak value (x) is 20 dBµA lower. It can be seen that there is only a minor difference between the normal (red) and the rectifier-ON-CEIs-OFF (green) operation; only the 300 kHz and 16 kHz CEI switching frequency stand out clearly. Therefore, the effect of the CM current on the operation of the LVDC distribution can be neglected. However, it was stated in Publication III that the CM current generates RF disturbances and makes the PLC communication challenging. Therefore, CM current filtering actions may be required.

With the PWM rectifying converter (Figure A.2b), the CM current level is notably higher, which can be seen in Figure 5.3b. This is due to the power electronics switches that are

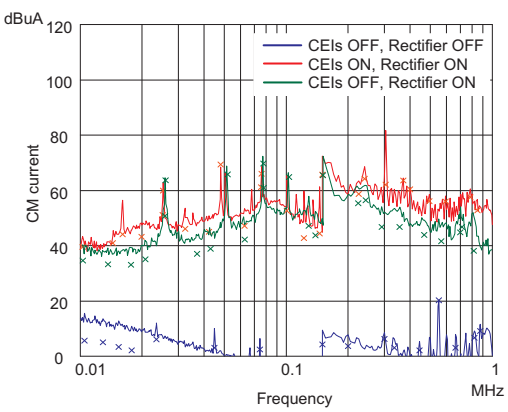

(a) Thyristor bridge (reproduced from Pub. IV)

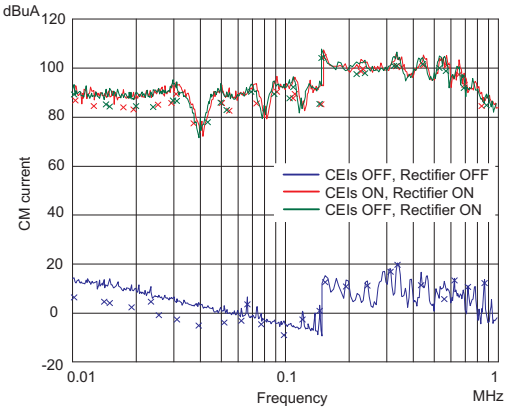

(b) PWM grid-tie rectifier, no filter

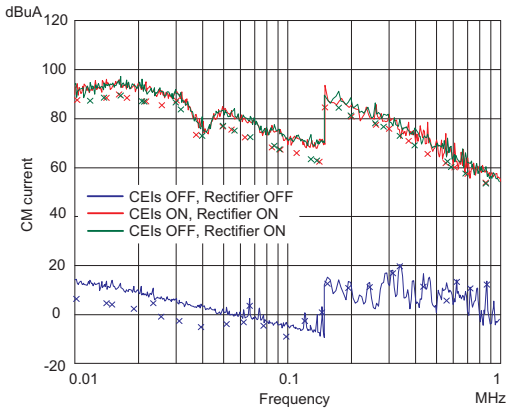

(c) PWM grid-tie rectifier with a CM choke

Figure 5.3: Measured DC network CM currents with the thyristor bridge rectifier (a) and the PWM rectifying converter. For the PWM converter, results are available with (b) and without (c) a CM choke. Note different y-axis scaling in subplot a.

actively controlled during the normal operation. The current throughout the frequency range is higher than with the thyristor bridge rectifier. It is also evident by comparing the red and green curves that the CEIs have no effect on the CM current. When the highest CM current with the thyristor bridge rectifier was 70 dBµA (10 mA), it is now 105 dBµA (251 mA). This degrades the feasibility of the PLC. In this application, the manufacturer advices that the EMC filter of the converter unit should be removed because of the unearthed IT DC network. This was done according to the manual.

To decrease the CM current, two similar CM chokes were built and installed at the rectifying substation. A 3D model of the choke is shown in Figure 5.4b. The chokes are connected according to Figure 5.4a. The CM current after the filter installation can be seen in Figure 5.3c. The currents at the frequencies below 30 kHz are not affected, which results from the CM circuit structure: the capacitance to earth plays a significant role

and therefore, the frequency dependence of the CM circuit impedance corresponds to the capacitive reactance. At low frequencies, the effect of the filter is insignificant because the CM circuit impedance is notably higher than the filter impedance. Reduction at the higher frequencies is significant, 10–35 dBμA. For instance at 500 kHz, the current is decreased from 108 dBμA (251 mA) to 72 dBμA (4 mA). The current is still higher than with the thyristor bridge rectifier, but the curves converge at 1 MHz. The CM choke produces some losses, which can be seen in Figure 5.4c, where an infrared camera photo of the choke under normal operation is shown. The filter and EMI issues with the PWM rectifying converter are discussed in more detail in a future publication.

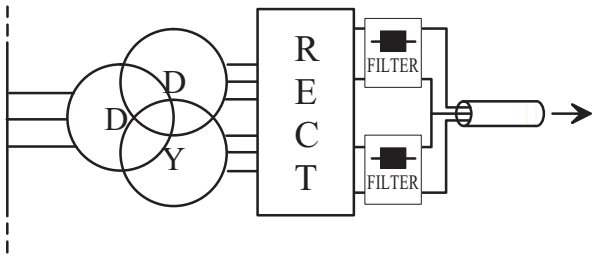

(a)

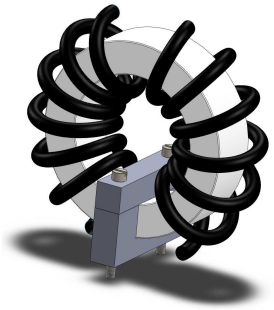

(b)

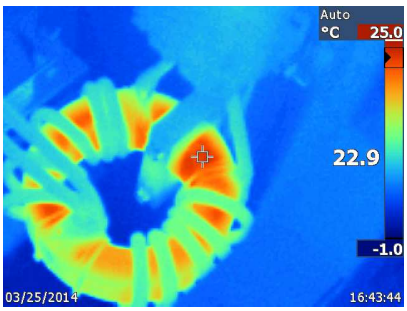

(c)

Figure 5.4: A) Location of the filters in the system, b) a 3D model of the CM choke, and c) an infrared camera photo of the operating choke.

5.3 Customer-end network

CEIs connected to the DC network produce CM voltage against earth. As a result, the CM current is injected to the customer-end network. The dominating frequencies are the switching frequency and its harmonics. Again, no standardized levels are available for those frequencies, and therefore, in Publication III, the customer-end CM currents were analyzed from the electrical safety point of view; the analysis is based on measurements conducted on the LVDC research site. The results are from the system with the thyris-

tor bridge rectifier. The standard IEC 60479-2 (IEC, 1987) introduces a frequency factor F_{f}, which is a ratio of the threshold current for the relevant physiological effects at the frequency f on the threshold current at 50 Hz. The frequency factor differs for perception, let-go, and ventricular fibrillation. In Figure 5.5a, the frequency factor for the let-go threshold is shown. It can be seen that the required current increases with the frequency. The curve in the standard ends at 1 kHz, but according to Perkins, the curve can be extended to 1 MHz (b), which is "the long standing dividing frequency between electrical safety and EMC, and the extension is based upon the published data plus a general medical understanding of the conduction of current within the body that allows for a continual increase in the allowed current to the end frequency carrying on the same reduction in effects specifically measured" (Perkins, 2014). As a conclusion, the electrical safety of the LVDC distribution network can be ensured if the CM current can be kept below the limits. This is not associated with the safety issues with 50 Hz, because the customer-end network is already built safe for the line frequency currents, and the analysis is performed to reveal possible issues with the higher frequencies originating from the CEI.

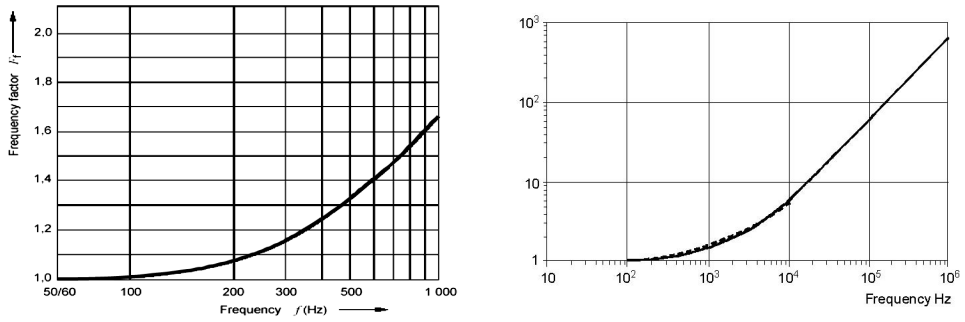

(a) (b)

Figure 5.5: A) Variation of the threshold of let-go within the frequency range 50/60 Hz to 1000 Hz (IEC, 1987). B) Extended frequency factor curve (Perkins, 2014).

The CM current has to be low enough not to degrade electrical safety or affect the operation of the devices on the customer premises. In other words, the CEIs have to be fully compatible with the existing customer-end networks, designed for the conventional AC supply. The key element in the CM current path to the customer-end network is the isolation transformer, located at the output of the CEI. Figures 5.1b and A.2 show that the CM current can only flow through the impedance between the transformer primary and secondary, consisting of resistance, inductance, and capacitance. When the isolation transformer used on the LVDC reseach site was measured, the resistance and inductance in the measurements were so high that they have no effect on the impedance of the parallel RLC circuit between the primary and the secondary. Hence, the transformer impedance $Z_{\mathrm{transf.}}$ in the CM current circuit can be calculated using the frequency f and the transformer capacitance $C_{\mathrm{transf.}}$ as

$$Z_{\text{transf.}} = \sqrt{R^2 - X^2} = X_{C_{\text{transf.}}} = \frac{1}{2\pi f C}. \quad (5.1)$$

The impedance depends on f, which is the CEI switching frequency (or its harmonic), and $C_{\text{transf.}}$ which depends on the transformer structure, also if the transformer is inside the galvanically isolating DC/DC converter. When higher switching frequencies are enabled by modern SiC and GaN transistors, the size of the isolation transformer in the DC/DC converter decreases. In addition, the DC/DC converter itself is a CM current source. Finally, the power requirement of the customer affects the structure of the CEI; is the optimal structure achieved by using a single high-power CEI or several parallel-operating CEIs? These are the issues that have to be taken into account when designing the CEI.

The impedance was calculated for the CEI isolation transformer of the LVDC research site. With the measured capacitance $C_{\text{transf.}}$=290 pF and the switching frequency f=16 kHz, $Z_{\text{transf.}} \approx 34$ kΩ. When the maximum voltage against earth is 750 V in the worst case, the CM earth current becomes 22 mA. In Figure 5.6, the measured CM currents $i_{\text{CM,cust1}}$, $i_{\text{CM,cust2}}$, and $i_{\text{CM,cust3}}$ of the customer-end networks 1, 2, and 3, respectively, are depicted. The switching frequency of the CEI and its harmonics are clearly shown in the red curves, but single harmonics disappear after 150 kHz, which is due to the different EMI test receiver settings. The maximum measured currents are 4 mA, 0.25 mA, and 8 mA (72 dBµA, 48 dBµA, and 75 dBµA in the figure, respectively). It can be seen that the customer-end network structure and devices connected to the network have an influence on the CM current magnitude. Because customer 2 is a summer cottage and the measurements were conducted in wintertime, there are fewer devices connected to the network. Therefore, the difference between an energized (red) and a de-energized (blue) network is small, resulting from a high-impedance CM current path. In networks 1 and 3, CM current magnitudes are more similar and differences between the red and blue graphs are significant. The measurements show that the CM currents in the customer-end networks are essentially lower than the calculated worst-case current, and the different user-end network structures have an effect on the CM current.

5.3.1 EMI filters and residual current devices

Many electronic devices include an EMI filter for high-frequency interference attenuation. The attenuation depends on the selected filter, but the frequencies desired to be filtered are notably higher than the line frequency, as can be seen in Figure 5.7a. Therefore, there is no attenuation at the 50 Hz frequency. However, with the CEI supply, there are frequencies higher than 50 Hz originating from the CM current injection, with a higher magnitude than in a normal AC supply. This can lead to three situations:

1. The current through the filter to the earth (Figure 5.7b) can be higher than the filter rating, which can result in filter overheating, equipment failure, and a risk of fire.

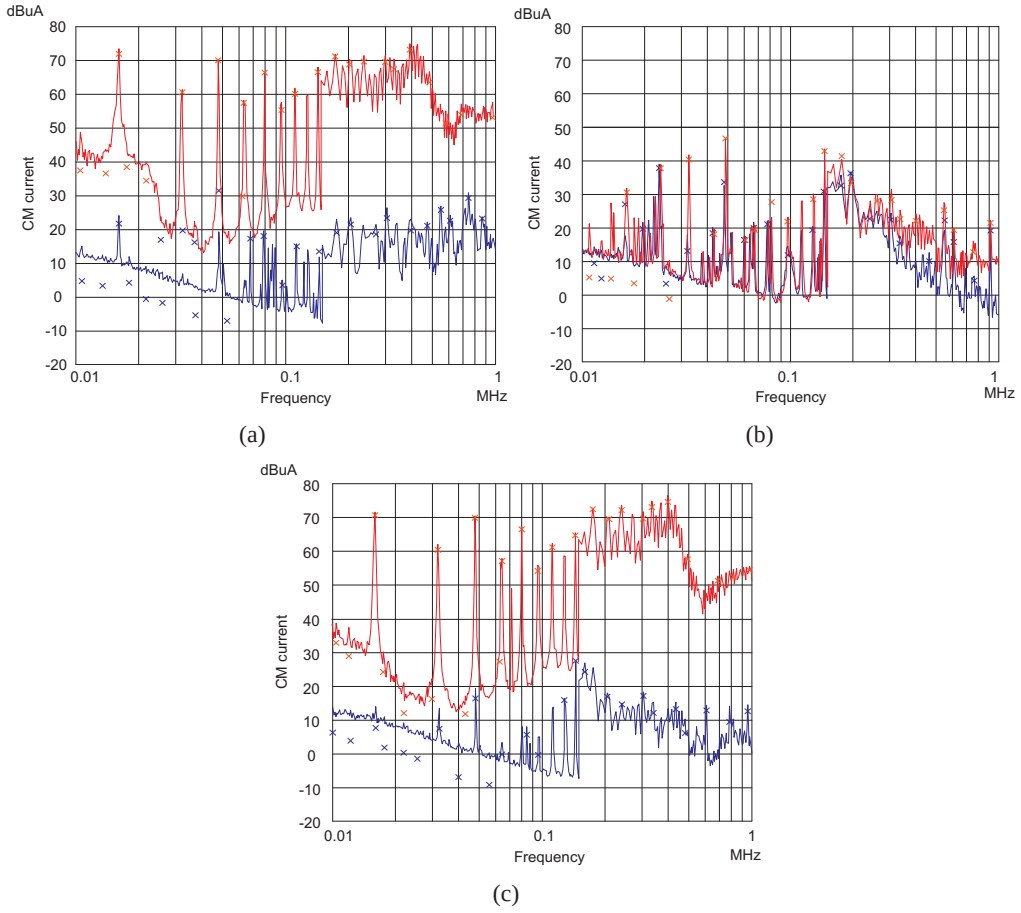

Figure 5.6: Measured customer-end network CM currents $i_{\mathrm{CM,cust1}}$ (a), $i_{\mathrm{CM,cust2}}$ (b), and $i_{\mathrm{CM,cust3}}$ (c). The red color indicates the CM current when the CEI under test is operating, and the blue color the current with the CEI turned off (adapted from Publication III).

2. If the EMI-filtered device is supplied through a residual current device (RCD), it may trip in normal operation. In particular, this is the case if there are several devices with EMI filtering supplied with a single RCD.
3. If a device with an EMI filter is connected to an unearthed socket, the potential of the device may rise, and touching the device could cause an electric shock.

In (Freschi, 2012), the behavior of RCDs at frequencies higher than the rated one is analyzed using type AC and A RCDs, which are intended for sinusoidal alternating currents and pulsating direct current, respectively. Freschi concluded that the behavior of RCDs at a high frequency is more strongly influenced by the typology rather than by the values assumed by their physical parameters, and the measurements at high frequencies show that all AC/d- and A/e-type RCDs have a tripping time below the values prescribed by the IEC standards. Hence, it can be concluded that the RCDs do not trip below the rated

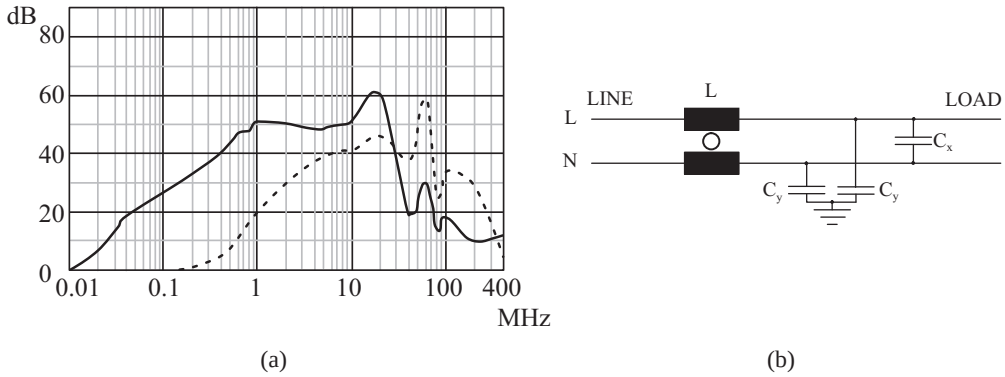

(a) (b)

Figure 5.7: Attenuation loss curve (a) and schematics (b) of a Schurter 5500.2002 EMI filter used in the measurements. In a), the solid line indicates common mode and the dashed line differential mode (Publication III).

current at high frequencies, especially, because the frequency in this application is higher than the 1 kHz Freschi used. Figure 5.8 illustrates the measured earth currents $i_{\mathrm{earth,EMI}}$ for two EMI filters connected to the output of the CEI, as shown in Figure 5.2a, and the currents are measured at the protective earth conductors of the EMI filters, also shown in the figure. When no filter is connected, the current equals $i_{\mathrm{CM,cust1}}$. The filters are typical AC-side line filters dimensioned to attenuate frequencies above 100 kHz. This may also result from the lack of the 2–150 kHz frequency band in the standardization, and therefore, filtering at those frequencies is not relevant for the manufacturers.

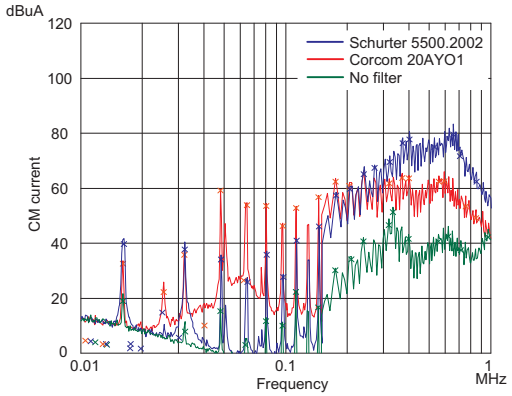

Figure 5.8: Measured CM earth currents $i_{\mathrm{earth,EMI}}$ through the studied EMI filters connected to the CEI output (reproduced from Publication III).

It was expected that the switching frequency and its harmonics are evident also in this measurement. Filter b (blue) has a better attenuation at lower frequencies, but filter a (red) attenuates better at higher frequencies. The current magnitude at high frequencies

increases by 20–40 dBμA when EMI filters are connected, depending on the filter, when compared with the no filter (green) curve. Hence, it can be assumed that the filter produces a parallel low-impedance path for the CM current, which conducts the majority of the current. The highest measured currents between 10 and 150 kHz are 40–60 dBμA (0.1–1 mA). Filter b (red) attenuates better at the higher frequencies, which was expected because of the attenuation properties of the filters. Therefore, it can be concluded that there are no challenges with the aforementioned issues 1, 2, and 3, and in this respect, no electrical safety degradation occurs.

5.4 Radio frequency EMI

The DC network is constructed using a three-conductor underground AC cable with an earthed concentric conductor, but it could also be built using a four-conductor AC cable without a concentric conductor. It can be assumed that the cable with an earthed sheath decreases the RF EMI, but the DC network is 1.7 km long, and therefore, it is not reasonable to test different underground cable types. Hence, the results are provided for the three-core concentric cable. The RF measurements were conducted with a Rohde & Schwartz HFH 2-Z2 loop antenna, which was located at a 50 m range from the overhead line (Figure 5.9), as instructed in CISPR 18-2 (CISPR 18-2, 2010). The EMI test receiver settings are shown in Table 5.1. According to CISPR 18-2, the measurements should be conducted at certain silent frequencies, and in that case, information concerning other frequencies would be lost. Therefore, standardized measurements could not be performed.

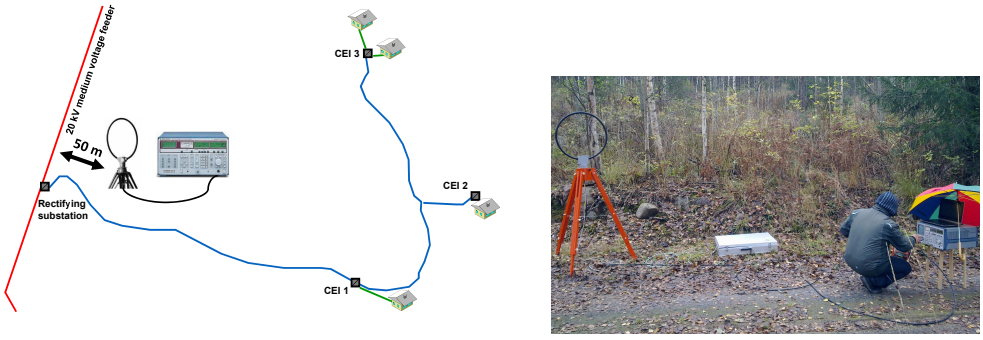

(a) (b)

Figure 5.9: Measurement scheme for RF EMI measurements (a) and the actual measurement setup (b).

The main objective was to compare the results from the normally operating system with the de-energized network. The results are depicted in Figure 5.10. It can be seen that the RF EMI originating from the system with the thyristor bridge rectifier (Figure 5.10a) is insignificant. It is stated in Publication III that the LVDC network converters have an impact on the measured frequency spectrum, but the field strengths of the frequencies originating from the LVDC network can be neglected. The situation is different with the

PWM rectifying converter (Figure 5.10b), which was expected on the grounds of the CM current measurements. The shape of the curve is also similar with the CM current curve. Because the converter uses hysteresis modulation, no single switching frequency or its harmonics are noticeable. When the difference in the field strengths between the 'system ON' and 'system OFF' conditions was a few dBμV/m, it is 50 dBμV/m at worst with the PWM rectifying converter without the CM filter. The highest field strengths also occur at high frequencies. It was assumed that the interference will decrease when the CM chokes are installed. In Figure 5.10c, a dramatic reduction, especially at the higher frequencies, can be seen. The difference between the energized and de-energized systems is small. Without clear standardized limits for the RF radiation, it can be assumed from the results that the radiation originating from the LVDC research site is at an acceptable level.

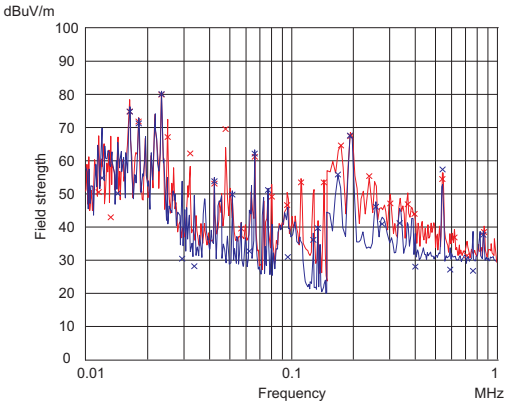

(a) Thyristor bridge

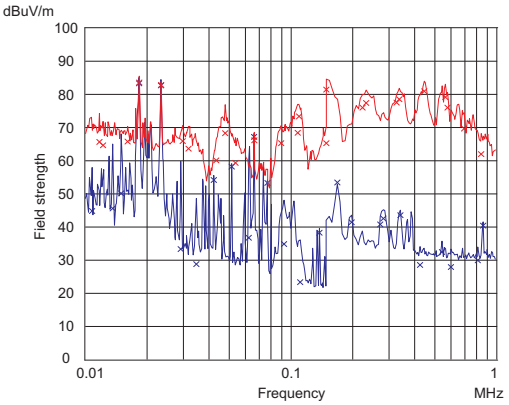

(b) PWM grid-tie rectifier, no filter

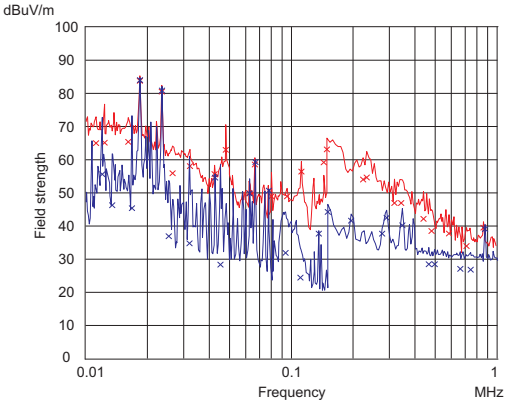

(c) PWM grid-tie rectifier with CM choke

Figure 5.10: Measured RF EMI with the thyristor bridge (a) rectifier and the PWM rectifying converter. For the PWM converter, results are available with (b) and without (c) a CM choke. The red color indicates the normally operating system and the blue color the de-energized network. The results are from measurements with a maximum antenna direction.

5.5 Conclusions

Common-mode and radio-frequency issues concerning the LVDC distribution were addressed. The analysis was based on measurements of CM currents in the customer-end networks and the DC network, and RF interferences close to the LVDC research site. It can be concluded that with the thyristor bridge rectifier, both the CM current in the DC network and the RF interferences can be neglected. When the thyristor bridge was replaced with a PWM rectifying converter, disturbances increased significantly. To improve the situation, CM chokes were designed and installed near the rectifier. As a result, the CM current decreased dramatically, which led to a lower RF interference. Actually, the difference between the thyristor and the PWM rectifiers became small. The impact of the PWM rectifier on the interferences of the LVDC research site will be analyzed in more detail in a future publication. The results of the customer-end network CM current measurements reveal that in this application, currents are at a sufficient level to provide safe electricity supply. However, the LVDC research site is developed further, and new measurements and analyses are required when the converters in the system are modified.

6 Public network research site

The structures of the power electronics addressed in this doctoral dissertation use well-studied topologies currently available. It was clear from the beginning that the research will be strongly influenced by the experimental work, because the main focus of the work was to adapt these topologies to this application. Of course, simulations and calculations had to be performed before actual implementation, but the main results are gathered from the experimental setups in the laboratory ((Nuutinen et al., 2011b)) and the public distribution network. For some results such as the short-circuit operation and the EMI issues, the setups were essential. In this chapter, the public network setup, which has been the most important target for the development, is introduced. It has the following features:

- 12-pulse half-controlled thyristor bridge rectifier (Jun. 2012–Oct. 2013)
- Two grid-tie rectifying converters (Nov. 2013 onwards)
- 1.7 km long bipolar DC network, replaces a 1000 V AC installation
- Three three-phase CEIs with galvanic isolation, similar to the three-phase laboratory setup
- Four actual electricity end-users
- Converterless directly connected BESS (Oct. 2014 onwards)
- Battery charge/discharge control using the rectifier
- Web-based control and monitoring solution

The research site was established to enable comprehensive practical studies concerning different areas of the LVDC distribution. The objective was to implement a combination of a fully functional LVDC system and a flexible research platform to a public distribution network. The network is operated by the distribution system operator (DSO) Järvi-Suomen Energia Oy and owned by the power company Suur-Savon Sähkö Oy, and the site was built in collaboration between LUT and the company. While writing this dissertation, the research site has experienced two aforementioned major upgrades. Publication IV lists the following research objectives, among which new objectives concerning the use of BESS in this application are introduced.

- Verification of the LVDC network and μGrid functionalities.
- Verification of the system planning principles.
- Verification of the developed technical solutions, functionalities, analysis methodology, and design methods.
- Verification and development of the system design, control algorithms, and management systems.
- Experiences of the durability and reliability of the electronic components in a demanding distribution network environment.
- Feedback for the equipment development.
- Installation inspections and authorized approval of structures.
- Experiences from the electricity end-users and installation and operations personnel.
- Practical experiences to support LVDC system standardization.
- Development of optimal control strategies for the BESS.
- Evaluation of the operational life of the BESS in this application.

The setup is built in a 1/0.4 kV AC supply area, which was considered to be the best location available from the LVDC point of view: (1) the transmission distances were suitable, (2) the number of customers (four) was not too high for a research setup, (3) the network was already undergrounded with a compatible cable, (4) the installation of optical fiber cables for communication was possible, and importantly, (5) the customers were willing to participate in the study. Because the system to be built is a novel solution for this purpose, the power electronics had to be designed and built by the researchers, and the reliability at the beginning was considered not that good. Hence, it takes about half an hour to return the original AC supply to use, which is essential in the case of a failure in the LVDC system. However, the backup supply had to be unexpectedly used only for two times over the last three years. In Figure 6.1, the LVDC research site is shown, and in Table 6.1, the properties of the system are listed.

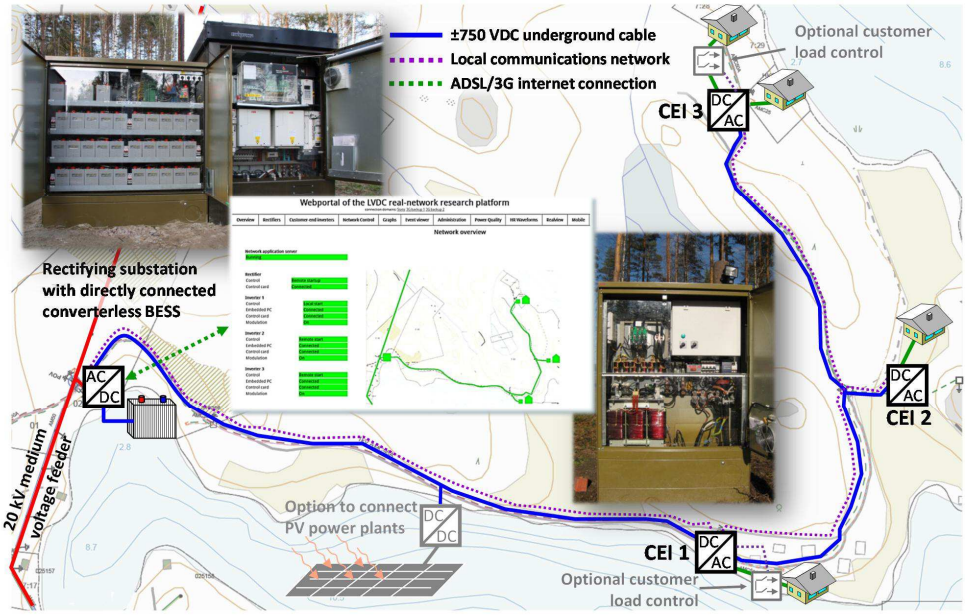

Figure 6.1: LVDC research site located on the map (reproduced from Publication IV).

6.1 Rectifier and DC network

The DC network is supplied from the 20 kV MV network through a 100 kVA double-tier transformer and the rectifier, which are installed in a transformer substation depicted in Figure 6.2a. At the beginning, bidirectional power transmission was not required, and a half-controlled thyristor bridge rectifier topology was selected. With its simplicity and sufficient control options, it provided a quick way to implement the rectifier. The thyristor bridge rectifier was later replaced by a grid-tie rectifying converter, constituting commercial converter units, because bidirectional power transmission and control over the DC

Table 6.1: System specifications and technical design criteria.

System	Property	Value
Earthing	DC network	IT
	Customer-end network	TN-(C)-S
Supply transformer		3-phase double-tier 50 Hz
	Nominal power	100 kVA
	Group	Ddy0y5
	Ratio	Pri: 20.5(±2x2.5%
		Sec: 0.53/0.53 kV
	Impedance	4%
Rectifier 1	Structure	12-pulse half-controlled thyristor bridge
	Nominal power	50+50 kVA
	Short-circuit capacity	>2 kA
	Output voltage U_{DC}	±750 V
	Distortion	max. pulsation 10%, no THD limit
	Network capacitance	12 mF
	Measurements	$U_{\mathrm{DC}-}$, $U_{\mathrm{DC}+}$, u_{AC}, U_{ctrl} $I_{\mathrm{DC}-}$, $I_{\mathrm{DC,M}}$, $I_{\mathrm{DC}+}$ T_{rect}, R_{earth}
Rectifier 2	Structure	PWM grid-tie converter
	Nominal power	35+35 kVA
	Short-circuit capacity	>2 kA
	Output voltage U_{DC}	±750 V
	Distortion	max. pulsation <1%, no THD limit
	Network capacitance	12 mF
	Measurements	$U_{\mathrm{DC}-}$, $U_{\mathrm{DC}+}$, $u_{\mathrm{AC}-}$, $u_{\mathrm{AC}+}$ $I_{\mathrm{DC}-}$, $I_{\mathrm{DC,M}}$, $I_{\mathrm{DC}+}$, $I_{\mathrm{AC}-}$, $I_{\mathrm{AC}+}$ U_{ctrl}, T_{cabinet}, T_{filter}, R_{earth}
CEIs	Structure	3-phase with galvanic isolation
	Nominal power	16 kVA
	Short-circuit capacity	200 $\mathrm{A_{rms}}$
	Output voltage u_{AC}	230/400 V
	Frequency	50 Hz±0.1%
	Variation (normal)	±1%
	(Island operation max.)	-15%
	Distortion	$\mathrm{THD_U}$<5%
	Isolation transformer	3-phase 50 Hz
	Nominal power	16 kVA
	Group	Dyn11
	Ratio	400/400 V
	Impedance	<4%
	Measurements	u_{L1}, u_{L2}, u_{L3}, U_{DC}, U_{ctrl} i_{L1}, i_{L2}, i_{L3}, i_{N}, i_{sum}, I_{DC} T_{IGBT}, T_{cabinet}
BESS A/B	Nominal capacity	30 kWh
	Fully charged voltage	790 V (3.36 V cell voltage)
	Fully discharged voltage	710 V (3.02 V cell voltage)
	Maximum charging power / current	30 kW / 1C
	Maximum discharging power / current (nominal)	30 kW / 1C
	Maximum discharging power / current (peak)	60 kW / 2C
	Number of cells	235
Battery cells	Type	$\mathrm{LiFePO_4}$
	Capacity	40 Ah
	Nominal voltage	3.2 V
	Upper limit voltage	3.65 V
	Cut-off voltage	2.5 V
	Cycle life	2000 @ 80% DOD, 0.2C discharge

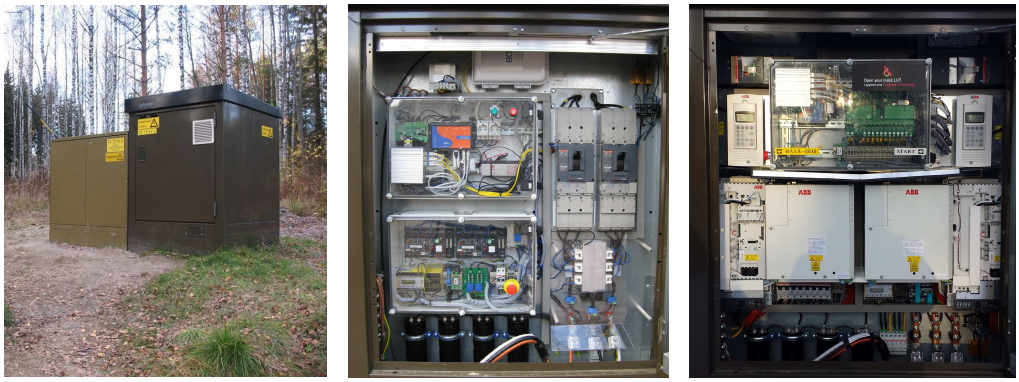

(a) (b) (c)

Figure 6.2: a) Rectifying substation with the BESS on the left, b) half-controlled thyristor bridge rectifier, and c) PWM grid-tie rectifying converter.

network voltage were required for the BESS. In Figure 6.2, the thyristor bridge rectifier (b) and the PWM rectifying converters (c), installed in the low-voltage side of the substation (a), are presented. In Figure A.2, the structures of the rectifiers are also shown. When the rectifier was upgraded, an additional measurement card was installed to enable high-resolution measurements and disturbance recording also at the rectifier-end of the network. With the thyristor bridge rectifier, the resolution was insufficient. The measurement card, developed first for the CEI control, is installed in the transparent box shown in Figure 6.2c.

The DC network is a 1.7 km long undergrounded bipolar network, constructed as a terrain-isolated functionally unearthed (IT) system. As was discussed above, the electrical safety issues require the use of an unearthed structure. The cable is a PVC-insulated AC cable, which was already in use with the 1/0.4 kV AC distribution. Because of the earthing arrangement, an insulation monitoring device is used to monitor the level of insulation of the DC network. The device controls the molded-case circuit-breakers before the rectifier, also used in the short-circuit protection, to disconnect the supply if the duration of an earth fault is long enough. The standardization requires an earth resistance of at least 1 MΩ.

6.2 CEIs

When the three-phase CEI was designed, the requirements were set to enable full hardware and software customization. With the experiences from the single-phase laboratory setup, the target was to reduce restrictions that prevent studies, tests, or implementations of advanced functionalities. As a result, commercial solutions were rejected. Currently, the site comprises three CEIs; one connected to the minus pole and two to the plus pole of the bipolar DC network (Figure A.2). The CEIs provide 230/400 VAC voltage to four end-users as presented in Figure 6.1. The galvanic isolation enables the interconnection of the IT DC network and the functionally earthed TN customer-end network. As it is

discussed in Chapter 3, the 50 Hz transformer-based isolation is not the best option, but it enabled the CEI to be operational at short notice. The CEI is designed to supply short-circuit current, which is studied in Chapter 4. The installation of the CEI in an outdoor cable distribution cabinet is shown in Figure 6.3a, and the components of the CEI are depicted in Figure 6.3b.

(a) (b)

Figure 6.3: a) CEI 3 located by the road and b) an inside view of the CEI cabinet.

The CEIs require adequate performance for power electronics control, measurement data recording, and protection and fault ride through (FRT) functions. The control board comprises two Texas Instruments TMS320F28335 digital signal processors (DSP). DSP 1 is used for the IGBT control purposes only, and DSP 2 is responsible for all other CEI functions. Two DSPs enable the development of power electronics control algorithms separately from the other functionalities, which is a significant advantage in a research setup. The board includes 16 measurement channels with a resolution of 12 bits. The same control board is used in the rectifier measurements and for the BESS control and monitoring, but only with a single processor installed. The CEI control board and the signals and the peripherals of the DSPs are presented in Figure 6.4.

6.3 BESS

The output voltage of the rectifier can be adjusted between 710 V and 790 V, and it has no effect on the customer-end voltage level and quality. Thus, the BESS was designed to be directly compatible with the DC network voltage levels. The objective was to use the rectifier to manage the charging and discharging of the BESS. In (Nuutinen et al., 2015), the implementation of the BESS is covered, and the BESS is also discussed in (Lana et al., 2014a) and (Lana et al., 2015b). Because of the bipolar network structure (Figure A.2b), the BESS consists of two similar sets of batteries, A and B, both with control devices, measurements, and battery management systems of their own. Photographs of the BESS

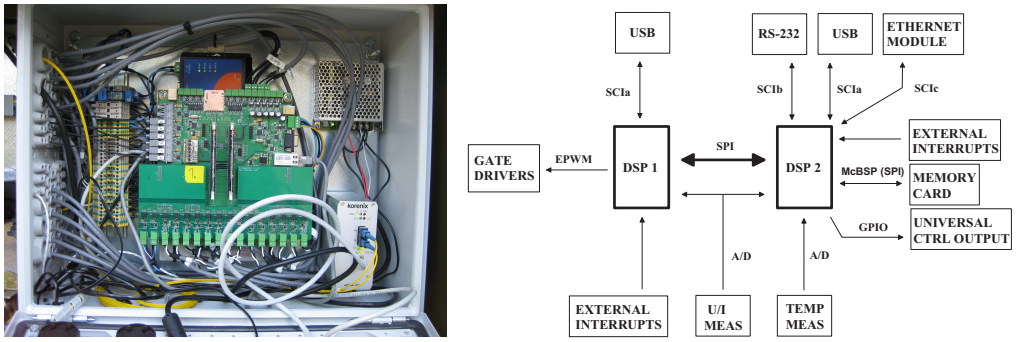

(a) (b)

Figure 6.4: Control board of the CEI (a) and signals and peripherals of the control board (b) (Publication IV).

are presented in Figure 6.5, and the main power and control circuits in Figure 6.6. The BESS is installed by the rectifying substation, shown in Figure 6.2a. Currently, the BESS enables the following functionalities:

- BESS current/power control
  - Constant current (CC) stage during charging and discharging
- DC network voltage control
  - Constant voltage (CV) stage during charging and discharging
- Rectifier current/power control
  - MV grid supply power control (enables load leveling)
- Island mode
  - Rectifier zero-current mode
  - Disconnection from the MV network
- MV grid local frequency control (not yet fully implemented)

6.4 Control and monitoring system

The research site is located tens of kilometers away from both the DSO and LUT. Hence, a remote supervision and management system was developed. The web-based system allows the remote control over the rectifier, the CEIs, and the BESS, and enables system supervision, disturbance recording, and display of high-resolution measurement data. The rectifier, the CEIs, and the BESS comprise industrial box PCs interconnected through a fiber optic communication network. The master unit is located in the rectifier substation. The access to the control system is established either with an asymmetric digital subscriber line (ADSL) connection or with a mobile data connection used for backup. The control and monitoring system is covered in (Lana, 2014) and (Lana et al., 2015a).

(a) (b)

Figure 6.5: Back-to-back installed A and B cabinets with pull-out battery shelves. The main circuit control components are installed in cabinet A (a) and the control electronics in cabinet B (b) (Publication IV).

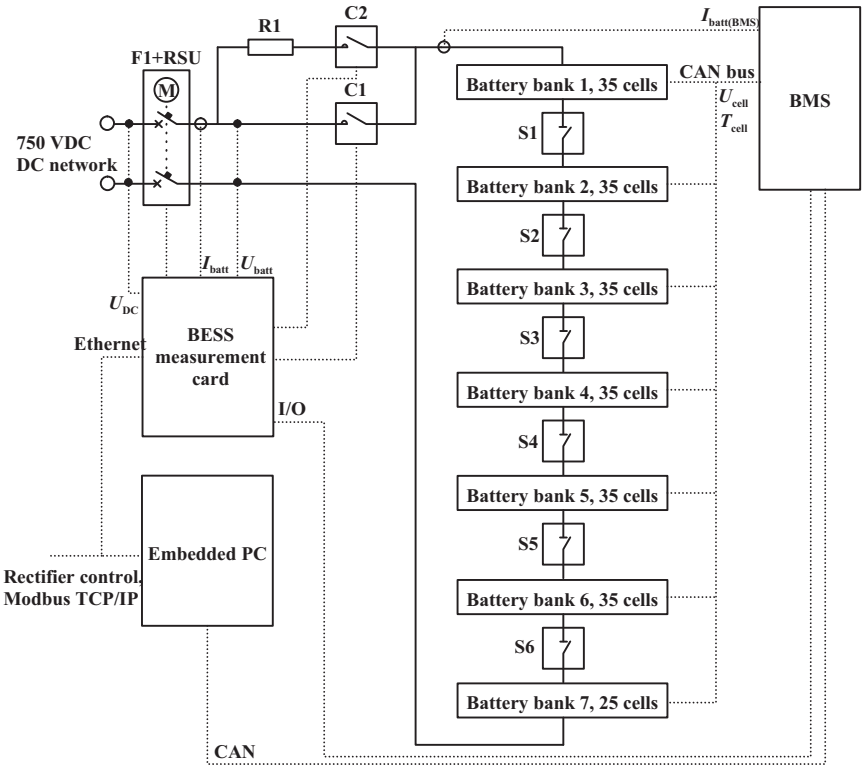

Figure 6.6: Control electronics and devices and the main circuit of the BESS.

6.5 Experiences from use

The site has produced a large amount of measurement data, but it has also provided experiences from the use of an LVDC distribution in an actual environment. Climatic overvolt-

ages, natural hazards, operating conditions, and unexpected situations have been valuable for the system development. Despite some failures in the system, sometimes caused by the user error, the result has always been an improvement to the system. There have been many minor faults and situations, involving hardware and software, that have caused short interruptions, but they have been anticipated in the first implementation. Also, it took almost 8000 hours before the backup AC supply had to be used for the first time. In this section, some of the experiences are introduced, and they are also addressed in (Kaipia et al., 2012), (Nuutinen et al., 2012), (Nuutinen et al., 2013) and Publication IV.

6.5.1 Climatic overvoltages

For protection against both the DC network overvoltage and the (climatic) overvoltage against earth, surge protectors are installed in the rectifying substation and in the CEI cabinets. However, these protectors are connected to the DC network. During thunderstorms, climatic overvoltages caused main power stage, gate driver, and current sensor failures, which occured only at CEI 1. The latest event also destroyed the ADSL modem and the embedded PC. An investigation revealed the reason for this: the ADSL line surge protectors, installed in a separate cabinet beside the CEI cabinet, have a poor connection to earth. The internet service provider installed the cabinet and never connected it to the available earthings to which the CEI cabinet was connected. A 90 Ω resistance was measured between the cabinets. Therefore, when overvoltage occurred in the ADSL line, it surged through the modem to the 12 V supply circuit in the CEI cabinet, breaking other devices connected to the circuit. After the earthing was corrected, no problems have occurred ever since. An overvoltage in the DC network has not been an issue, as can be seen in Figure 6.7, where an overvoltage event is depicted. It can be seen that the increase in the voltage of the DC network is slow, and as a result, the CEI shuts itself down and restarts after the voltage decreases below 770 V. The situation is controlled, and no overvoltage occurs in the customer-end network. In this case, the thyristor bridge rectifier was in use and the BESS was not yet installed.

6.5.2 HSARs and longer interruptions

With the thyristor bridge rectifier in use, the capacitors in the DC network supplied the network during the HSAR. The capacitors were dimensioned to be capable of feeding the network for 0.5 s when the power per pole was less than 1.5 kW. The HSAR situation is depicted in Figure 2.5. It can be seen that the customer-end voltage is kept constant until the the DC network voltage reaches 610 V, where the output voltage is decreased by 15% to increase the supply time of the capacitors. When the rectifier was replaced by the grid-tie rectifying converter and the BESS was installed, longer interruptions could be exdeeded by an island operation. In Figure 6.8, the power and state of charge (SOC) of the plus-pole-connected BESS B is shown over one day. It can be seen that the DC network is supplied with a variable power during the 5 h interruption in the MV network. After the interruption, the BESS is charged, but there are a few short interruptions also during the charging process. Over this time, nominal voltage is supplied to the customer.

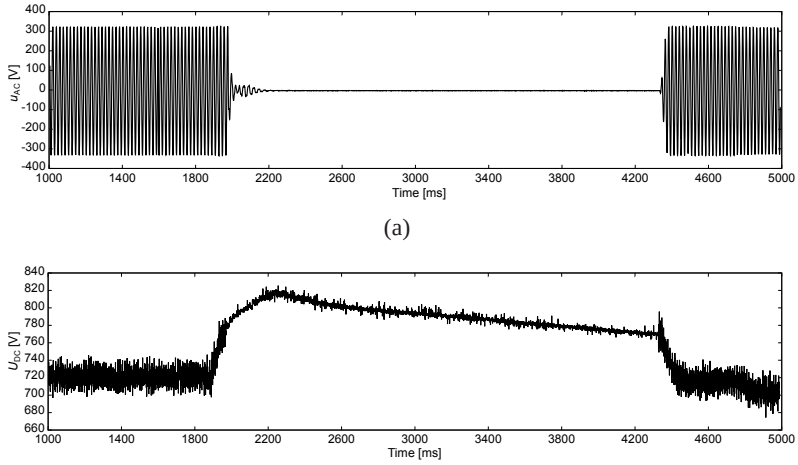

Figure 6.7: Phase a voltage of the CEI 3 (a) and the DC network voltage of the plus pole (b) during a DC network overvoltage situation, followed by an HSAR (Publication IV). Thyristor bridge rectifier is in use.

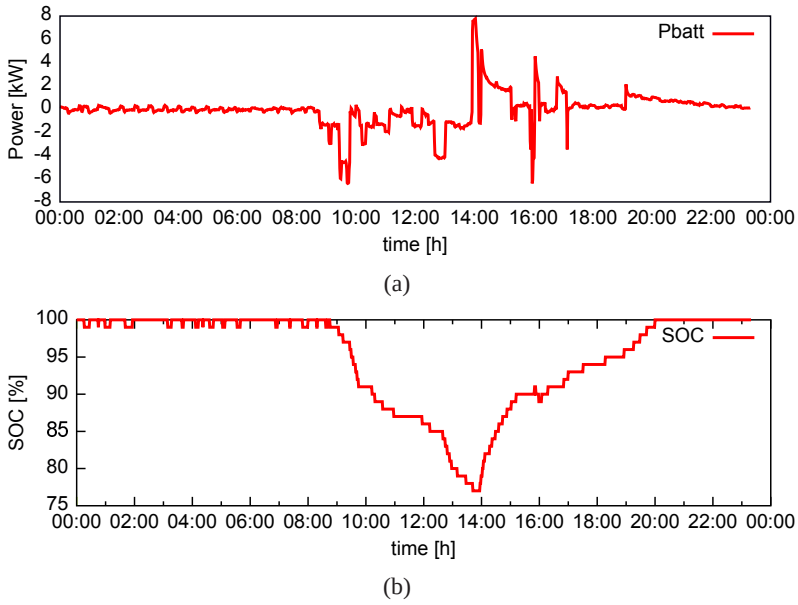

Figure 6.8: The power (a) and SOC (b) of BESS B during supply network interruption.

6.5.3 Insulation resistance

The insulation resistance of the DC network varied between 20 MΩ and 30 MΩ, when the site was commissioned. After nine months of use, a thunderstorm caused the aforementioned faults in CEI 1. After that, the insulation resistance also decreased almost to

10 MΩ, where it has remained for the last two years. The situation was investigated, and it seems that the lightning has caused some damage to the underground cable of customer 2. This is, however, an unreliable result and requires more measurements. However, the resistance is still notably higher than the required 1 MΩ, and no further actions are necessarily required.

In the DC voltage and current measurement circuit, small isolating DC/DC converters with a 1500 V isolation withstand voltage are used. Even though the voltage is double the maximum voltage over the component, many of components broke down. This sometimes decreased the insulation resistance of the DC network, which resulted in the trip of the insulation monitoring device and the system shutdown. Similar components in the customer-end side measurement circuits operate well. After the DC-network-connected components were replaced by a version with a higher isolation voltage rating, there have been no issues with the DC/DC converters.

6.5.4 Customer-end voltage quality

The CEI enables constant customer-end voltage regardless of the power level used. The CEI includes a delta-wye transformer, and after the first tests, it was clear that a significant voltage unbalance occurs with unbalanced loads. Therefore, a voltage unbalance correction was added to the control algorithm. In Figure 6.9, customer-end phase voltages and powers from the LVDC research site are shown. It can be seen that the 1% voltage unbalance cannot be achieved in every situation; with a small power consumption, the unbalance is less than 1% most of the time, but when the power unbalance increases, the phase voltage error exceeds 2%. However, the voltage unbalance is proportional to the relative load unbalance between the phases, not to the absolute power consumption. The output voltage control will be improved in the future.

The correction was operating sufficiently at CEIs 1 and 2. However, it caused voltage flicker in certain operating conditions at CEI 3. It was found out that during a start-up sequence of a heat pump of the customer, the unbalance correction algorithm caused flicker. It could be detected only by observing a light bulb, not by using an oscilloscope or a power quality meter. The algorithm was developed and tested, but the problem remained. Therefore, the only option was to turn the feature off. This is one of the issues that requires further study in the future.

6.5.5 Operating conditions

The components of the setup have experienced operating conditions varying from +30°C summer days to rough winter conditions with the temperature of -30°C. Still, no failures caused by the operating conditions have occurred. The rectifier and the CEIs have only a cooling fan for the hot conditions. In wintertime, the losses of the converter keep the temperature at a sufficient level. This application is good from the thermal design point of view; the highest powers are used in cold weather, and vice versa. Hence, relatively small

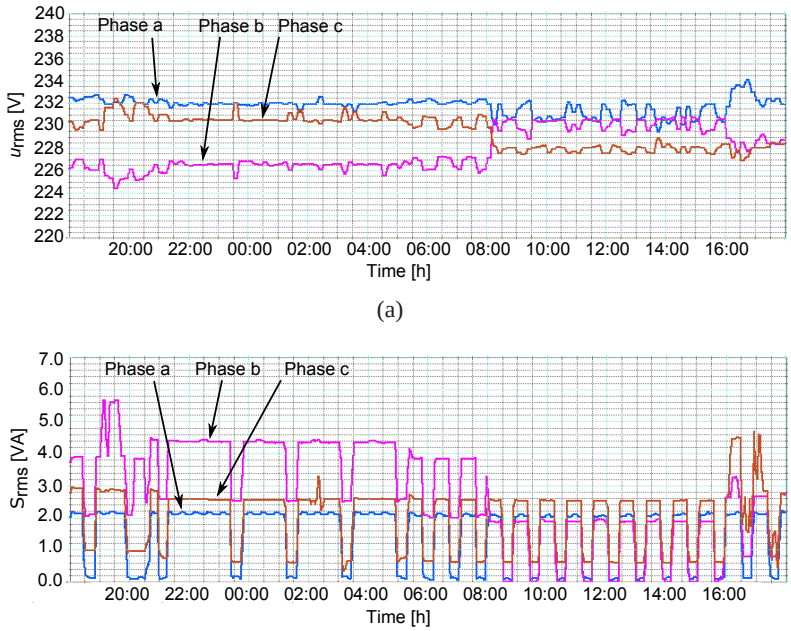

Figure 6.9: Phase voltages (a) and powers (b) of the CEI over a 24 h period (Publication IV).

cooling solutions suffice. However, when the efficiencies of the next-generation converters are higher, the situation may be different, and humidity issues have to be addressed in the design.

Because the BESS is installed by the rectifier, the losses are used to heat the BESS in cold weather. The experiences have shown that the temperature of the BESS can be kept 15–20°C above the ambient temperature. The battery cells require at least 0° and -20° temperatures for the charging and discharging process, respectively. Therefore, additional heating is required to ensure that the low temperature causes no additional aging of the cells.

6.6 Future development and research

The BESS was installed less than a year ago, and the LVDC system has been developed step by step to enable various smart grid functionalities. Currently, the BESS enable island operation during interruptions and also in normal operation. With the BESS, power taken from the MV network could also be regulated. In the future, PV panels will be installed to enable more advanced island operation together with the BESS. Thus, results from the use of a battery energy storage in this kind of an application will be gathered, and the operating life of the BESS can be evaluated. The network power flow can be controlled to maximize the network energy efficiency and minimize electricity costs. Further, the control over the

customer-end loads will be implemented to enable demand response functionalities. As was dicussed in Chapter 3, the losses of the CEIs are currently high, and hence, the CEIs will be upgraded to the next generation low-loss devices. ICT-based protection will be among the research issues, because the converters in the LVDC network already involve protection functions. However, the current standardization prohibits the use of power electronics for protection.

7 Conclusions

In this doctoral dissertation, power electronic converters in a public LVDC distribution network were analyzed, and the requirements set by this application were addressed. When compared with the present 400 V AC electricity distribution, the use of the $\pm$750 V DC voltage level significantly increases the transmission capacity with the same low-voltage cables. As a result, the LVDC distribution system can be used to renovate present MV branch lines and low-voltage networks, and it is also a potential solution for a new network design. From the power electronics point of view, the LVDC distribution system consists of a rectifier and CEIs for the end-user electricity supply. In addition to the power electronics, the rectifier substation includes a double-tier transformer for MV network interconnection and, of course, the undergrounded DC network itself. The LVDC distribution network can be considered a smart grid: the rectifier and CEIs enable various functionalities, such as remote monitoring, control, metering, protection functions, and power flow control both in the DC and customer-end networks. In the course of the research, a research site was implemented in an actual distribution network, providing electricity supply for four customers. When writing this dissertation, the system has been in operation for over 1000 days. The research setup has been used to verify most of the results presented in this work. The laboratory setups have also been of a high value.

After the introduction, suitable rectifier topologies were introduced and analyzed. It was concluded that the thyristor bridge rectifier is applicable, if the unidirectional power transmission is adequate and no DC voltage control is required. This inexpensive, low-loss, and easy-to-control solution has been used for over one year on the LVDC research site without any challenges. When there is a need for bidirectional power transmission and/or DC network voltage control, the PWM grid-tie rectifier enables both these functionalities. This topology was also an upgrade of the LVDC research site rectifier. In the next chapter, the CEI was introduced. After the discussion of the requirements, single-phase and three-phase topologies were analyzed, and three applicable topologies were selected: a single-phase full-bridge, a three-phase four-leg, and a modular three-phase one. Loss calculation for these topologies was made, using nine commercial switch components. Because the CEI is used to supply actual customers, the electrical safety is important. This was studied in the following two chapters. At first, the short-circuit operation of the CEI was discussed. In Publication I, a single-phase CEI in the laboratory was used, and in Publication II, the short-circuit behavior of the three-phase CEI used in the LVDC research site was analyzed. It was concluded that in order to meet the requirements set by the present standards, the CEI has to provide adequate short-circuit current for the protection devices. This results in challenges in the CEI design and implementation. Other protection methods, currently not allowed by the standards, were introduced and verified by measurements.

Because the LVDC network involves power electronics, the electromagnetic interference produced by the system had to be studied. The analysis in Publication III is based on measurements conducted on the LVDC research site. The analysis is divided into three sec-

tions: common-mode current in the DC network, common-mode current in the customer-end network, and radio-frequency EMI originating from the research site. The main results are from the system with the thyristor bridge rectifier, and they are backed up with the measurements gathered from the latest, PWM rectifier supplied system. It can be concluded that with a proper galvanic isolation, CM current in the customer-end network is very low and it does not degrade the safety of the end-user. The CM current in the DC network has no effect on the electrical safety, but it affects the feasibility of PLC, what was briefly discussed in Publication III. The RF interference was also low, but there are deficiencies in the current standardization that prevent a proper analysis. As can be seen, the public network research site plays an important role in the research; it has been the most important setup, and it has been continuously developed over the last three years. Hence, in the final chapter, it was addressed in detail.

7.1 Generality of the results

Some of the results of this dissertation can be well generalized in other LVDC applications. The CEI structures, loss analysis, and the short-circuit operation are not dependent on the network structure or properties. Similarly, the rectifier structures are also applicable to different types of LVDC systems. On the other hand, the results from the interference analysis are obtained from this particular LVDC network. Many things affect the magnitude of the interference and the required countermeasures: the rectifier and CEI structures, galvanic isolation, possible overhead-line DC network, or different cable types, earthing of the DC network in good grounding conditions, and also the size of the network and the number of the customers. Still, the promising results with the self-manufactured converters indicate that the interference is not an issue in other networks, either. The use of the highest available $\pm$750 V voltage levels is a lifeline for long rural-area LVDC, but in other applications, for instance in urban areas, other voltage levels are also possible. This has also an effect on the interferences. From the CEI point of view, the DC network voltage level was briefly discussed in this study. The selection of the voltage level is also analyzed in (Karppanen et al., 2015).

7.2 Suggestions for future work

In the course of the research, two issues have been discovered to pose the major challenges: the customer-end short-circuit protection and the losses of power electronics. The developed low-current protection methods require both standard approval and commercially available components to become feasible. Before that, the CEI has to be compatible with present protection devices, which results in overdimensioning of the components. This is, however, an important issue that requires further work. The losses of the power electronics are crucial to the feasibility of the LVDC distribution. In particular, the losses of the CEI have to be decreased. The author is confident that with DC/DC converter-based galvanic isolation and novel CEI structures, together with modern SiC and GaN switches, significant improvements can be made. The losses of the rectifier are also important. The LVDC distribution requires a new way of thinking. The most important aspects are the

life-cycle losses of the power electronics; the CEIs operate most of the time at low power levels, and therefore, optimization of the CEI based on that is more important than the nominal power efficiency. This has been studied in a publication by the research team (Mattsson et al., 2015b). It is also important to gather results from other LVDC networks and compare them with these results to see the effects of the changes. This is important for the generalization, and it also facilitates the network design and converter development.

From the results obtained, we may conclude that the LVDC research site, based on the power electronics engineered during the research, has been supplying four customers quite reliably for over three years, which verifies the feasibility of the LVDC distribution system concept. The challenges encountered are not overwhelming, and hence, with the aforementioned improvements, the concept is ready for commercial use.

References

Alahuhtala, J. and Tuusa, H. (2008). “Space vector modulated four-wire unidirectional three-phase/level/switch (VIENNA) rectifier with an additional leg for DC link voltage balancing.” In *Proc. of APEC 2008*. 24–28 Feb. 2008, Austin, Texas, USA.

Burkart, R. and Kolar, J.W. (2012). “Overview and Comparison of Grid Harmonics and Conducted EMI Standards for LV Converters Connected to the MV Distribution System.” In *Proc. of PCIM 2012*. 11–13 Sept. 2012, Saõ Paulo, Brazil.

Chen, B., et al. (2015). “Analysis and Suppression of Circulating Harmonic Currents in a Modular Multilevel Converter Considering the Impact of Dead Time.” *IEEE Trans. Power Electron.*, 30(7), pp. 3542–3552.

CISPR 18-2 (2010). *Edition 2.0 2010-06: Radio interference characteristics of overhead power lines and high-voltage equipment. Part 2: Methods of measurement and procedure for determining limits*. International Electrotechnical Commission, Geneva, 2010.

Cree Inc. (2014). *Casady, J. and Palmour, J.: Power products commercial roadmap for SiC from 2012-2020 and power products rel. data & pricing forecasts for 650V-15kV SiC power modules, MOSFETs & diodes*. Available: http://www.nist.gov/pml/high_megawatt/upload/Approved-Cassady_Palmour.pptx.

Cvetkovic, I., et al. (2012). “A Testbed for Experimental Validation of a Low-voltage DC Nanogrid for Buildings.” In *Proc. of EPE-PEMC 2012 ECCE Europe*. 4–6 Sept. 2012, Novi Sad, Serbia.

Demirkutlu, E. and Hava, A.M. (2009). “A Scalar Resonant-Filter-Bank-Based Output-Voltage Control Method and a Scalar Minimum-Switching-Loss Discontinuous PWM Method for the Four-Leg-Inverter-Based Three-Phase Four-Wire Power Supply.” *IEEE Trans. Ind. Appl.*, 45(3), pp. 982–991.

Dong, D., et al. (2012). “Common-mode EMI noise reduction for grid-interface converter in low-voltage DC distribution system.” In *Proc. of APEC 2012*. 8–9 Sept. 2012, Vladivostok, Russia.

Eden, R. (2013). *SiC & GaN Power Semiconductors - 2013 by IHS Technology*. Available: http://www.apec-conf.org/wp-content/uploads/2013/09/is1.4.2.pdf.

EN 50 065-1 (1991). *Signalling on low voltage electrical installations in the frequency range 3 kHz to 148.5 kHz – Part 1: General requirement, frequency bands and electromagnetic disturbances*. CENELEC, Brussels, Belgium, 1991.

EN 50160 (1994). *Voltage characteristics of electricity supplied by public distribution systems*. CENELEC, Brussels, Belgium, 1991.

Freschi, F. (2012). “High-Frequency Behavior of Residual Current Devices.” *IEEE Trans. Power Del.*, 27(3), pp. 1629–1635.

Haakana, J. (2013). *Impact of reliability of supply on long-term development approaches to electricity distribution networks*. Doctoral dissertation, Acta Universitatis Lappeenrantaensis 547, Lappeenranta University of Technology, Lappeenranta, Finland, 2013, 85 p.

Hayashi, Y., Toyoda, H., Ise, T., and Matsumoto, A. (2014). "Design consideration for contactless DC connector in high power density future 380 V DC distribution system." In *Proc. of ECCE 2014*, pp. 5690–5697. 14–18 Sep. 2014, Pittsburgh, PA, USA.

He, L., Zhang, K., Xiong, J., and Fan, S. (2015). "A Repetitive Control Scheme for Harmonic Suppression of Circulating Current in Modular Multilevel Converters." *IEEE Trans. Power Electron.*, 30(1), pp. 471–481.

IEC (1987). *IEC60479-2: Effects of current passing through the human body - Part 2: Special aspects*. International Electrotechnical Commission, Geneva, 1987.

IEC (2006). *IEC 60071-1: Insulation co-ordination - Part 1: Definitions, principles and rules*. International Electrotechnical Commission, Geneva, 2006.

IEC (2013). *IEC60947-2: Low-voltage switchgear and controlgear - Part 2: Circuit-breakers*. International Electrotechnical Commission, Geneva, 2013.

IEC (2015). *IEC TS 62578:2015-04: Power electronics systems and equipment - Operation conditions and characteristics of active infeed converter (AIC) applications including design recommendations for their emission values below 150 kHz*. International Electrotechnical Commission, Geneva, 2015.

Islam, M.R., Youguang, G., and Jianguo, Z. (2014). "A High-Frequency Link Multilevel Cascaded Medium-Voltage Converter for Direct Grid Integration of Renewable Energy Systems." *IEEE Trans. Power Electron.*, 29(8), pp. 4167–4182.

Kaipia, T., et al. (2012). "Field Test Environment for LVDC Distribution – Implementation Experiences." In *Proc. of CIRED Workshop 2012*. 29–30 May 2012, Lisbon, Portugal.

Kaipia, T., et al. (2013). "A System Engineering Approach to Low-Voltage DC Distribution." In *Proc. of CIRED 2013*. 10–13 Jun. 2013, Stockholm, Sweden.

Kaipia, T. (2014). *EPE 2014 tutorial: Low-Voltage Direct Current (LVDC) Power Distribution for Public Utility Networks – Considerations of Converter and System Design*.

Kaipia, T., Salonen, P., Lassila, J., and Partanen, J. (2006). "Possibilities of the Low Voltage DC Distribution Systems." In *Proc. of NORDAC 2006*. 20–21 Aug. 2006, Stockholm, Sweden.

Kakigano, H., Miura, Y., and Ise, T. (2010). "Low-Voltage Bipolar-Type DC Microgrid for Super High Quality Distribution." *IEEE Trans. Power Electron.*, 25(12), pp. 3066–3075.

Karppanen, J., et al. (2015). “Effect of Voltage Level Selection on Earthing and Protection of LVDC Distribution Systems.” In *Proc. of ACDC2015*. 10–12 February 2015, Edgbaston Stadium, Birmingham, UK.

Kerekes, T. (2009). *Analysis and Modeling of Transformerless Photovoltaic Inverter Systems*. Doctoral dissertation, Aalborg University, Institute of Energy Technology, Aalborg, Denmark, 2009.

Kim, J.H., Sul, S.K., Kim, H., and Ji, J.K. (2004). “A PWM Strategy for Four-Leg Voltage Source Converters and Applications to a Novel Line Interactive UPS in a Three-Phase Four-Wire System.” In *Proc. of IAS 2004*. 3–7 Oct. 2004, Westin Hotel, Seattle, United States.

Kolar, J.W. and Zach, F.C. (1997). “A novel three-phase utility interface minimizing line current harmonics of high-power telecommunications rectifier modules.” *IEEE Trans. Ind. Electron.*, 44(4), pp. 456–467.

Lana, A. (2014). *LVDC power distribution system: computation modelling*. Doctoral dissertation, Acta Universitatis Lappeenrantaensis 583, Lappeenranta University of Technology, Lappeenranta, Finland, 2014, 177 p.

Lana, A., et al. (2011). “On Dimensioning LVDC Network Capacitancies and Impact on Power Losses.” In *Proc. of CIRED2011*. 6–9 Jun. 2011, Frankfurt, Germany.

Lana, A., et al. (2014a). “Consideration on Battery Energy Storage System for an LVDC Distribution System.” In *NORDAC 2014*. 8–9 Sep. 2014, Stockholm, Sweden.

Lana, A., et al. (2014b). “On Low-Voltage Dc Network Customer-End Inverter Energy Efficiency.” *IEEE Trans. Smart Grid*, 5(6), pp. 2709–2717.

Lana, A., et al. (2015a). “Control and Monitoring Solution for the LVDC Power Distribution Network Research Site.” In *Proc. of ICDCM 2015*. 31 Mar.–1 Apr. 2015, Charleston, SC, USA.

Lana, A., et al. (2015b). “Control of directly connected energy storage in LVDC distribution network.” In *Proc. of ACDC 2015*. 10–12 February 2015, Edgbaston Stadium, Birmingham, UK.

Lassila, J., et al. (2008). “Is there economical potential for the low voltage DC electricity distribution?” In *Proc. of NORDAC 2008*. 8–9 Sept. 2008, Bergen City, Norway.

Lassila, J., et al. (2009). “Potential and strategic role of power electronics in electricity distribution systems.” pp. 1–5. 8–11 Jun., Prague, Czech Republic.

Li, F.e.a. (2010). “Smart transmission grid: vision and framework.” *IEEE Trans. Smart Grid*, 1(2), pp. 168–177.

Lohjala, J. (2005). *Haja-asutusalueiden sähkönjakelujärjestelmien kehittäminen – erityisesti 1000 V jakelujännitteen käyttömahdollisuudet*. Doctoral dissertation, Acta Universitatis Lappeenrantaensis 205, Lappeenranta University of Technology, Lappeenranta, Finland, 2005, 201 p.

Lohjala, J., et al. (2005). "Potentiality and effects of the 1 kV low voltage distribution system." In *Proc. of FPS 2005*. 16–18 Nov. 2005, Amsterdam, The Netherlands.

Lucía, ., et al. (2013). "Design of Home Appliances for a DC-Based Nanogrid System: An Induction Range Study Case." *IEEE Trans. Emerg. Sel. Topics Power Electron.*, 1(4), pp. 315–326.

LUT (2010). *Power electronics in electricity distribution, part 2/2*. Technical report. Lappeenranta University of Technology (LUT), 2010. In Finnish.

LVD (2006). *Low voltage directive (LVD) 2006/95/EC*. European Commission, 2006.

Makarabbi, G., Gavade, V., Panguloori, R., and Mishra, P. (2014a). "Compatibility and Performance Study of Home Appliances in a DC Home Distribution System." In *Proc. of PEDES 2014*. 16–19 Dec. 2014, IIT Bombay, Mumbai, India.

Makarabbi, G., Lohia, K., Panguloori, R., and Mishra, P. (2014b). "Solid State Protection for Appliances in 220V DC Home Distribution System." In *Proc. of ICAGE 2014*. 17–18 Dec. 2014, Melbourne, Australia.

Mattsson, A., et al. (2013). "Modular Customer-end Inverter for an LVDC Distribution Network." In *Proc. of PCIM Europe 2013*. 14–16 May 2013, Nuremberg, Germany.

Mattsson, A., et al. (2014a). "Galvanic Isolation and Output LC Filter Design for the Low-Voltage DC Customer-End Inverter." *IEEE Trans. Smart Grid*, 5(5), pp. 2593–2601.

Mattsson, A., et al. (2014b). "Implementation design of the converter-based galvanic isolation for low voltage DC distribution." In *Proc. of IPEC-Hiroshima 2014*. 18–21 May 2014, Hiroshima, Japan.

Mattsson, A., et al. (2014c). "Implementation of a Modular Customer-end Inverter for a Low Voltage DC Distribution Network." In *Proc. of EPE 2014*. 26–28 Aug. 2014, Lappeenranta, Finland.

Mattsson, A., et al. (2015a). "Evaluation of Isolated Converter Topologies for Low Voltage DC Distribution." In *Proc. of IECON 2015*. 9–12 Nov. Yokohama, Japan.

Mattsson, A., et al. (2015b). "Life-Cycle Cost Analysis for the Customer-end Inverter Used in Low Voltage DC Distribution." In *Proc. of ICDCM 2015*. 31 Mar.–1 Apr. 2015, Charleston, SC, USA.

Mohan, N., Undeland, T., and Robbins, W. (2003). *Power Electronics: Converters, applications and design, 3rd edition*. Wiley. 802 p.

Niiranen, J., et al. (2010). "Experiences from a Back-to-Back Converter fed Village Microgrid." In *Proc. of ISGT 2010*, pp. 1–5. 11–13 Oct. 2010, Gothenburg, Sweden.

Nuutinen, P., Lana, A., Salonen, P., and Silventoinen, P. (2011a). "Start-up of the LVDC Distribution Network." In *Proc. of CIRED 2011*. 6–9 Jun. 2011, Frankfurt, Germany.

Nuutinen, P., Pinomaa, A., and Silventoinen, P. (2016). "Grid-Tie Rectifying Converter Impact on Common-Mode and RF EMI in a Low-Voltage DC Distribution Network." *IEEE Trans. Smart Grid*. In review.

Nuutinen, P., et al. (2011b). "Implementing a Laboratory Research Platform for an LVDC Distribution System." In *Proc. of IEEE SmartGridComm 2011*. 17–20 Oct. 2011, Brussels, Belgium.

Nuutinen, P., et al. (2012). "Commissioning Inspection of an LVDC Distribution Network." In *Proc. of NORDAC 2012*. 10–11 Sept. 2012, Espoo, Finland.

Nuutinen, P., et al. (2013). "Experiences from Use of an LVDC System in Public Electricity Distribution." In *Proc. of CIRED 2013*. 10–13 Jun. 2013, Stockholm, Sweden.

Nuutinen, P., et al. (2015). "Implementing a Battery Energy Storage System with a Converterless Direct Connection to an LVDC Distribution Network." In *Proc. of CIRED 2015*. 15–18 Jun. 2015, Lyon, France.

Peltoniemi, P. (2010). *Phase voltage control and filtering in a converter-fed single-phase customer-end system of the LVDC distribution network*. Doctoral dissertation, Acta Universitatis Lappeenrantaensis 404, Lappeenranta University of Technology, Lappeenranta, Finland, 2010, 177 p.

Peltoniemi, P. and Nuutinen, P. (2013). "Fault Detection Method for Phase-to-Ground Faults in Three-Phase Inverter Applications." In *Proc. of IECON13*. 10–13 Nov. 2013, Vienna, Austria.

Peltoniemi, P., Nuutinen, P., and Pyrhonen, J. (2013). "Observer-based Output Voltage Control for DC Power Distribution Purposes." *IEEE Trans. Power Electron.*, 28(4), pp. 1914–1926.

Peltoniemi, P., et al. (2008). "Output Filtering of the Customer-end Inverter in a Low-Voltage DC Distribution Network." In *Proc. of EPE-PEMC'08*, pp. 1763–1770. 1–3 Sep. 2008, Poznan, Poland.

Perkins, P. (2014). "What does your touch current look like? Making proper touch current measurements." In *Proc. of ISPCE 2014*, pp. 25–28. 5–7 May 2014, San Jose, CA, USA.

Pinomaa, A. (2013). *Power-line-communication-based data transmission concept for an LVDC electricity distribution network – Analysis and implementation*. Doctoral dissertation, Acta Universitatis Lappeenrantaensis 557, Lappeenranta University of Technology, Lappeenranta, Finland, 2013, 92 p.

Pinomaa, A., Ahola, J., Kosonen, A., and Nuutinen, P. (2014). “Applicability of narrow-band power line communication in an LVDC distribution network.” In *Proc. of IEEE ISPLC 2014*. 30 Mar. –2 Apr. 2014, Austin, Texas, USA.

Rashed, M., Klumpner, C., and Asher, G. (2010). “High performance multilevel converter topology for interfacing energy storage systems with medium voltage grids.” In *Proc. of IECON 2010*. 7–10 Nov. 2010, Glendale, Arizona, USA.

Rekola, J. and Tuusa, H. (2011). “Comparison of line and load converter topologies in a bipolar LVDC distribution.” In *Proc. of EPE2011*. 30 Aug.–1 Sept. 2011, Birmingham, UK.

Rekola, J., Virtanen, A., Jokipii, J., and Tuusa, H. (2012). “Comparison of converter losses in an LVDC distribution.” In *Proc. of IECON 2012*. 25–28 Oct. 2012, Montreal, QC, Canada.

Rodríguez-Otero, M.A. and O’Neill-Carrillo, E. (2008). “Efficient Home Appliances for a Future DC Residence.” In *Proc. of IEEE Energy2030*. 17–18 Nov. 2008, Atlanta, GA USA.

Salato, M., Zolj, A., Becker, D., and Sonnenberg, B. (2012). “Power system architectures for 380V DC distribution in telecom datacenters.” In *Proc. of INTELEC 2012*. 30 Sept. – 4 Oct. 2013, Scottsdale, Arizona, USA.

Salonen, P., et al. (2008). “A Study of LVDC Distribution System Grounding.” In *Proc. of NORDAC 2008*. 8–9 Sept. 2008, Bergen City, Norway.

SFS 6000 (2012). *Low Voltage Electrical Installations and Safety at Electrical Work*. SESKO standardization, Finland, 2012.

Simanjorang, R., et al. (2010). “A high output power density 400/400V isolated DC/DC converter with hybrid pair of SJ-MOSFET and SiC-SBD for power supply of data center.” In *Proc. of APEC 2010*, pp. 648–653. 21–25 Feb. 2010, Palm Springs, CA, USA.

Viitanen, T. and Tuusa, H. (2002). “A Steady-State Power Loss Consideration of the 50kW VIENNA I and PWM Full-Bridge Three-phase Rectifiers.” In *Proc. of PESC02*. 23–27 Jun. 2002, Cairns, Queensland, Australia.

Zahedi, B. and Norum, L.E. (2013). “Modelling and simulation of hybrid electric ships with DC distribution systems.” In *Proc. of EPE 2013*. 2–6 Sep. 2013, Lille, France.

Zhang, R. (1998). *High performance power converter systems for nonlinear and unbalanced load/source*. Doctoral dissertation, Virginia Polytechnic Institute and State University, 1998.

Appendix A: Laboratory and public network setups

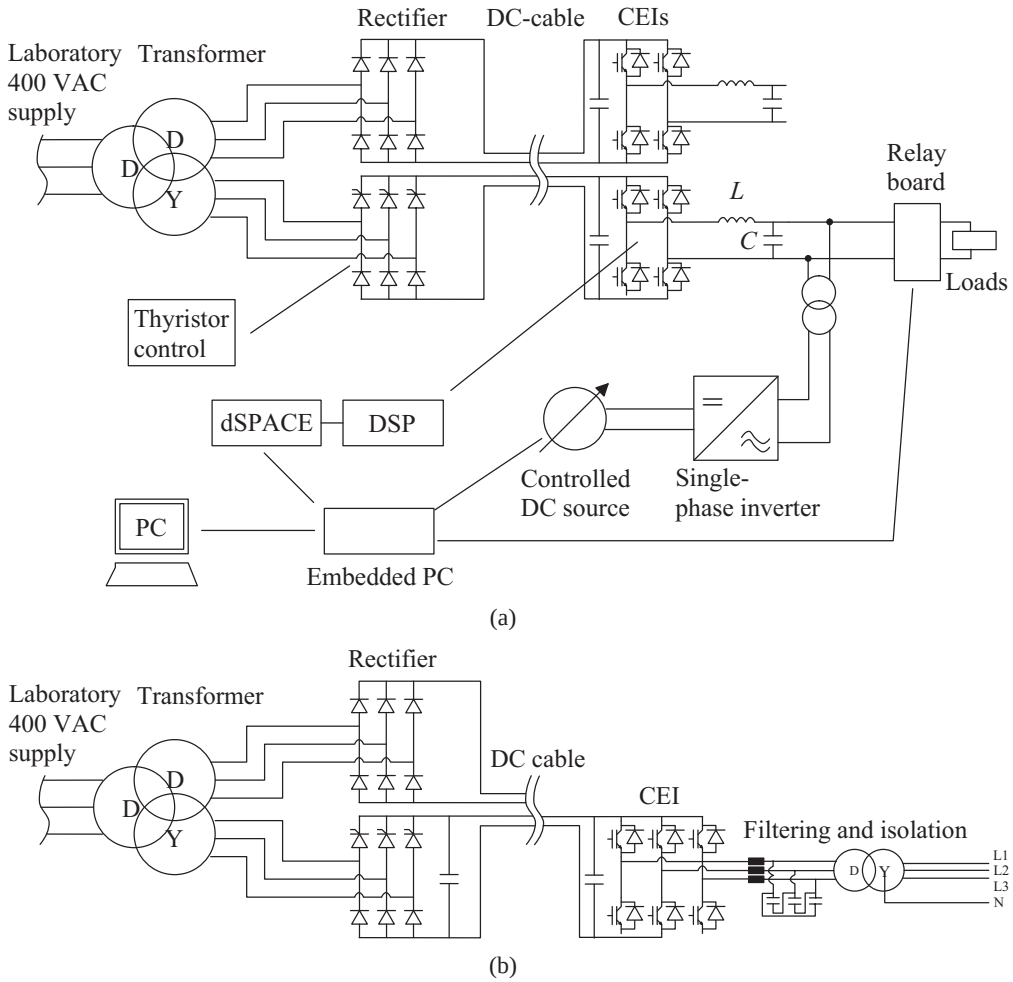

Figure A.1: Structure of a) single-phase and b) three-phase laboratory setups.

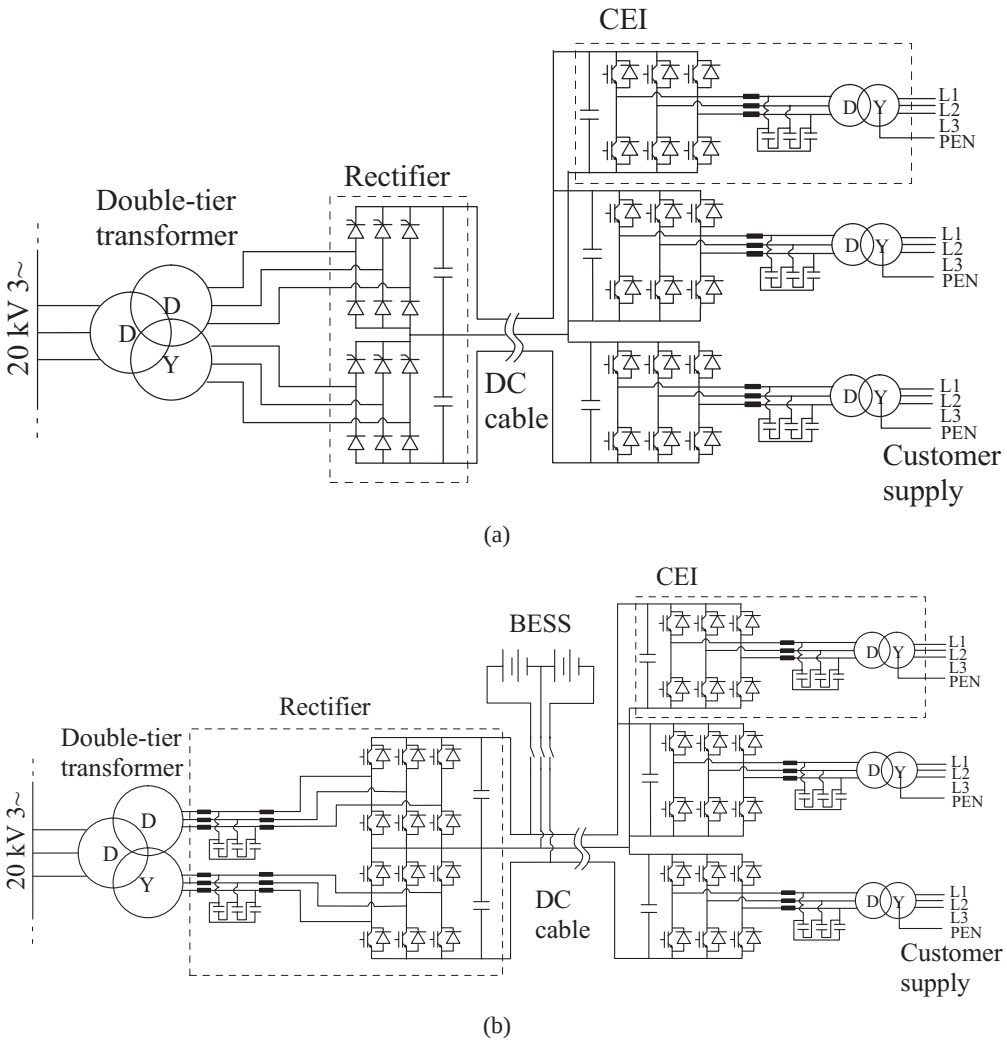

Figure A.2: Structure of the LVDC research site with a) thyristor bridge rectifier and b) PWM grid-tie rectifying converter and a battery energy storage system (BESS).

ACTA UNIVERSITATIS LAPPEENRANTAENSIS

640. RATAVA, JUHO. Modelling cutting states in rough turning of 34CrNiMo6 steel. 2015. Diss.

641. MAYDANNIK, PHILIPP. Roll-to-roll atomic layer deposition process for flexible electronics applications. 2015. Diss.

642. SETH, FRANK. Empirical studies on software quality construction: Exploring human factors and organizational influences. 2015. Diss.

643. SMITH, AARON. New methods for controlling twin configurations and characterizing twin boundaries in 5M Ni-Mn-Ga for the development of applications. 2015. Diss.

644. NIKKU, MARKKU. Three-dimensional modeling of biomass fuel flow in a circulating fluidized bed furnace. 2015. Diss.

645. HENTTU, VILLE. Improving cost-efficiency and reducing environmental impacts of intermodal transportation with dry port concept – major rail transport corridor in Baltic Sea region. 2015. Diss.

646. HAN, BING. Influence of multi-phase phenomena on semibatch crystallization processes of aqueous solutions. 2015. Diss.

647. PTAK, PIOTR. Aircraft tracking and classification with VHF passive bistatic radar. 2015. Diss.

648. MAKKONEN, MARI. Cross-border transmission capacity development – Experiences from the Nordic electricity markets. 2015. Diss.

649. UUSITALO, ULLA-MAIJA. Show me your brain! Stories of interdisciplinary knowledge creation in practice. Experiences and observations from Aalto Design Factory, Finland. 2015. Diss.

650. ROOZBAHANI, HAMID. Novel control, haptic and calibration methods for teleoperated electrohydraulic servo systems. 2015. Diss.

651. SMIRNOVA, LIUDMILA. Electromagnetic and thermal design of a multilevel converter with high power density and reliability. 2015. Diss.

652. TALVITIE, JOONAS. Development of measurement systems in scientific research: Case study. 2015. Diss.

653. ZUBEDA, MUSSA. Variational ensemble kalman filtering in hydrology. 2015. Diss.

654. STEPANOV, ALEXANDER. Feasibility of industrial implementation of laser cutting into paper making machines. 2015. Diss.

655. SOKOLOV, MIKHAIL. Thick section laser beam welding of structural steels: methods for improving welding efficiency. 2015. Diss.

656. GORE, OLGA. Impacts of capacity remunerative mechanisms on cross-border trade. 2015. Diss.

657. AURINKO, HANNU. Risk assessment of modern landfill structures in Finland. 2015. Diss.

658. KAIJANEN, LAURA. Capillary electrophoresis: Applicability and method validation for biorefinery analytics. 2015. Diss.

659. KOLHINEN, JOHANNA. Yliopiston yrittäjämäisyyden sosiaalinen rakentuminen. Case: Aalto-yliopisto. 2015. Diss.

660. ANNALA, SALLA. Households' willingness to engage in demand response in the Finnish retail electricity market: an empirical study. 2015. Diss.

661. RIABCHENKO, EKATERINA. Generative part-based Gabor object detector. 2015. Diss.

662. ALKKIOMÄKI, VILLE. Role of service and data reuse in enterprises. 2015. Diss.

663. VÄNTSI, OLLI. Utilization of recycled mineral wool as filler in wood plastic composites. 2015. Diss.

664. KLEMOLA, KATJA. Tuottavuuden, vaikuttavuuden ja kustannusvaikuttavuuden arviointi alueellisesti integroiduissa sosiaali- ja terveyspalveluissa – palvelujen käyttöön perustuva malli ja esimerkkejä. 2015. Diss.

665. HEROLD, KRISTIINA. Impact of Word-of-Mouth on consumer decision-making: An information processing perspective in the context of a high-involvement service. 2015. Diss.

666. OLABODE, MUYIWA. Weldability of high strength aluminium alloys. 2015. Diss.

667. VANHALA, ERNO. The role of business model in computer game development organizations. 2015. Diss.

668. SALAMPASIS, DIMITRIOS. Trust-embedded open innovation: Towards a human-centric approach in the financial industry. 2015. Diss.

669. DE SMET, DIETER. Innovation ecosystem perspectives on financial services innovation. 2015. Diss.

670. PORRAS, PÄIVI. Utilising student profiles in mathematics course arrangements. 2015. Diss.

671. SALMINEN, JUHO. The role of collective intelligence in crowdsourcing innovations. 2015. Diss.

672. ROSAS, SAILA. Co-operative acquisitions – the contextual factors and challenges for co-operatives when acquiring an investor-owned firm. 2015. Diss.

673. SINKKONEN, TIINA. Item-level life-cycle model for maintenance networks – from cost to additional value. 2015. Diss.

674. TUUNANEN, JUSSI. Modelling of changes in electricity end-use and their impacts on electricity distribution. 2015. Diss.

675. MIELONEN, KATRIINA. The effect of cationic-anionic polyelectrolyte multilayer surface treatment on inkjet ink spreading and print quality. 2015. Diss.

676. OMAJENE, JOSHUA. Underwater remote welding technology for offshore structures. 2015. Diss.